Identification of kick-back from normal situations due to activation of flexible demand

Han, Xue; Bindner, Henrik W.; Hansen, Henrik; Rasmussen, Kåre Seest; Cajar, Peder Dybdahl; Ding, Yi; Tackie, David Victor

Publication date:
2014

Document Version
Publisher's PDF, also known as Version of record

STRATEGIC PLATFORM FOR INNOVATION AND RESEARCH IN INTELLIGENT POWER [IPOWER]

Identification of kick-back from normal situations due to activation of demand flexibility

Category	**Report**
Identifier	**WP 3.6.2 (original WP 4.5.2)**
Status	**Final Document**
Version	**Version 1.0**
Access	**WorkPackage 3.6**
Editors	**Xue Han, DTU**
Date	**February 17, 2014**

Funding: Joint by partners and Danish Government (iPower platform has been granted support from SPIR - Strategic Platform for Innovation and Research).

DOCUMENT CONTROL

Members of the iPower Consortium

Danish Energy Association	DE
DONG Energy	DONG
DTU Centre for Electric Technology	DTU CET
Risø DTU	RISØ DTU

List of Contributors

Xue Han, RISØ DTU	WP3.6 participant
Henrik W. Bindner, RISØ DTU	WP3.6 participant
Henrik Hansen, DE	WP3.6 participant
Kåre Seest Rasmussen, DONG	WP3.6 participant
Peder Dybdal Cajar, DONG	WP3.6 participant
Yi Ding, DTU CET	WP3.6 working group leader
David Victor Tackie, DE	WP3 leader

List of Reviewers

Latest Version of this Document

Related Documentation

iPower Glossary
Flexibility Interface – Information Modeling for Direct Control (iPower WP 4.6.2 & Cross-WPs)

Summary of Changes

Version 0.1 24/11/2013, Xue Han	Preliminary version prepared
Version 0.2 19/12/2013, Xue Han	Comments from co-authors incorporated
Version 0.3 20/01/2013, Xue Han	Modelling details updated & recommendation updated
Version 1.0 17/02/2013, Xue Han	Identified mistakes corrected, recommendation & conclusion updated

CONTENTS

1 Introduction

1.1 Background

The integration of renewable energy sources increases in the last decade and will keep growing in the future [1]. The commission of the European Countries has set the target of 20 % renewables by 2020 [2]. The Danish government has promoted a long term target of achieving 100% renewable energy supply by 2050 [3]. Meanwhile, the power system is moving from a system energized by a few centralized conventional large power plants to a system with a large population of distributed smaller production units [4]. With large quantities of intermittent renewable energy sources, and decentralized power generations, more ancillary services are required from the power system operation, in order to balance the consumption and production, and to secure the reliable power supply. One of the approaches in a smart grid concept is to utilize distributed energy resources (DERs) to provide services [5] [6].

DERs are small units that produce energy or have the ability to adjust their consumption. They are normally installed at the end-users in low-voltage (LV) distribution grid: small production units, such as small wind turbines and photovoltaic systems (PVs); and flexible consumption units, such as electrified space heating and cooling systems and electric vehicles (EVs) [7]. The provision of services from DER units requires appropriate aggregating approaches and control strategies to scale up the volume of power and energy.

To accomplish the environmental goal of 2020 and 2050 [2] [3], the Danish government is pushing forward greener and more efficient energy usage in the whole society. Consequently, electric vehicles and heat pumps are anticipated to play major roles in the future energy structure in Denmark. In this subtask, we mainly focus on these two types of units as a portfolio to provide demand flexibility from residential customers.

1.1.1 Demand side DER and its flexibility

In [7] from iPower Work Package 4, the flexibility of demand side DERs are explicitly classified into three categories – *Buckets, Batteries*, and *Bakeries*:

- **Buckets** – A bucket type DER has limited ability to store energy under power limitation with a given quality of the storage. The quality of the storage decides how much energy is lost along time. Example: space heating system.
- **Batteries** – The battery represents a customer that has larger flexibility of energy consumption within certain energy and power limit. A time limit is set to ensure certain amount of energy is stored in the defined period: the charging period can be freely determined as long as the state of charge can reach specific level at certain time. Example: electric vehicle.
- **Bakeries** – A bakery type DER has a certain consumption profile that is not changeable. But it is allowed that the appearance of the consumption can be shifted within certain time constraints. Example: tumble dryer.

Different flexible demand categories exhibit different behaviours, not only on what type of flexible products they can serve, but also on the nature of kick-back effects. Thus, it is interesting to observe and to compare the behaviours of electric vehicles and heat pumps that belongs to different categories.

1.1.2 LOAD KICK-BACK EFFECT

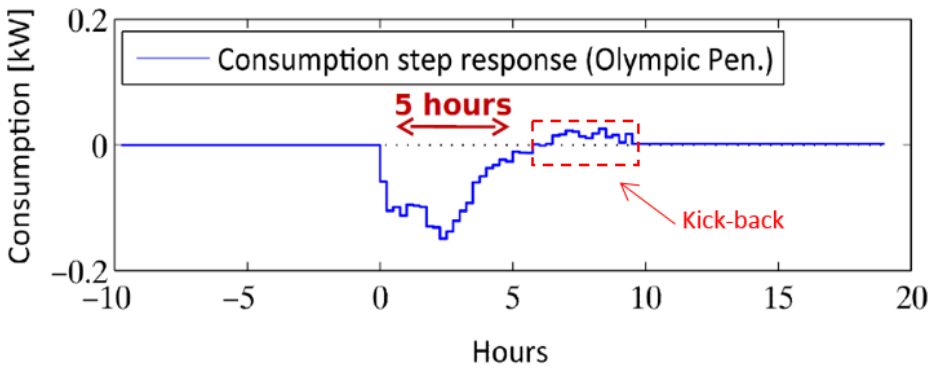

Figure 1: Load kick-back due to demand flexibility [8].

Load kick-back effect (Figure 1), a.k.a, "energy payback effect", "load recovery", "load rebound", and "load pick-up", are investigated originally under the circumstances of restoration from power system outages [9]. The phenomenon is described as "*initial load demand after an outage can exceed the load demand that would have been observed at any time before the outage*". It is due to the fact that the usual diversity of different loads is lost, and all of them have synchronized behaviour. Under the smart grid frame, the kick-back effect may happen as well: the ancillary services instruct the DER units to perform same or similar actions to their flexibility. The harmonized actions of a large quantity of homogeneous DERs would not fade off easily. For example, after a period when the demand consumption are curtailed, the customers energize the loads to restore the normal operation (e.g., normal room temperature). The diversity of electric element usage is lost in this occasion. Such phenomenon is called "**kick-back effect**".

Lee and Wilkins [10] presented their energy pay back models of water heaters with predefined load control strategies (e.g., the water heater is switched off between 4:00 PM and 6:00 PM). The payback curve (see the figure on the right side) is formulated as a function of reduced energy during each 15-minute interval (quadratic in the first interval and linear afterwards until 2 hours later) using regression method. Similarly, Kurucz, Brandt, and Sim [11] defined the payback patterns in consecutive 15-minute intervals (see Table 1 for water heater). In [12], the software EnergyPlus is used to identify the payback effects of the components inside the building (e.g., space-heating and air-conditioning systems). Figure 2 shows how the payback pattern would be (in dashed line). Paoletti, and *et al.* [13] presented a time series model for the load forecasting in active distribution networks. In their model, the payback effect is given as a reversed proportion of reduced energy and its duration is assumed to be half of the duration of the service. The kickback effects are also observed from modelling a large population of thermostat loads in some studies [14] [15]. Some control strategies to reduce the kick-back effects are proposed in [16]. ADDRESS delivery 1.1 [17] also underlines the energy payback effects as one of the main risk of activation of active demand.

1.2 MOTIVATION

Under such circumstances, the kick-back load is higher than the pre-event load. The peak generated by the kick-back effect may increase the network load and power imbalance, and furthermore produce corresponding consequences, such as increase of energy bills, and impacts on market price [17]. Given the increasing importance of demand response in the distribution grid operation, the dynamic behaviours of the aggregated DER performance and subsequently the impact on

Control duration	Payback duration	Energy payback [MWh]	Payback demand [MW]
1-5	1	1-5	1-5
6-8	2	8	5,3
9-10	3	10	5,3,2
11-12	4	1	5,3,2,1
13	5	12	5,3,2,1,1

Table 1: Payback curve of a water heater in consecutive 15-minute intervals [11].

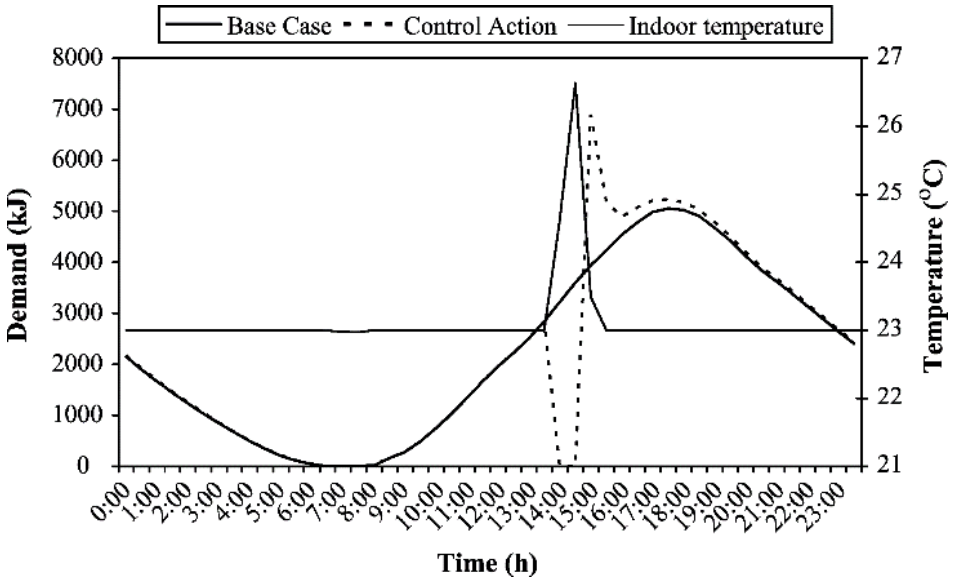

Figure 2: Thermal load consumption curves for a residential air conditioner [12].

the grid should be sufficiently addressed. Thus, this subtask will look into this phenomenon and investigate the kick-back effect of various DER units (e.g., electric vehicles and heat pumps) when applying different control methods in the normal operation conditions.

1.3 METHOD

The study consists of four parts: modelling, scenario defining, case study, and recommendations (see Figure 3).

A real medium-voltage (MV) distribution grid area operated by DONG Energy A/S [18] is used for the grid study. It includes 19 feeders and 326 nodes. Two representative bottlenecks (a MV feeder and a MV/LV transformer) are identified by analysing the load flow results at the most critical time instant. The customer consumption information under each node is specified in the provided grid model in NEPLAN [19]. A bottom-up approach is used to investigate the aggregated behaviours of DER units: corresponding models are built, and individual behaviours are simulated. Two groups of control strategies are defined to activate the demand flexibility.

After the above modules are prepared, a scenario tree can be built to study the impact of different factors on the shape and the size of the kick-back load. Meanwhile, the grid effect of the kick-backs are investigated by focusing on the bottlenecks

of the grid. To explicitly analyse the aggregated response of DER units, several control methods are applied to a large portfolio of DERs to observe the kick-back load.

Based on the simulation results, recommendations are provided to mitigate the kick-back effects. Some procedures are evaluated via simulations.

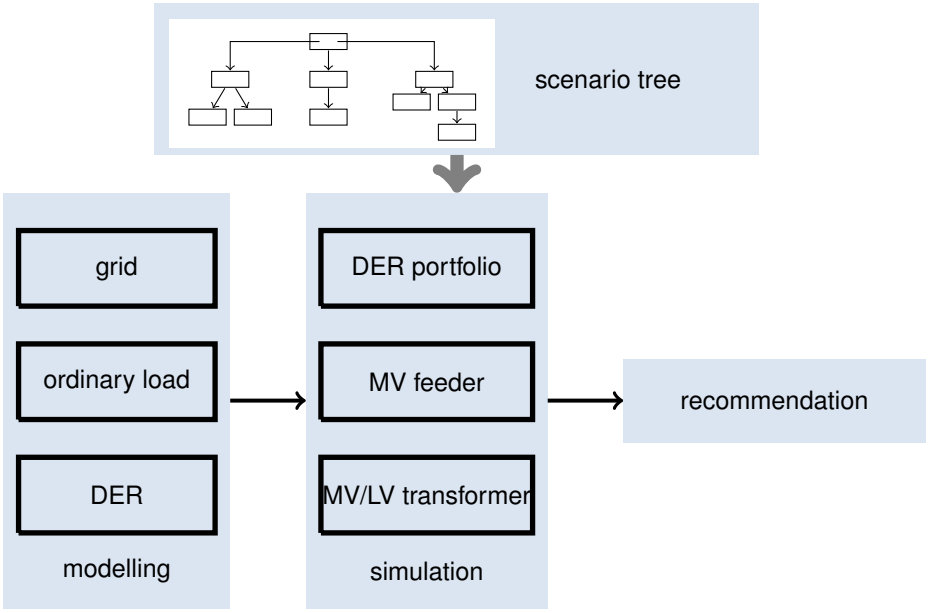

Figure 3: Diagram of study method

1.4 STRUCTURE OF THE REPORT

The remaining part of this report is structured as follows. Initially, grid models, load models, and their components are introduced in Section 2. The investigated control methods are presented in the same section. It is followed by the description of scenarios and their each dimensions in Section 3. Based on the knowledge in Section 2 and Section 3, the simulations and analysis is conducted in Section 4. Some recommendations are provided to avoid the critical kick-back effects when designing a control solution in Section 5. In the end, Section 6 concludes the study and presents the future work.

2 STUDY SET-UP

The modelling details of different modules in Figure 3 "modelling" block will be presented in this section. The grid consists of 3 primary substation connections (A, B, and C), 19 feeders and 326 nodes, including both MV nodes and LV nodes at the secondary side of MV/LV transformers. All 19 feeders are in radial topology in the normal operation condition. The MV feeders are tied by cables that are with normally opened breakers. This configuration can increase the reliability of constant and stable power delivery to the end users. DONG Energy has categorized customers in two groups: large customers with their own specific load profiles along a year (active and reactive power [1]), and small customers that are categorized into 27 types and each of which have typical load profiles based on Velander formula[2] (annual energy consumption and constant power factor [3]). The yearly curves indicate that the most severe conditions appear in the winter during weekdays. Figure 4 – Figure 6 illustrate the loading of elements and the voltage deviations in the grid. Although the long term load growth and the integration of DER units (in our case, electric vehicles and heat pumps) are exhibited in the set-up, the further reinforcement of the grid facilities are not yet considered in this study. It is due to the fact that one of the major interests on developing and introducing demand response is to postpone or avoid later reinforcement of the grid.

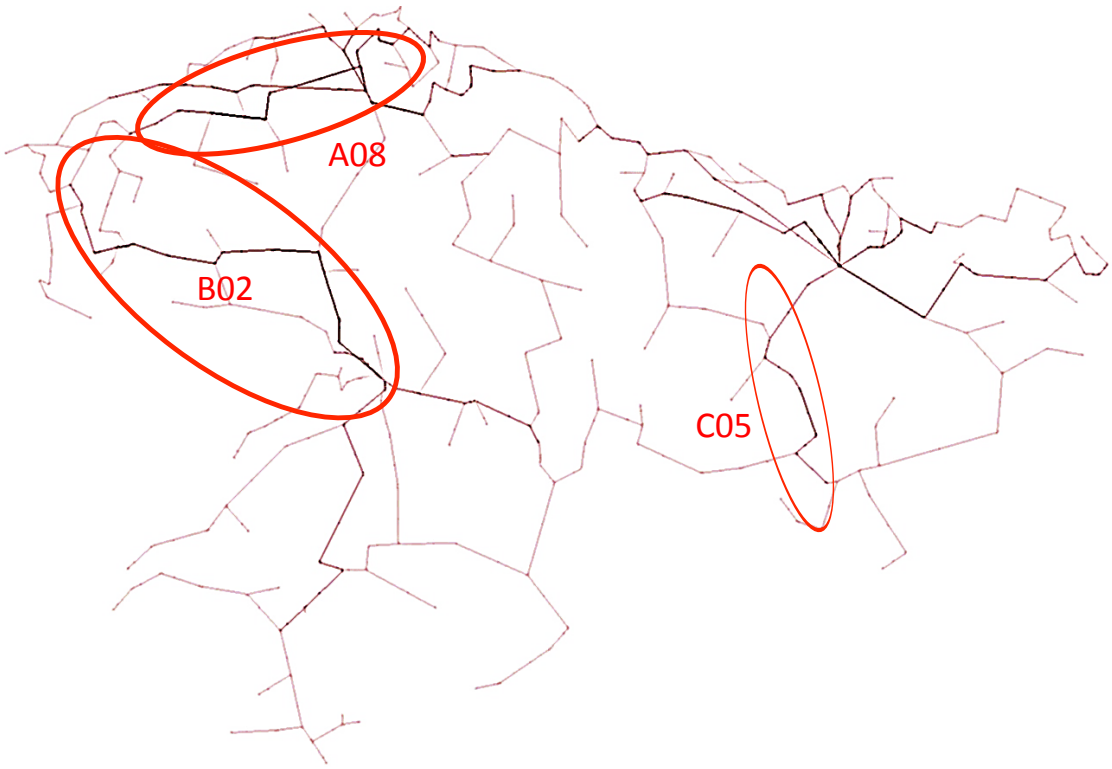

Figure 4: Line loading of the entire grid area (darker and thicker lines indicate higher loading factor) at 11-12-2013 18:30.

[1] PQ load: active power and reactive power are provided to identify the load profile.

[2] The maximal power consumption P_{max} [kWh/h] is calculated by $P_{max,i,k} = \alpha_k \times E_{i,k} + \beta_k \times \sqrt{E_{i,k}}$, where $E_{i,k}$ is the annual consumption [MWh] of this particular load category k, under a certain node i. α_k and β_k are the parameters for the category. Details are in Appendix B

[3] EC load: annual consumption and power factor are provided to identify the load profile.

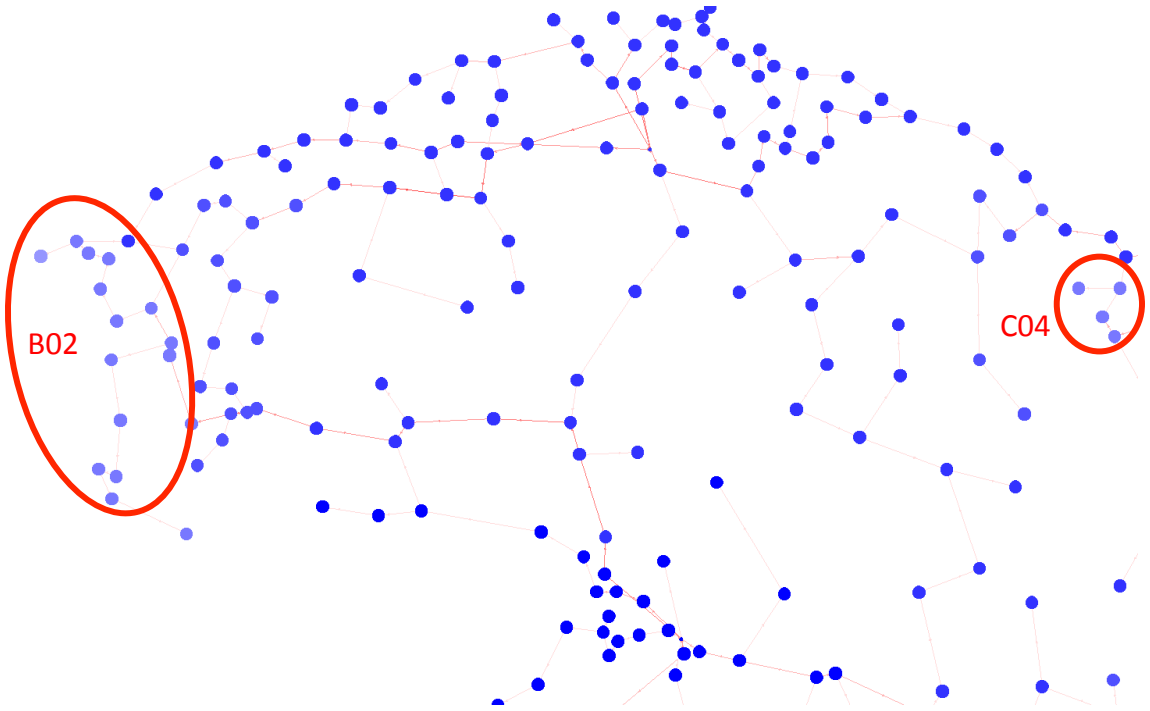

Figure 5: Voltage deviations (lighter points indicate lower voltage magnitudes) at 11-12-2013 18:30.

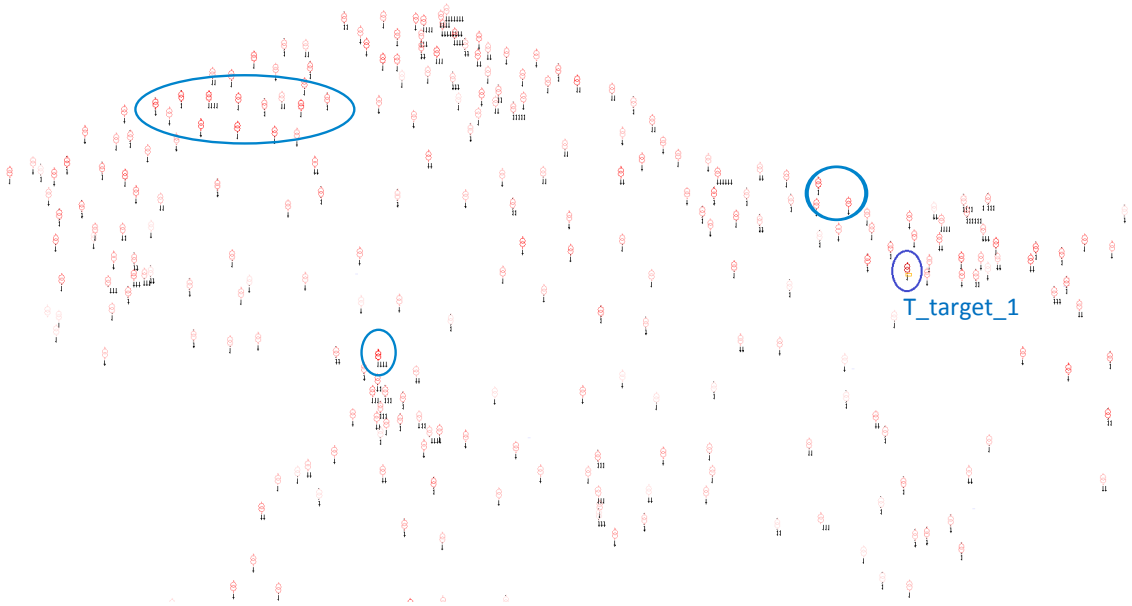

Figure 6: MV/LV transformer loading in the grid area. (darker symbols indicate higher loading factor) at 11-12-2013 18:30.

2.1 GRID MODEL

2.1.1 OPERATION CONSTRAINTS TO ASSESS THE KICK-BACKS

Three essential operation constraints are chosen to measure the grid operation performance:

- Node voltage: according to EU Standard EN50160 [20], the variation of voltage magnitude 10-minute average rms value should be within $\pm$10% of the nominal value for 95% of time [4]. Considering the fact that MV distribution area and LV area share the range of $\pm$10%, and a suboptimal position of fixed tap-changer at secondary substation, $\pm$5% is set as an indicator of critical voltage deviation situation in our study.
- Line loading: considering the "N-1" criterion, 30% of the cable capacity is reserved for emergency operation condition. So two measuring points are set. 70% loading is the indicator of heavy loading condition, and 100% loading is the hard limit of overloading. The capacity of lines (cables) are defined in current [Amp].
- Transformer loading: similar to line loading, 70% loading and 100% loading are the two measuring points for transformer loading conditions. The capacity of transformers are defined in apparent power [kVA].

2.1.2 CHOICE OF MV/LV TRANSFORMER AND MV FEEDER

To narrow down the objectives in the grid model, a MV/LV transformer and a MV feeder are selected to represent severe conditions in the grid area. The loading of individual transformers and lines, and the voltage deviations from the nominal voltage values (i.e., 10 kV in MV grid and 0.4 kV in LV grid) are calculated for the peak period (7^{th} December 2013 – 20^{th} December 2013) without integration of electric vehicles and heat pumps.

The voltage drop along the radial feeder and the line loading mostly depend on the connected loads in the feeder. Figure 4 illustrates that most critical lines are located close to the primary transformer. From the figure, it can be identified that two feeders marked by the red circles are heavier loaded than the rest. Figure 5 tells that the nodes within the read circles have largest voltage drop. Several heavily loaded transformers are marked by the blue circle in Figure 6. One of them is T_target_1. There are three overloaded LV transformers in the grid in the current scenario, winter case.

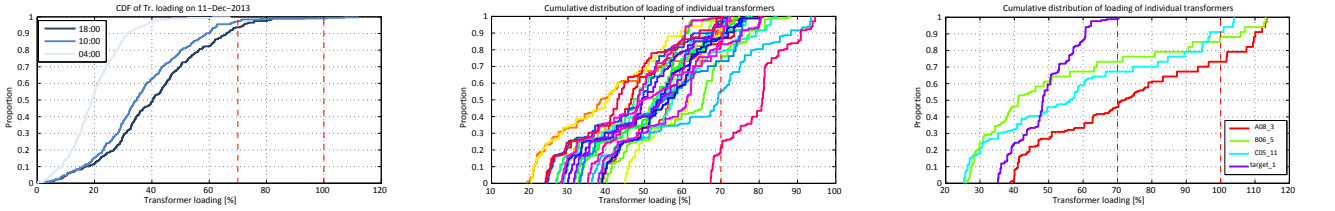

(a) CDF of different time instant (b) CDF of heavily loaded transformers along time (c) CDF of overloaded transformers and the selected transformer T_target_1

Figure 7: Cumulative distribution of line loadings in a peak period in December 2013.

[4] The LV grid areas are modelled as lumped loads in the grid model. Hence, the voltage drop in LV grid areas will not be considered in our study

Figure 7 shows the loading of MV/LV transformers in the grid model within the chosen peak period in December 2013. Heavily loaded conditions occurs on 26 transformers in this period, among which 3 transformers has been through overloading. Figure 7 (a) shows the cumulative curve of the loading values of all the transformers at three different time instants on 11-12-2013. 4:00 is the time instant that lines are most lightly loaded. 10:00 and 18:00 are the observed morning and evening peaks through a day. 90% of the population are loaded at or below 31%, 60%, and 67% of their capacity [kVA] respectively. Figure 7 (b) presents cumulative distribution of the transformer loading values in the simulated period of the transformers, which exhibit heavy loading conditions. In Figure 7 (c), we can find the cumulative distribution curves of the loading factor of the overloaded transformers, and a particular one that is selected for the further analysis. Considering the load yearly increase and the sharing of electric vehicles and heat pumps, there is very little space for these 3 transformers to shift and reshape the load profile. However, the loading condition is severe in the selected transformer, 'T_target_1' (in feeder C04), but could be restricted within the safe region if applying demand response. Hence, it is selected as the representative MV/LV transformer for the further analysis.

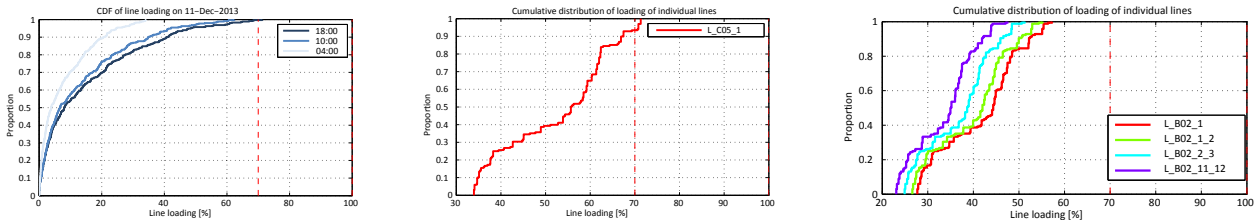

(a) CDF of different time instant (b) CDF of heavily loaded line along time (c) CDF of selected lines in B02 feeder

Figure 8: Cumulative distribution of line loadings in a peak period in December 2013.

Figure 8 shows the loading of lines in the grid model. In general, line loading conditions are less critical than the transformer loading. Figure 8 (a) shows the cumulative curve of the loading values of all the transmission lines (cables) at three different time instants on 11-12-2013. 90% of the population are loaded at or below 20%, 36%, and 41% of their capacity [A] respectively. There is only one heavily loaded line in the grid. It is the first line in Feeder C05. The loading of the line is over 70% of its capacity in approximately 7% of the simulated period (Figure 8 (b)). By sorting the lines with their loading factors, it is identified that the loading of selected lines in Feeder B05 are severe but not extremely critical (Figure 8 (c)). The most loaded conditions lie in 45% – 55% of their capacities.

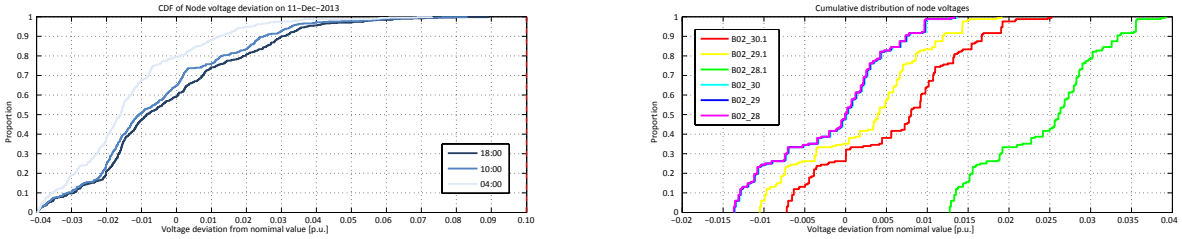

(a) CDF of different time instant (b) CDF of selected nodes in B02 feeder (LV & MV)

Figure 9: Cumulative distribution of node voltage deviations in a peak period in December 2013.

In Figure 9 (a), the voltage deviations (positive value: drop, negative value: rise) from the nominal values of all the nodes are illustrated given certain time instants. Meanwhile, the cumulative curves of voltage deviations along time of certain nodes are plotted in Figure 9 (b). It can be seen that voltage deviation conditions are not as critical as transformer loading. The largest voltage drop in MV grid occurs at 18:00 11-12-2013 at the last node in Feeder C05, which is 3.3%

of the nominal value, while the largest one in LV occurs at the same time in Feeder C04, which is 7.3% of the nominal value. By sorting the nodes with their voltage deviations, it is identified that the voltage of selected nodes in Feeder B05 are comparably severe but not extremely critical (Figure 9 (b)). Considering all criteria, Feeder B05 is selected as the representative MV feeder for the further analysis in Section 4.

Under the transformer T_target_1, 5 types of customers compose the load consumption in the load YL_target.1. Table 2 lists the portions of all types. Table 2 shows, under Node target.1, the power factors of the loads varies from 0.981 to 0.995, and the difference between apparent power and active power is very little. Subsequently, for the analysis of T_target_1, active power is used to approximate the overall power flowing through the transformer. The rated power of the transformer is 400 kVA. The detailed information of the transformer is presented in Figure 10. In Section 2.2, the details about different loads will be presented.

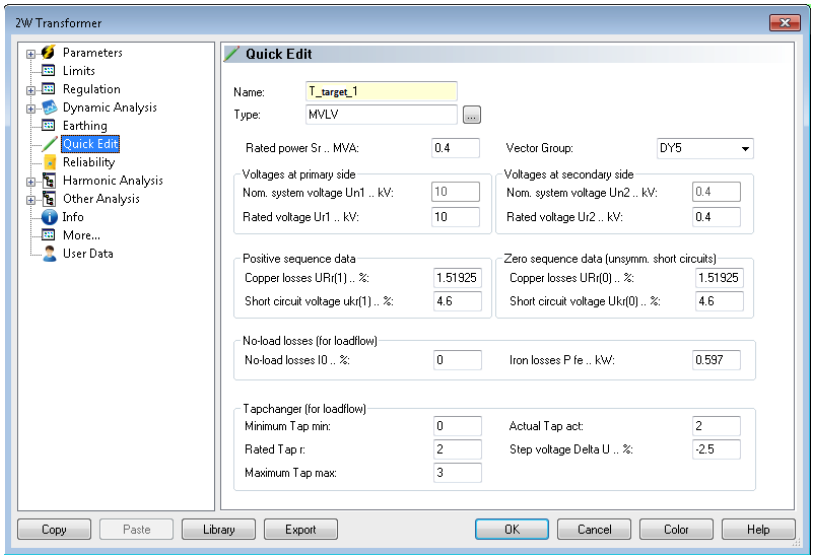

Figure 10: Detailed parameters of MV/LV Transformer T_target_1.

Annual Consumption [MWh]				1230.582
Portion	**Category**	α	β	**cosϕ**
0.50%	DETAILHANDEL	0.21	0.85	0.981
31.10%	ELVARMEBOLIG	0.27	0.56	0.995
7.80%	ENFAMILIEHUS_U_ELVARME	0.28	1.25	0.995
0.40%	FAELLESFORBRUG_LEJLIGHED	0.16	2.3	0.995
60.20%	FRITIDSHUSE	0.24	3.1	0.995

Table 2: The property details in the load YL_target.1 under the transformer T_target_1 .

Feeder B02 contains 31 nodes, including 26 small customer groups (i.e., connecting point of MV and LV grid) and 14 large customers. Figure 11 shows the current measurement in the week from 10-12-2012 to 16-12-2012. From the figure, we can tell there are two peaks during a day, where the most critical point is 178.8 A at 18:00 13-12-2012. The largest voltage deviation from the nominal value appears at the same time at 18:00 13-12-2012. It is 5.3% at MV level and is 8.3% at LV side (without considering the voltage drop in LV feeders).

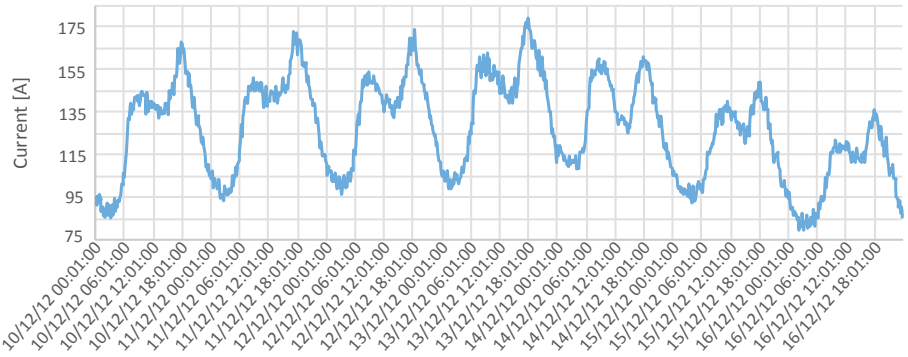

Figure 11: Current measurement of feeder B02 from 10-12-2012 to 16-12-2012.

2.1.3 Model rebuilt and simulation platform

The grid model consist of 19 radial feeders, which have junctions with each other by normally opened breakers. The load flow calculation in the original grid model takes many iterations to converge. It takes time to look inside the grid and to find the information needed. Thus, the feeder model of B02 is rebuilt by exporting the partial information related to the feeder to a new project in NEPLAN (see Figure 12). To insert the simulated electric vehicle charging patterns and heat pump consuming patterns, some text files with certain format are used to exchange the information between Matlab and NEPLAN. New loads named as 'LD_'+(node ID) are used to duplicate the additive load patterns from Matlab.

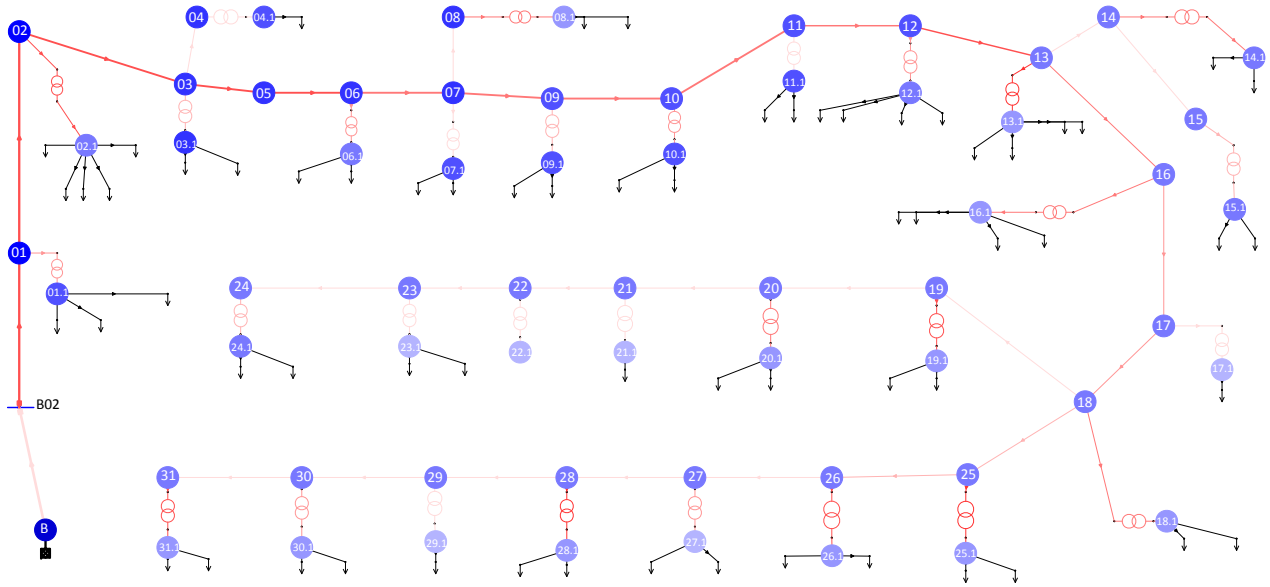

Figure 12: The rebuilt B02 feeder in NEPLAN with load flow information.

2.2 LOAD MODEL

As previously mentioned, two types of loads are specified in the grid model: large customer (PQ load) and small customer (EC load).

2.2.1 LARGE CUSTOMERS (PQ LOAD)

The naming of large customers start with "LO", which is followed by the corresponding node ID and a number string (e.g., "LO_2000.1_123456789012345678" represents a large customer load under node 2000.1). In the grid model, there is no particular time series defines the consumption curve. Both active power and reactive power keep constant for all the time as predefined value.

2.2.2 SMALL CUSTOMERS (EC LOAD)

This load type represents small customers that can be categorized into 27 predefined load categories by DONG Energy. is an example of this type. The naming of small customers start with"YL", which is followed by the corresponding node ID (e.g., "YL_2000.1" represents a small customer load under node 2000.1). Each load category has its own load templates covering the entire period of a year. A year is fragmented into 22 periods, during each of which a particular daily scaling factor curve is assigned. These 22 periods reflect the annual variation of the load affected by the ambient environment (e.g., weather condition and temperature) and special periods (e.g., Christmas holiday and autumn holiday). For each period, weekday curves and weekend curves are further separated into 2 templates. The nominal scale is the maximal peak load P_{max} [kWh] that is derived from the Velander formula and the estimated annual consumption as described in footnote 2. A long term estimate is represented by the yearly increase of the annual consumption. The increasing rate is 1.6% per year. The estimated energy consumption increase is 11.7% in 2020 and 30.9% in 2030 comparing to 2013. Figure 13 shows the load profiles (without considering electric vehicles and heat pumps)under node target.1 on a normal December weekday, and on a normal July weekday respectively in 2013, 2020, and 2030. The load profiles in 2013, 2020, and 2030 are marked with ●, ♦, and ▲ on the curves. Details are presented in Appendix A.

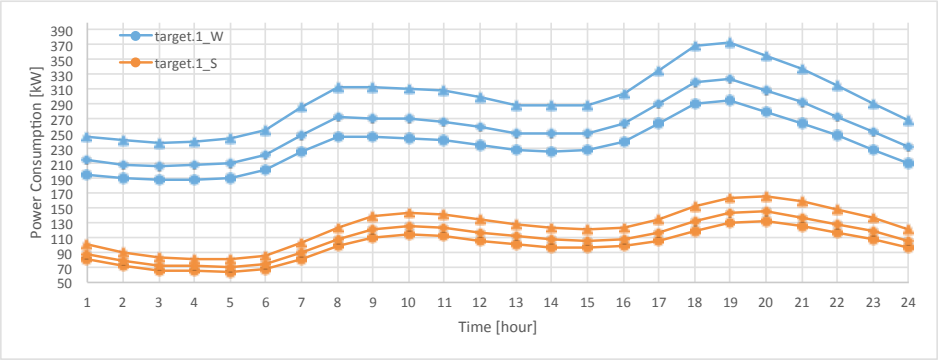

Figure 13: Load profiles (without electric vehicles and heat pumps) under node target.1 in winter (blue) and in summer (orange) in 2013, 2020, and 2030.

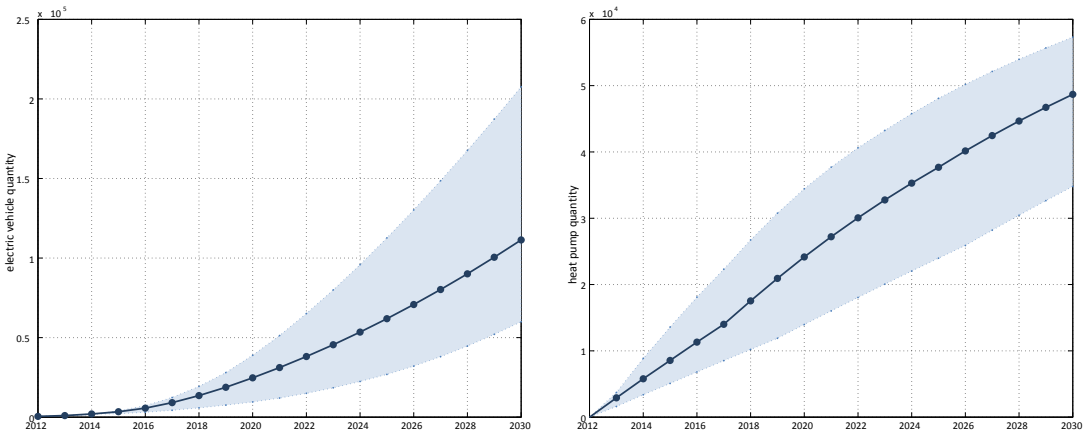

(a) Penetration estimation of electric vehicles

(b) Penetration estimation of heat pumps

Figure 14: Penetration estimation curves (base, low, and high scenarios) in DONG's grid.

The number of electric vehicles and heat pumps are associated with certain categories of small customers, and the yearly penetration level estimated for the future. According to the future estimate from DONG Energy A/S [18], electric vehicles are anticipated to be integrated with customer type 'ENFAMILIEHUS_U_ELVARME' and 'ELVARMEBOLIG'. The numbers of heat pumps placed in each nodes are associated with the numbers of 'Burde_Være_Olie_huse' (i.e., houses with oil-fired burners). The penetration levels of electric vehicles and heat pumps are illustrated in Figure 14 provided by DONG Energy A/S [18]. This study aggregates the power consumption of the populations of electric vehicles and heat pumps are modelled with a bottom-up approach, and combining their individual power requirements and human behaviour constraints. Thus, the penetration numbers at each node in the grid are rounded to the nearest integers. The numbers of DERs associated with individual nodes in 2013, 2020, and 2030 are listed in Appendix A.

2.3 TYPES OF DERS IN THE PORFOLIO

As introduced in Section 1, electric vehicles and heat pumps are chosen in this task as the potential DER units who serve flexible demand to power system services. They are associated with certain types of small customers, as explained in Section 2.2.2. The models to simulate the individual DER behaviours will be discussed here.

2.3.1 ELECTRIC VEHICLE MODEL

Electric vehicles are modelled as portable batteries, of which the availability (i.e., in this study, available when parking at home) and the state of charge (SOC) are determined by owners' driving patterns. In our study 'vehicle to grid' concept is not considered (i.e., no bi-directional power flow). The charging and discharging (to convert chemical energy to mechanical energy of motors) characteristics of batteries are simplified as defined power value regardless SOC conditions. The maximal charging rate $P_{rate,max}$ is 3.7 kW. The charging efficiency η_1 is approximated as 0.9, and the consumption efficiency η_2 is approximated as 0.87 [21]. The energy use $conv_e$ is approximately 32.5 kWh / 160 km [22]. The driving patterns are approached by randomly selecting driving records of vehicles in Denmark during workdays in a database [23] as sub-samples which represent the entire driving patterns in the database. Three parameters are used to capture the

patterns: time arriving at home, time leaving home, and driving distance in this period. The daily driving distance is limited within 160 km. Short at-home period (i.e., less than 2 hours) are ignored in the record. By having the above-mentioned properties, the behaviours of electric vehicles are captured in the model. Figure 15 shows the behaviour of a single electric vehicle. The control variables of electric vehicles are determined as whether it is allowed to charge (binary), and the charging rate (continuous) (see Figure 16).

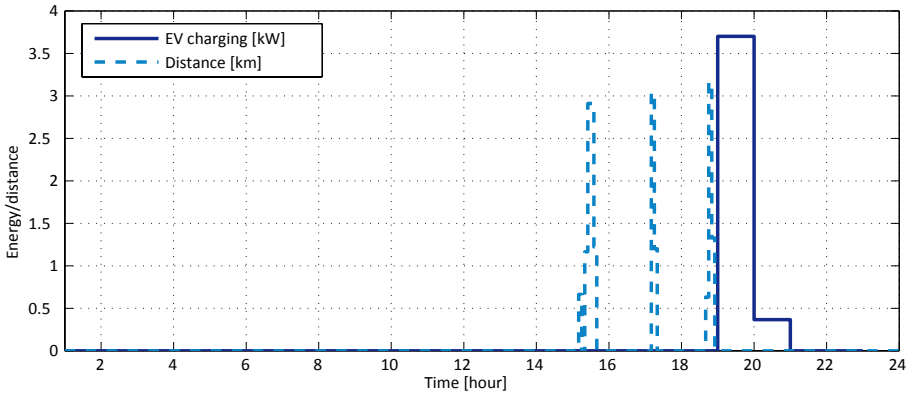

Figure 15: The behaviour of a single electric vehicle.

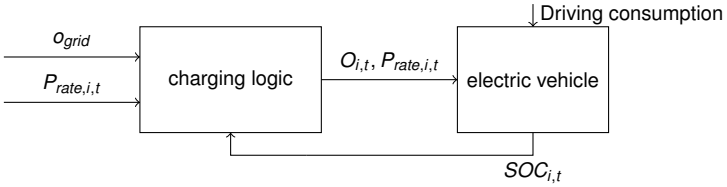

Figure 16: Electric vehicle model diagram.

The model can be explained by the following equations:

$$\begin{aligned} P^{e2m}_{i,t} &= \frac{1}{\eta_2} D_{i,t} conv_e, \\ P^{ch}_{i,t} &= O_{i,t}\eta_1 P_{rate,i,t}/E_{battery}, \\ SOC_{i,t+1} &= SOC_{i,t} + P^{ch}_{i,t} - P^{e2m}_{i,t}, \\ SOC_{i,0} &= SOC_{initial}, SOC_{i,t_{leave}} = 100\%, \\ 0 \leq P_{rate,i,t} &\leq P_{rate,max} P_{ev,t} = \sum_i O_{i,t} P_{rate,i,t}. \end{aligned} \tag{1}$$

where, $P^{e2m}_{i,t}$ [kW] is consumed power of EV i at time t, which depends on the driving distance $D_{i,t}$ [km] in this interval; $P^{ch}_{i,t}$ [kW] is the stored power and $E_{battery}$ [kWh] is the battery capacity; the customer behaviours are captured by the initial SOC $SOC_{initial}$ and the battery should be fully charged before leaving home, as indicated by $SOC_{i,t_{leave}}$. $P_{ev,t}$ [kW] is the aggregated electric vehicle consumption. The binary state $O_{i,t}$, indicator for charging is calculated by

$$\begin{aligned} O_{i,t} &= idx_{full} \cdot idx_{home} \cdot idx_{order}, \\ \text{where, } idx_{order} &= 1 - (1 - o_{grid})(1 - o_{owner}). \end{aligned} \tag{2}$$

where, idx_{full} indicate whether the battery is full, idx_{home} indicate whether the vehicle is at home, and idx_{order} indicate whether it is allowed to charge. idx_{order} is 'true' when either the the controller allows or the owner must charge.

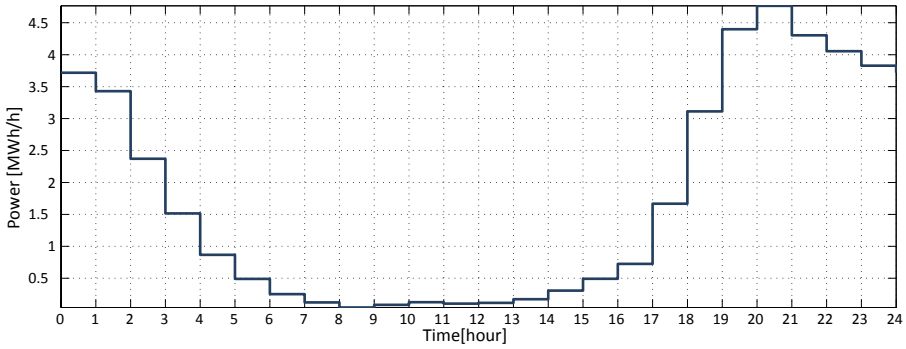

Figure 17: The total energy consumption of a fleet of electric vehicles at the amount of 4673.

Figure 17 illustrate the the energy consumption of a large population of electric vehicles (this number refers to the penetration in 2030 in the analysed grid area, see Table 3 in Section 3), assuming electric vehicles start to charge as soon as they arrive at home. Based on such model, the kick-back effect will be analysed when curtailment is added into the management.

2.3.2 SPACE HEATING SYSTEM USING HEAT PUMP

The space heating system model consists of two parts: heat pump (thermostat), and the associated house (the energy buffer) as shown in Figure 18.

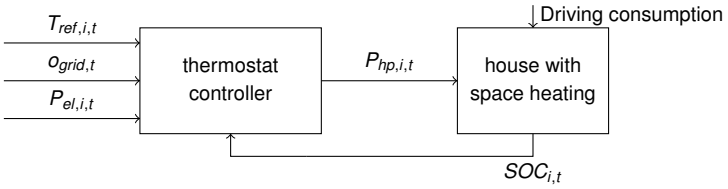

Figure 18: Heat pump model diagram.

The heat pump circulates a refrigerant and transmit the energy from one volume to another in a closed loop, energized by electricity. Coefficient of performance (COP) indicates how efficient the heat pump uses electric power to heat the house. It varies depending the outdoor temperature or the temperature difference between indoor temperature and outdoor temperature (or underground temperature). COP in conjunction with the temperature difference between indoor and outdoor is investigated in [24] and [25]. The performance of COP is thus implemented as illustrated in Figure 19. COP is larger if the temperature difference is larger. COP is derived as follows.

$$COP = \frac{P_{hp}}{P_{el}} \tag{3}$$

where P_{hp} is the heating power generated from heat pump, and P_{el} is the actual electric consumption from the power system.

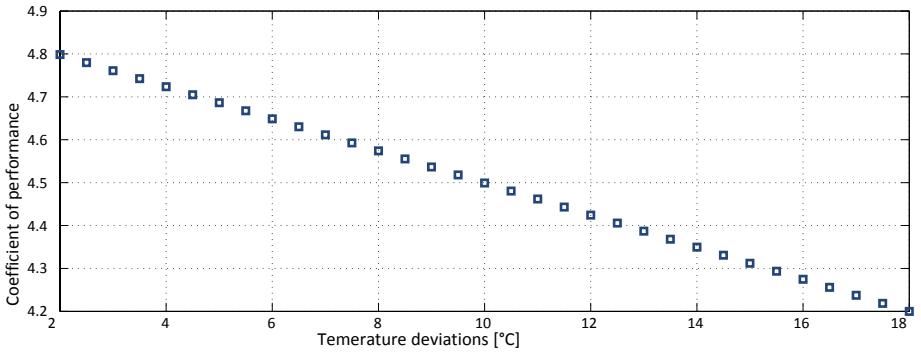

Figure 19: Scatter plot of the relation between COP and temperature difference.

According to [26], the size of heat pump $P_{hp,rated}$ is defined as 3 kW, and the capacity of auxiliary heating resister P_{res} is 6 kW. If COP is less than a threshold value, the heating resister will start to generate heat. The start-up consumption spike is defined as 1 kW lasting 10 minutes. Each building of the population is equipped with a thermostat which controls the indoor temperature according a set-point T_{ref}. The threshold of the thermostat controller is $\pm 1°$C and it is assumed the same for all the buildings.

A simplified first order house model is used. The value of indoor temperature T_{in} [°C] represents the amount of energy stored in the house. It is affected by the outdoor temperature T_{out} [°C] because the insulation of the house could hardly be perfect, and energy would flow through wall, ceiling, floor, etc. Meanwhile, the heating energy input from the heat pump system P_{hp} [kW] would compensate the loss of thermal power. The discretized expression of the model using k as the sample time is expressed as

$$\begin{aligned} T_{in,j}(k+1) &= A_j T_{in,j}(k) + B_{0,j} P_{hp,j} + B_{1,j} T_{out,j}, \\ A_j &= 1 - \frac{1}{RC_j},\ B_{0,j} = \frac{1}{C_j},\ B_{1,j} = \frac{1}{RC_j}. \end{aligned} \tag{4}$$

where, the value of the thermal heat resistance R [°C/kW] is kept constant across the population, the heat capacitance C_j [kWh/°C] is proportional to S_j, the size [m^2] of the building j. S_j of each building follows a Gamma distribution and it is given in Equation 5 [27]. In [27], the distribution in Equation 5 and the associated parameters k, θ have been obtained performing a statistical analysis of the size of the class of buildings from the data provided by Danish National Register of Buildings (BBR) [28]. The histogram of 10^5 houses realizations is shown in Figure 20. The initial indoor temperature (at steady state) follows uniform distribution.

$$S_j \sim \Gamma(k, \theta) \quad \text{with } k = 22.35 \vee \theta = 1/6.71 \tag{5}$$

Given the above features, the cluster of houses of same type but with slightly different characteristics are modelled. The simulation results for a single heat pump is presented in Figure 21. The temperature is taken from the measurements in Power Flexhouse January 2013 [29].

By having a large group of heat pumps, the variations of consumption is smoothed out. Figure 22 shows the power consumption of a group of heat pumps at quantity of 40 and of 2975 (this number refers to the penetration in 2030 in the analysed grid area, see Table 3 in Section 3). The variation is approximately 10% and 3% respectively of the average

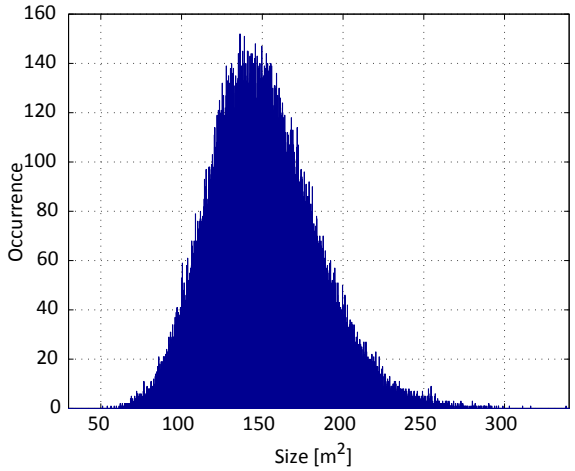

Figure 20: Stochastic realizations from the Gamma distribution in Equation 5. [27]

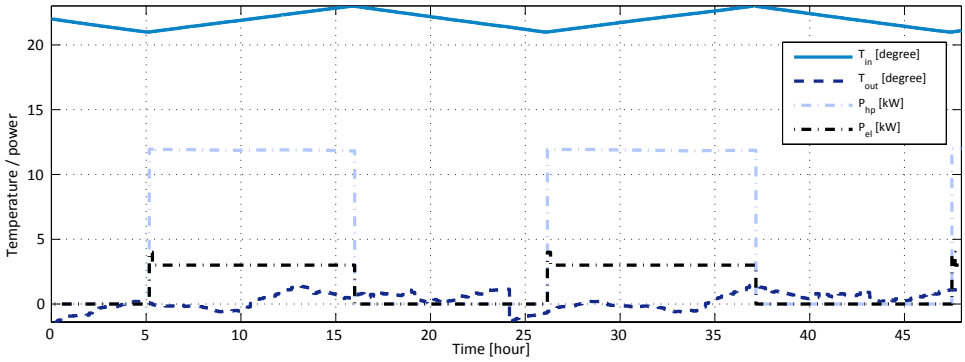

Figure 21: Simulation results of a single heat pump running for two days in winter.

steady state consumption. The potential control variables of heat pumps are whether the heat pump is allowed to consume (binary), the room temperature set-point (continuous), and the heating rate (continuous).

2.4 CONTROL STRATEGIES

To investigate the kick-back effects after activating flexible demand, several control strategies are defined in this subsection. To identify different factors that may affect the occurrence and the size of kick-back effect, we select several simple methods (off-line), which have larger opportunities to be implemented in practice. The control strategies can be applied for ancillary services (e.g. secondary reserve), and for distribution grid operation (e.g., congestion management, and peak shaving). In applications of flexible demand, e.g., for voltage regulation in grid with large penetration of photovoltaic, solar radiation, and the ambient temperature should be considered in provoking the control algorithms.However, in this report, we will not discuss much about the services and applications, but focus on the kick-back effects themselves.

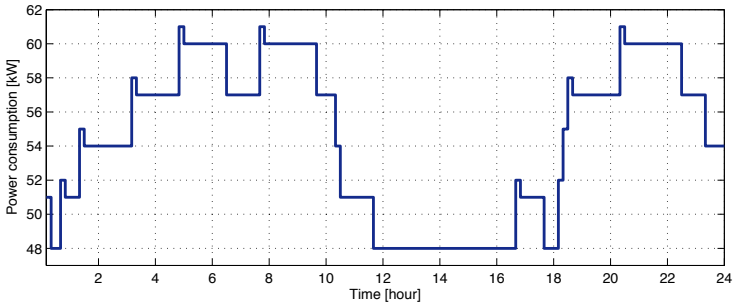

(a) 40 heat pumps

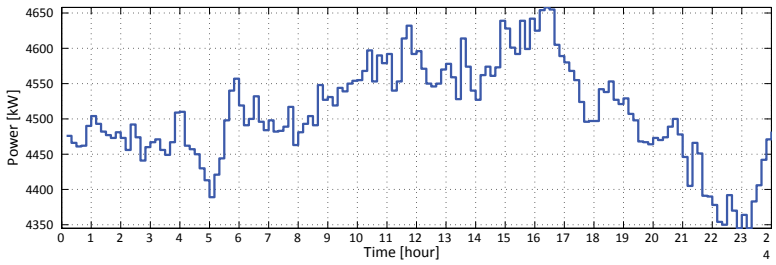

(b) 2975 heat pumps

Figure 22: . Simulation results of power consumption of a group of heat pumps in winter time.

2.4.1 STOP CONTROL

As the simplest version of direct control, stop control (illustrated in Figure 23) is used in the study. The DERs respond as what is requested as long as the quality of their primary services are guaranteed (see Figure 24). In the control loop, the remote controller can determine the inputs individually, and have the possibility to receive messages from individual DERs. Two strategies are investigated:

- **Partial stop** – curtailing part of the available controllable units to fulfil the objectives unless the local constraints are violated. The signals are randomly assigned to the available units. The control signal is determined by the power limit, the current process states, and the size of available flexibility (contained in the feedback loop).
- **Complete stop** – all the available controllable units are forbidden to consume power during the curtailment period (control period) unless the local constraints are violated.

2.4.2 INCENTIVE-BASED CONTROL

In indirect control method, the incentive/price signal broadcast is sent to the controllable units to influence the load shapes as presented in Figure 26 (a). The units can decide their behaviours based on the incentive signal [5]. A typical signal

[5]The purple circles in DER units represent the individual local responsive control strategies.

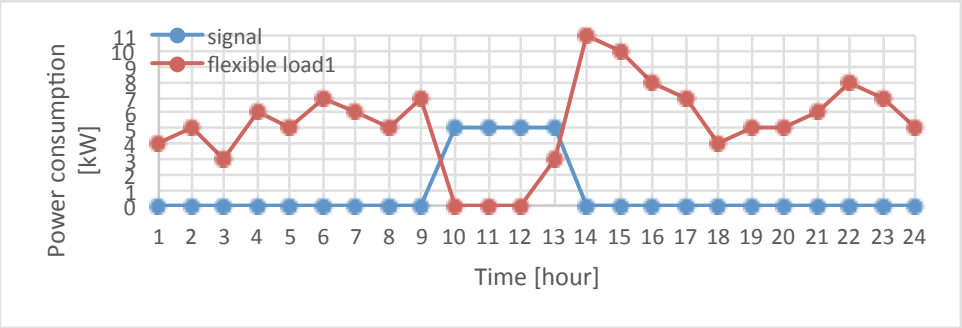

Figure 23: Illustration of stop control applied on an arbitrary load.

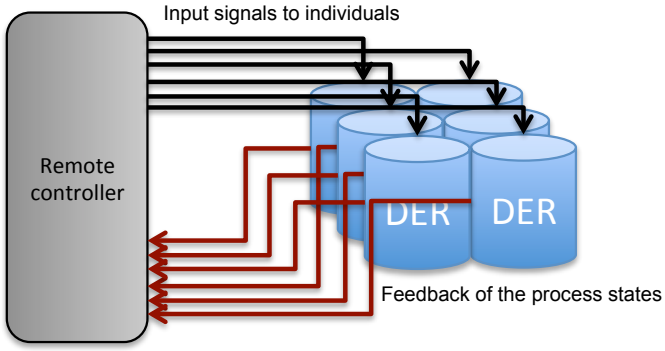

Figure 24: Sketch diagram of direct control method.

curves is used (see Figure 25):

- A spot price curve [DKK/MWh] taken from Nordpool (13 December 2012 DK1).

In this case, the customers have the possibility to react following their preference on power usage. Hence, the reaction may vary. The incentive signal is elaborated by the local responsive control strategies as a function of the incentive signal. The function can be resembled by different forms: threshold values, linear relationship, or a high-pass filter. The controllable variables of DERs can be in different form: binary states, step-wise, adjustable continuously, etc. The block diagram in Figure 26 (b) shows the factors that determine the customer behaviours.

Here lists some local reactive strategies:

- Binary – The consumption of load is completely curtailed when the incentive signal value is above the threshold value;
- Step-wise – The consumption of load is changed when the incentive signal value is in different ranges;
- Continuous – The load consumption is a function of the incentive signal (e.g., droop).

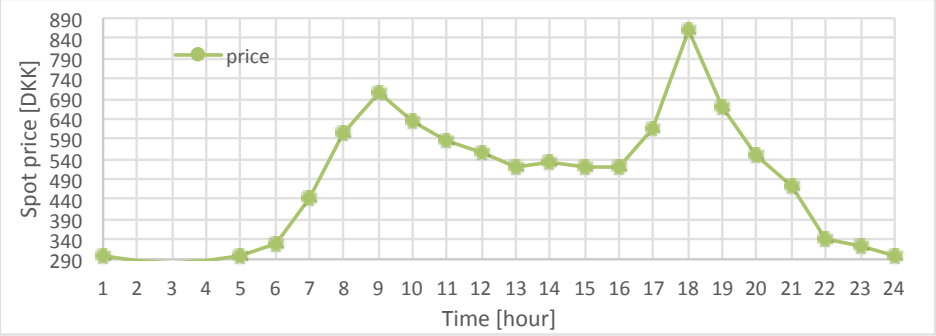

Figure 25: Illustration of stop control applied on an arbitrary load.

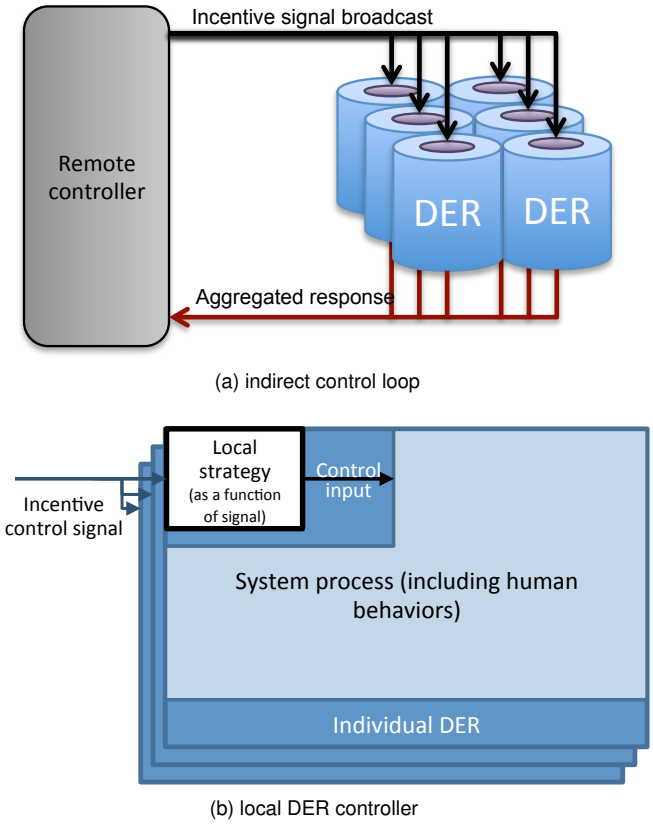

Figure 26: Sketch diagram of indirect control method.

3 SCENARIO DESCRIPTION

To investigate the kick-back effects under different conditions, a scenario space is built with three dimensions. The first dimension indicates the ratio of the flexible load to the total energy consumption, which is an important factor on the size of flexibility and the kick-back load. The second one considers and intend to compare different environment conditions (i.e., winter and summer in our case). The third one is the control strategies that are applied in controlling flexibility. The last dimension is the orientation and focus of the models.

3.1 DIMENSION 1 – PENETRATION LEVELS

Similar to the investigation of the contingency situations, several penetration levels are determined corresponding to years as shown in Table 3. As previously mentioned in Section2.2.2, the quantities defined in the table are calculated by rounding the numbers estimated by DONG Energy [18] to the nearest integers at each node. The purpose is to enable the aggregation of the individual behaviours simulated by the models defined in Section 2.3. The numbers of DERs associated with individual nodes in 2013, 2020, and 2030 are listed in Appendix A.

D1	Electric vehicle					Heat pump				
	Quantity (DONG)	Quantity (grid)	Quantity (B02)	Quantity (target.1)	penetration	Quantity (DONG)	Quantity (grid)	Quantity (B02)	Quantity (target.1)	penetration
Low (2013)	500	2	0	0	∼0%	0	0	0	0	0%
Medium (2020)	24716	3044	75	8	3%	23518	1475	122	5	8%
High (2030)	111356	4672	365	36	10%	47398	2975	242	10	20%

Table 3: Scenario space dimension 1 (D1) – penetration level of electric vehicles and heat pumps.

3.2 DIMENSION 2 – SEASON CONDITIONS

Among 22 periods (during each of which, the load profiles of different small customer category are defined) over a year, two boundary cases are selected to reflect the seasonal variations: 1 normal weekday in July (i.e., summer) and a normal weekday in December (i.e., winter). Figure 13 shows the difference between these two seasons. Correspondingly, we assume that the space heating system is not used in the summer cases (the water heating behaviour is ignored because too random to capture).

3.3 DIMENSION 3 – CONTROL STRATEGIES AND CONTROLLABLE INPUTS

Selected numbers of control strategies from the discussions in Section 2.4 are applied to the further simulations and analysis (detailed descriptions are presented in Section 2.4):

1. **Control strategy**
   (a) Stop control
      i. Complete stop: all the DER units are not allowed to consume power within certain periods

ii. Partial stop: part of the DER units are not allowed to consume power or the power limit is curtailed within certain periods.

(b) Incentive-based control

i. Threshold value control: the control action is triggered when the control signal is above the threshold value.

ii. Droop control: the controllable inputs are in a linear relation with the control signal.

2. **Controllable inputs**

(a) Electric vehicle

i. P_{rate}: the charging rate

ii. o_{grid}: the admission from the remote controller

(b) Heat pump

i. T_{ref}: indoor temperature set-point

ii. o_{grid}: the admission from the remote controller

iii. P_{el}: electric power consuming rate [6]

3.4 DIMENSION 4 – ORIENTATION AND FOCUS

To have different level of detailed analysis, the last dimension in the scenario tree is orientations and focuses. In this task, we will emphasis on a MV/LV transformer T_target_1 and the associated loads, a MV feeder B02 and all its belongings, and a large fleet of DER units without looking at specific grid infrastructure.

In the first group, we mainly look at how different factors can affect the size and the shape of the kick-back effects. The simulations in support of the discussion around kick-back effects is obtained by executing a specific control set-up. The dynamic performance associated with the DER portfolios will be visualized to facilitate the understanding of this phenomenon. The loading of the transformer is mainly investigated in the second group. The bottleneck filtering and the observations of line loading and node voltage are conducted in the last group.

3.5 SUMMATION OF THE STUDY CASES

Based on the above dimensions, a scenario tree is further developed to narrow down the number of cases in Section 4. Figure 27 and Table 4 sum up the 4 dimensions and the corresponding cases. Two typical days are selected, a normal working day in December, and a normal working day in July (as a comparable case). Three penetration levels are investigated (2013, 2020, and 2030). Different control methods are applied in the simulations to look at the kickback effect and its size. In addition, the state of a MV feeder, a MV/LV transformer under and after the activation of control strategies are investigated. The loading of grid elements, the voltage deviations during and after peak hours are observed and compared. Moreover, the sensitivities of the kick-back size is studied by simulating a large population of DER units. Hereby, all four dimensions are included in this tree.

[6] not yet implemented

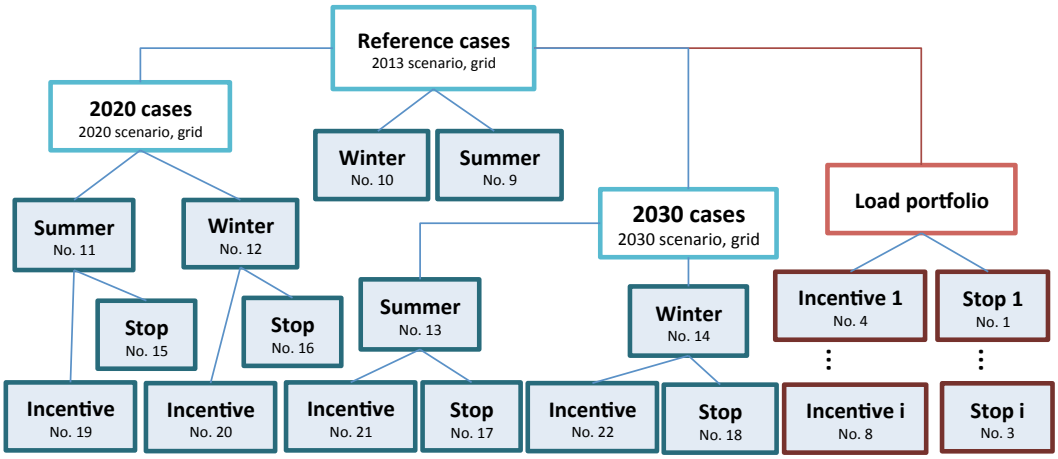

Figure 27: Scenario tree with the numbering of cases.

Case	D1	D2	Method	Input	Tr.	Feeder	DER fleet
1	–	–	stop, complete	o_{grid}, o_{grid}	–	–	X
2	–	–	stop, partial	o_{grid}, o_{grid}	–	–	X
3	–	–	stop, complete	T_{ref}, –	–	–	X
4	–	–	price, threshold	o_{grid}, o_{grid}	–	–	X
5	–	–	price, function	o_{grid}, o_{grid}	–	–	X
6	–	–	price, threshold	T_{ref}, –	–	–	X
7	–	–	price, function	T_{ref}, –	–	–	X
8	–	–	price, function	–, P_{rate}	–	–	X
9	2013	summer	–	–	X	X	–
10	2013	winter	–	–	X	X	–
11	2020	summer	–	–	X	X	–
12	2020	winter	–	–	X	X	–
13	2030	summer	–	–	X	X	–
14	2030	winter	–	–	X	X	–
15	2020	summer	stop, complete	o_{grid}, o_{grid}	X	–	–
16	2020	winter	stop, complete	o_{grid}, o_{grid}	X	X	–
17	2030	summer	stop, complete	o_{grid}, o_{grid}	X	–	–
18	2030	winter	stop, complete	o_{grid}, o_{grid}	X	X	–
19	2020	summer	price, threshold	o_{grid}, o_{grid}	X	–	–
20	2020	winter	price, threshold	o_{grid}, o_{grid}	X	X	–
21	2030	summer	price, threshold	o_{grid}, o_{grid}	X	–	–
22	2030	winter	price, threshold	o_{grid}, o_{grid}	X	X	–

Table 4: The summation of study cases in the scenario tree.

4 CASE STUDY AND SIMULATION RESULTS

4.1 SIMULATION OF A LARGE PORTFOLIO OF DER UNITS

In order to clarify the kick-back patterns of different types of DERs, we made the simulations on individual types of DERs. A sensitivity analysis is performed on a homogeneous (i.e., same kind but not same parameters in the models) population of 5000 space heating systems. So as for 5000 electric vehicles' charging profiles. Totally different characteristics are observed on the kick-back load curves in Figure 28. Hereby, electric vehicles and space heating systems are analysed separately.

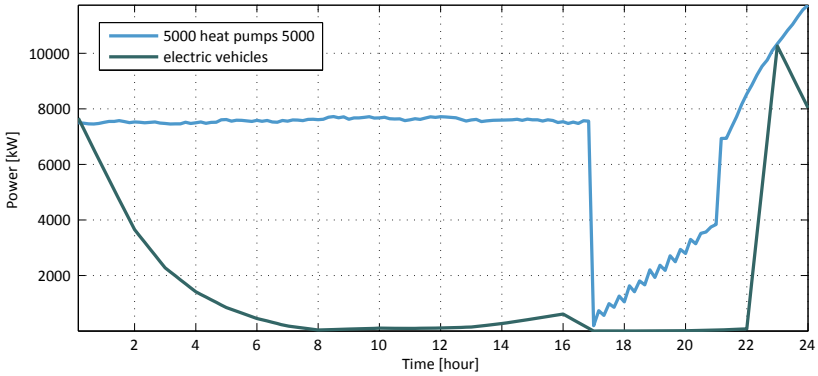

Figure 28: Kick-back effects of controllable thermostat loads and electric vehicles responding to stop control signals (Case1).

4.1.1 THE CONTROLLABLE THERMOSTAT LOAD FLEET

The dynamic behaviours of the aggregated load profile are investigated first (see Figure 29).

The states of individual units are observed in different stages during the dynamics in the following statements. "O" indicates a steady state of the aggregated power consumption before the control signals trigger the event. "O" exhibits the moment that the consumption of heat pumps starts to be curtailed. "O" marks the point when the curtailing period is finished. "O" shows the changes of states after the curtailment. "O" corresponds to the peak of the kickback effect. The consumption value at instant "O" is close to the value as in steady state ("O"). The histograms in Figure 30 shows the distribution of indoor temperatures and on/off states of associated heat pumps across the population. The units moving rightwards are those whose heat pump is "on", and those that pass the right thresholds are switching from "on" to "off". The units moving leftwards are those who switch off the heat pumps. The ones that pass the left thresholds are switching from "off" to "on".

- *Stage* "O" (Figure 30 (a)): The histogram shows that indoor temperatures are uniformly distributed across the population. The number of heat pumps that are "on" is statistically the same as the number of those are "off".
- *Stage* "O" (Figure 30 (b)): The indoor temperature histogram is similar to the one in Stage "O". However, almost all

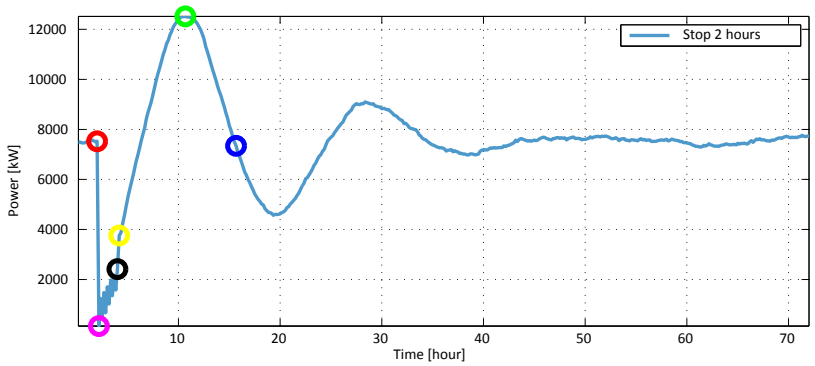

Figure 29: Kick-back effects of controllable thermostat loads responding to 2-hour stop control signals (Case 1).

the units are requested to turn off their heat pump to curtail the consumption. Only few heat pumps are on in order to keep the indoor temperature within the comfort thresholds.

- *Stage* "O" (Figure 30 (c)): The on/off state histogram is similar to the one in Stage "O". Slightly more units turn on the heat pumps to maintain the quality of their primary services. The indoor temperatures of a large population of buildings are around the lower threshold value because limited consumption is allowed to consume.
- *Stage* "O" (Figure 30 (d)): After the curtailing period, the units can follows their regular routines. More heat pumps are turned on, and less units have indoor temperature around the lower boundary (the normal states start to resume).
- *Stage* "O" (Figure 30 (e)): The histogram of the indoor temperatures shows that the temperatures are more evenly distributed. However, there are more units moving rightwards than ones moving leftwards. Most heat pumps are in "on" states, and thus the peak of kick-back effect comes at this moment.
- *Stage* "O" (Figure 30 (f)): here the aggregated consumption is close to the same value as at steady state (Stage "O"). However this situation does not result in a equilibrium point because the flow of units passing the right threshold value does not always equal the flow to the opposite side. By comparing the the histograms in Figure 30 (d), (e) and (f), it is noticeable that a "wave" is moving rightwards, hence composed by units that are heating up.

The oscillations are damped eventually, and the states of the population come back to steady state (Figure 31). The histograms shows that the indoor temperatures resemble a uniform distribution. The numbers of "on" and "off" heat pumps are almost equal.

Three control strategies are applied: complete stop (Case 1), partial stop with 500 kW curtailment (Case 2), and partial stop with 3000 kW curtailment (Case 2).

Figure 32 shows the aggregated load profile of 5000 heat pumps when applied complete stop control strategies. The binary state $O_{j,t}$ is the controllable input for building j at time t. The control strategy is thus formulated as:

$$O_{j,t} = \begin{cases} O_{grid,t} * O_{j,t}^{orig} & \text{if primary requirement is fulfilled} \\ 1 & \text{otherwise} \end{cases} \quad (6)$$

where, $O_{j,t}^{orig}$ is the original state that follows the thermostatic cycles.

During the stop period, the power consumption increases gradually to avoid the violation of the local primary constraints. Since there is no modification of the temperature set points, the flexibility is limited. If the curtailing period is long (e.g., 10

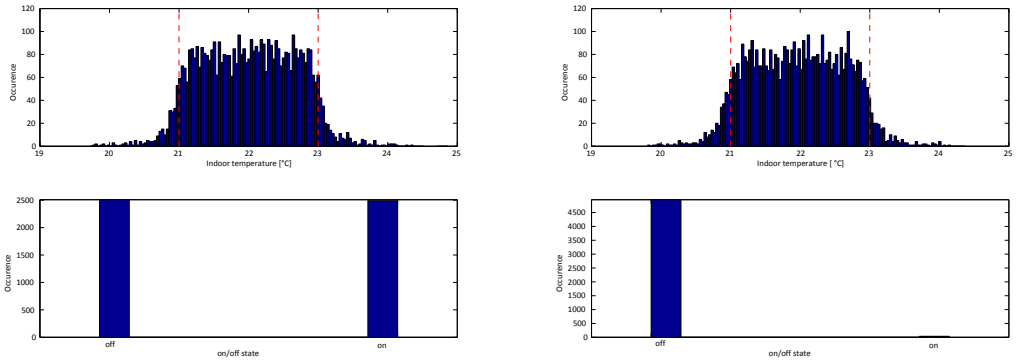

(a) stage "O"

(b) stage "O"

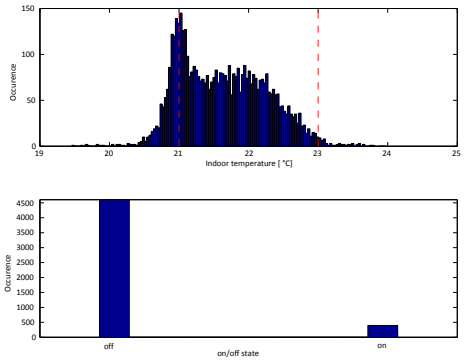

(c) stage "O"

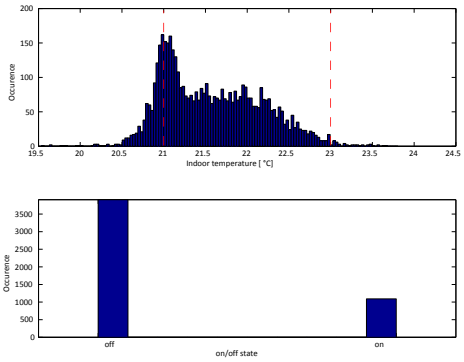

(d) stage "O"

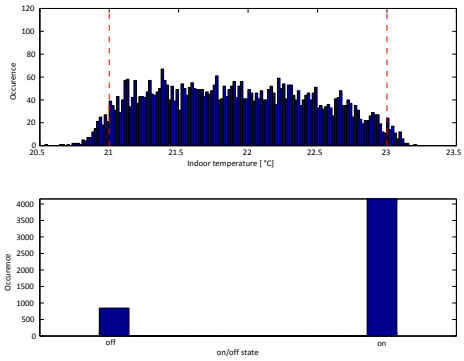

(e) stage "O"

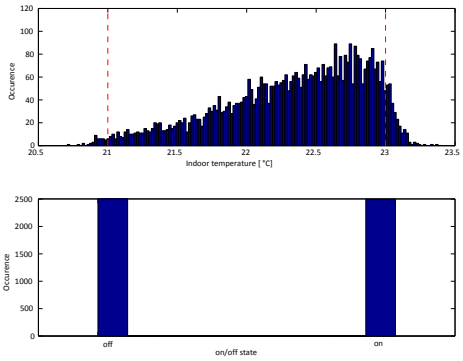

(f) stage "O"

Figure 30: Indoor temperatures and on/off states distributions.

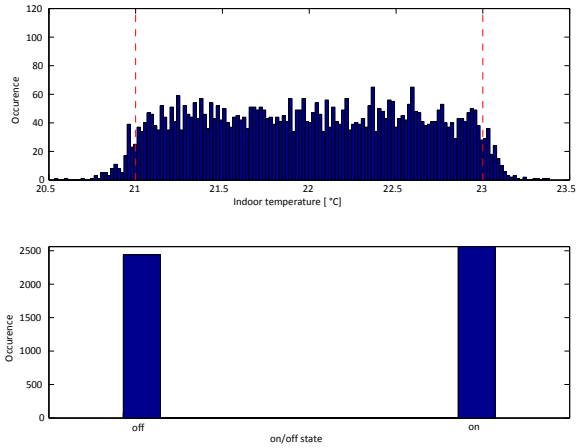

Figure 31: Indoor temperatures and on/off states distributions when back to steady state.

hours), the consumption during the curtailment will be the same or even higher than the steady state consumption. The peak introduced by kick-back effect may saturate (i.e., all the heat pumps are turned on, see the yellow curve in Figure 32). The little spikes are due to the modelled additional start up power.

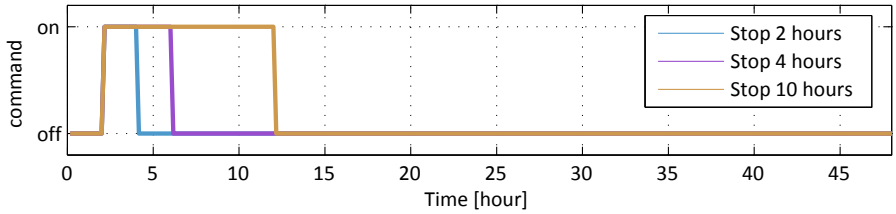

(a) control command O_{grid}

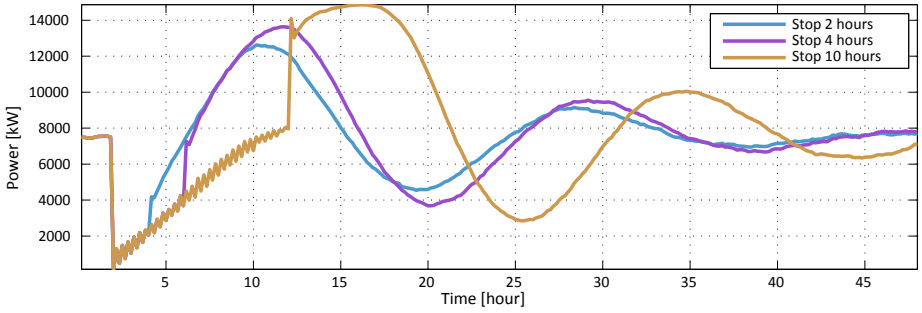

(b) load profiles

Figure 32: Case 1: 5000 heat pumps applied complete stop control strategies (on/off states as control inputs).

In Case 2 (partial stop case), thermostat controls in heat pumps are randomly selected. By knowing the current on/off states, and the corresponding indoor temperature of individual houses, the consumption in the next control time instant

can be estimated. This value determines the number of houses to be curtailed in the next control time instant. Because the control inputs for the houses in the current state have impact on the following period, the number of houses, which receive 'off' commands, is not a constant value, but is varying considering the estimated deviation from the last time step. The simulation results in Figure 33 shows that the oscillation frequency depends on the nature of the controllable load, and effect of external inputs (e.g., outdoor temperature), but not much on the formulation of commands. The largest peak occurs in 6 hours post the curtailing period. The size of the kick-back peak is depending on the amount of curtailed energy.

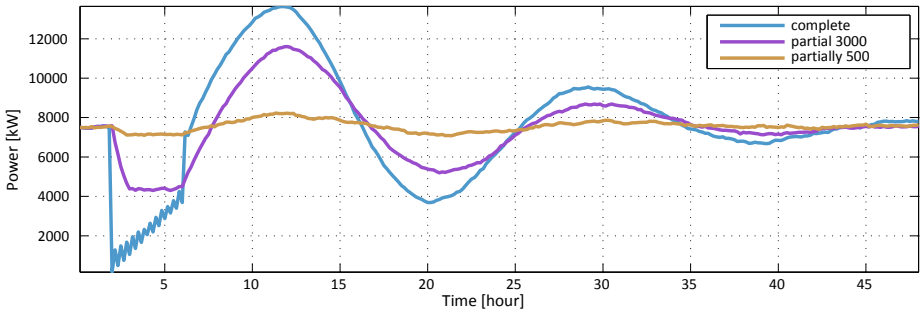

Figure 33: The overall load profiles of 5000 heat pumps applied different stop control strategies (Case 1 and Case 2).

Another noticeable phenomenon is that the oscillation is added on a step in Case 1, while there is not such step in Case 2. The reason is that in Case 1, some thermostat controllers remains the indoor temperature at their lowest boundary. This population start to run in a full load to resume the temperature back to the set-point after the curtailing period. However, there is very little accumulation in Case 2. Less houses are with the temperature hitting the lower boundary (only the houses with margins are chosen to curtail) in Case 16, because the availability and the size of flexible load is respected in the partial control strategies (i.e., the states are sent to the remote controller and considered when making decisions).

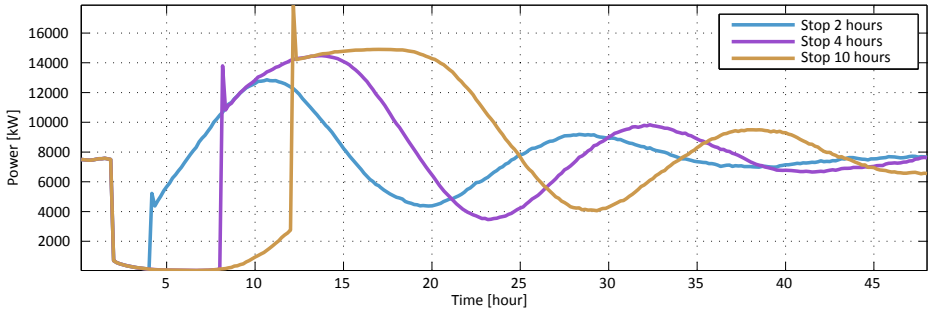

Figure 34: The overall load profiles of 5000 heat pumps applied complete stop control strategies with temperature set-points as control inputs (Case 3).

Figure 34 shows the simulation results when using temperature set-points as control inputs of the heat pumps lasting various curtailing periods. If the temperature reference is the control variable, the gradually increased consumption during the curtailing period would not come as fast as using on/off states as inputs because of larger lower margin is given in such case. We can see that after 4-hour curtailment, the consumption reaches the same level as the steady state if the on/off states are the control variables, while it takes more than 10 hours if the temperature reference is the control variable. The impulse spikes are larger if the temperature reference is chosen, due to the fact that more houses have lower and equal temperature as the original temperature set point. However, the size of the kick-back peaks are similar.

The kick-back peak of the yellow curve (stop 10 hours) also hit the maximal value, because all the heat pumps are on.

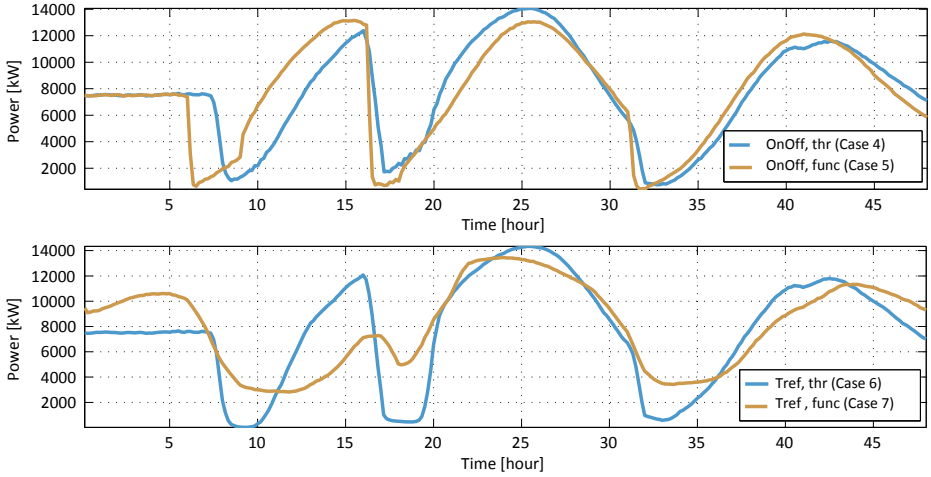

Figure 35: The overall consumption curves of 5000 heat pumps using incentive control signals.

Figure 35 shows the simulation results when the incentive control signal is applied (Case 4, 5 , 6 and 7), where the upper one shows the results using on/off state control and the lower one shows the results using temperature set point control.

In the threshold control strategy, the parameter threshold value $p_{threshold,i}$ [DKK] of individual unit i follows Gaussian distribution as explained in Equation 8. The mean is calculated as

$$\bar{p}_{threshold} = p_{mean} + 30\% \times (p_{max} + p_{min}) + \epsilon \tag{7}$$

where, p_{mean} [DKK] is the mean value of a daily spot price series, p_{max} and p_{min} [DKK] are the maximal and minimal prices correspondingly, and $\bar{p}_{threshold}$ is the mean of the Gaussian distribution. ϵ is a zero mean noise term, which stands for the deviation between the incentive signal and its prediction (i.e., raw market price).

$$p_{threshold,i} \sim \mathcal{N}(\bar{p}_{threshold}, (4.3\% \cdot \bar{p}_{threshold})^2) \tag{8}$$

In Case 5, the raw market price is elaborated by a high pass filter $H_j(s)$ for building j to trace the trend of the price variation. It is defined in Equation 9. The operating state of the heat pump will turn to "off", if $q_{j,t}$ is higher than a fixed value $q_{j,o}$.

$$H_j = \frac{q_j(s)}{p(s)} = \frac{a_j s}{s + \tau_j} \tag{9}$$

where, $a_j = 1$ is the sensitivity factor induced by the variation of price $p(t)$ [DKK], and τ_j is the filter time constant. To deviate the behaviours of the individual units, τ_j is designed to follow Gaussian distribution, which is also related to the size of the building S_j:

$$\tau_j \sim \frac{S_j - 150}{100} + \mathcal{N}(0.5, 0.15) \tag{10}$$

In Case 6, the strategy is similar to Case 4. The control input $T_{ref,j}$ will move to 20 if the price is higher than the threshold price $p_{threshold,j}$. In Case 7, a droop control strategy is utilized (see Equation 11). k_j is the slope of the droop of house j. Maximal temperature set-point $T_{ref,max}$ and minimal set-point $T_{ref,min}$ are defined as 24 and 20 respectively. Thus the temperature set-point is varying following the price signal.

$$T_{ref,j,t} = 22 - k_j * (p(t) - p_{mean}) \quad \text{if} T_{ref,min} \leq T_{ref,j,t} \leq T_{ref,max} \tag{11}$$

By comparing the simulation results of Case 4, 5 and 6, it can be seen that the shapes are similar but some shifts in time can be observed. The kick-back peak values are close to each other. During the curtailing period, the load consumptions are different by using different control inputs, which is identified in the previous discussion. The load curve is unique in Case 7. By have a droop control strategy, the space heating systems are able to over compensate the energy in the building while the price is low.

4.1.2 THE ELECTRIC VEHICLE CHARGING LOAD FLEET

Similarly, we simulated 5000 EVs for the analysis. The charging behaviours are investigated first (see Figure 36). Not as space heating system, there is not dynamic process in the models. However, the charging behaviours is strongly associated with human activities (driving patterns). More restrictive constraints are set to guarantee the quality of primary services.

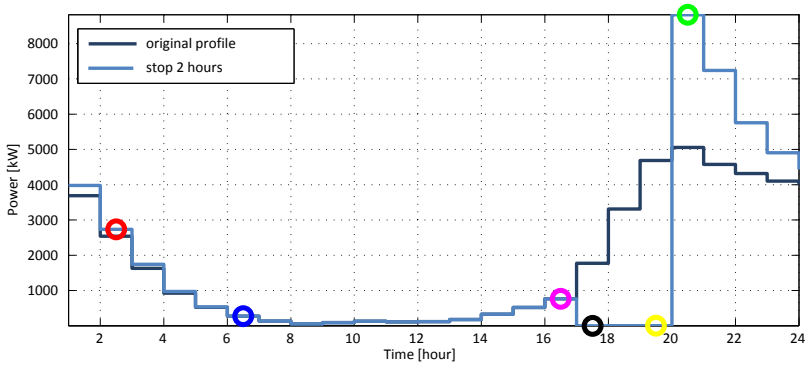

Figure 36: Kick-back effects of charging of electric vehicles responding to stop control signals from 17:00 to 19:00 (Case 1).

The states of individual units are observed in different stages during a day on hourly basis. The curtailment starts from 17:00 and stops at 19:00. "O" indicates the power consumption before the control signals trigger the event. "O" exhibits the moment that the consumption of electric vehicles starts to be curtailed. "O" marks the point when the curtailing period is finished. "O" shows the changes of states after the curtailment. It also marks the time when the kick-back peak appears. "O" corresponds to the early morning charging activities. The consumption value at instant "O" is close to the value as in original load curve ("O"). The empirical cumulative distributions in Figure 37 shows how much energy are required to be charged before the vehicle leave home. The histograms of on/off states indicate how many electric vehicles are being charged at different time instant.

- *Stage* "O" (Figure 37 (a)): The empirical cumulative distribution curves show that before the curtailment, the original one is the same as the new one. The number of electric vehicles that are charging is statistically the same in both cases.
- *Stage* "O" (Figure 37 (b)): When the control signal triggers the curtailing, all the charging electric vehicles stop charging and wait. The empirical cumulative distribution curves are the same but the numbers of vehicles that are charging is zero for the control case.
- *Stage* "O" (Figure 37 (c)): Due to the curtailment, more energy are required to be charged into the batteries in the

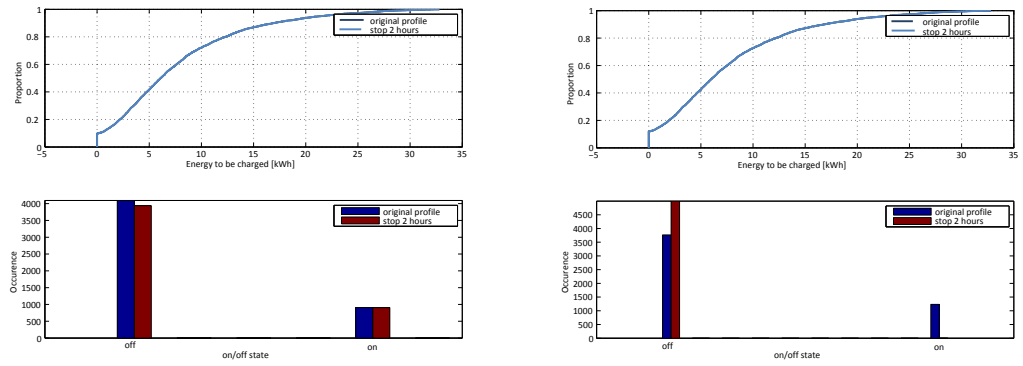

(a) stage "O" (b) stage"O"

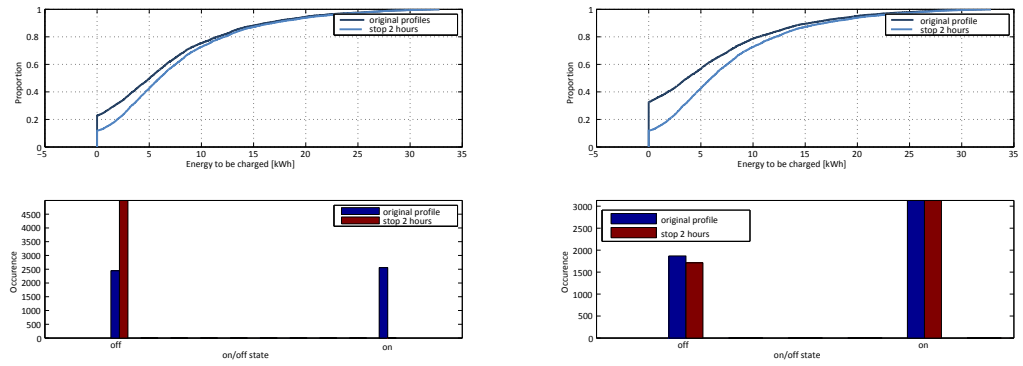

(c) stage "O" (d) stage "O"

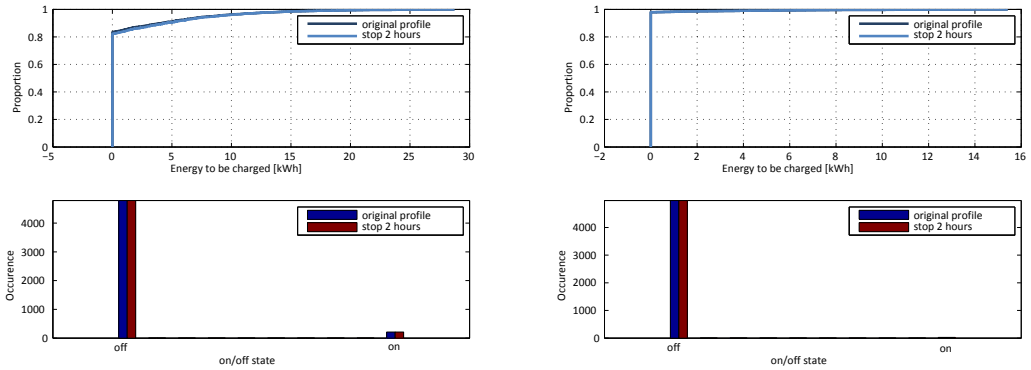

(e) stage "O" (f) stage "O"

Figure 37: Empirical cumulative distribution of energy to be charged in electric vehicles, and their charging states.

control case. Thus, we can see more numbers of vehicle batteries require little energy in the reference case. By observing the histogram, we can see that very few electric vehicles are charging at this stage.

- *Stage* "O" (Figure 37 (d)): After the curtailing period, the units can follows their regular routines. A lot of vehicle batteries start to charge. The difference of empirical cumulative distribution curves becomes larger compared to Figure 37 (c).
- *Stage* "O" (Figure 37 (e)): As time passing by, the difference between the two cases is mitigated. At this stage, 90% of the vehicle battery population are fully charged.
- *Stage* "O" (Figure 37 (f)): It is about the time that most vehicles leave home. Almost all the batteries are fully charged and are ready to run the trips in the coming day.

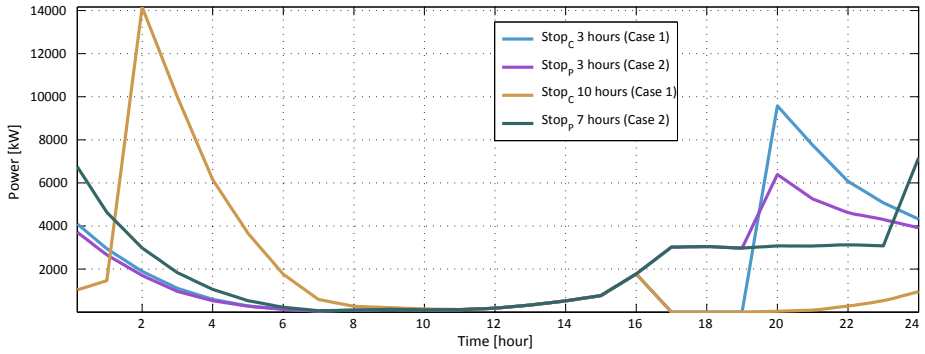

Figure 38: The overall consumption curves of 5000 electric vehicles using stop control.

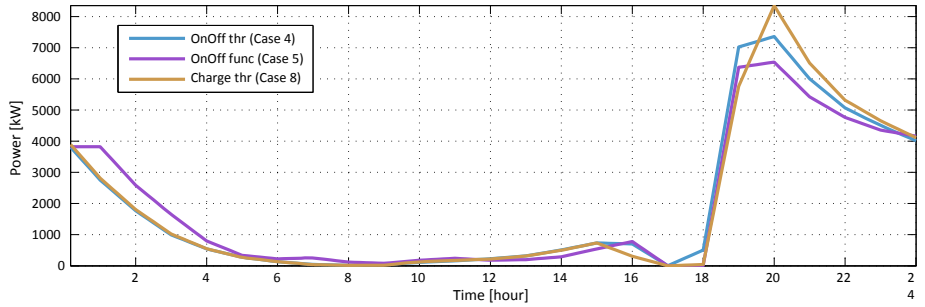

Figure 39: The overall consumption curves of 5000 electric vehicles using incentive control signals.

Figure 38 shows the results using stop control method in Case 1 and Case 2, where on/off state (i.e., charging or not) is the control variable. The control strategies are the same as for heat pumps. Similar to the results for heat pumps, the peak values depend on the curtailment period and the size of curtailed energy. Since there is no inertia in EV model, the peak comes faster is sharper than heat pumps. After 4-hour curtailment, some EVs requires charging in order to be fully charged before their next trip. Thus, we can observe some consumption from Hour 20. More importantly, the kickback effect of EVs are more time relevant. Thus, when to curtail the consumption is a factor to consider. More close to the leaving time the curtailing period is, more sensitive the charging behaviours would be (less flexible). The incentive signal driven results (Case 4, 5, and 8) are shown in Figure 39. It is seen that the modified signal curve may change the size and

shape of the charging curve. Comparing to Case 1 in Figure 38, the peak is smaller. The diversified responsive strategies can release the peak magnitude that is introduced by kick-back effect.

4.2 MV/LV TRANSFORMER ORIENTED SIMULATIONS

The numbers of DERs are too few to provide a generic performance of the modified load profiles with integration of electric vehicles and heat pumps. Thereby, average ones are simulated using Monte Carlo method. The electric vehicle charging patterns and the heat pump consuming patterns are randomly selected from a large population of patterns generated using the previously introduced models. The stochastic terms in the electric models are the driving patterns, including the at-home period, energy consumption in transportation, initial SOC states. The stochastic terms in the space heating system are the initial indoor temperature, and the thermostat parameters of houses. The dash-dot lines are the modified profiles with electric vehicles and heat pumps by taking the average of 2000 simulations. The solid lines are the original profiles calculated based on the node properties following the procedure in Appendix B. The numbers of electric vehicles and heat pumps can be found in Table 3.

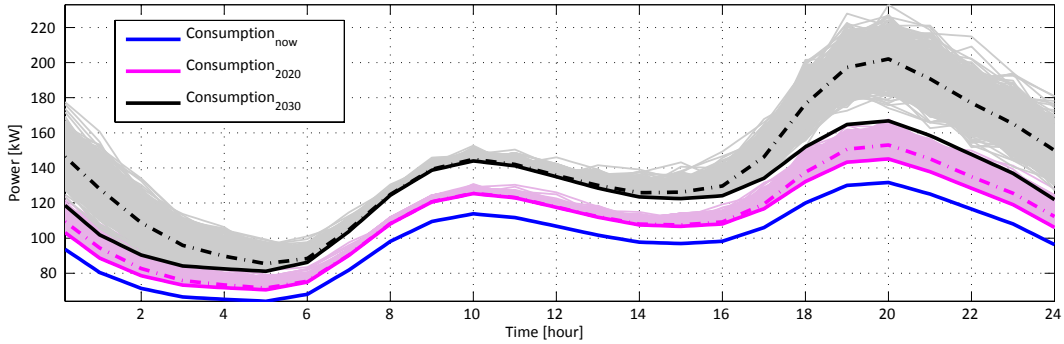

(a) summer cases No. 9, 11, & 13

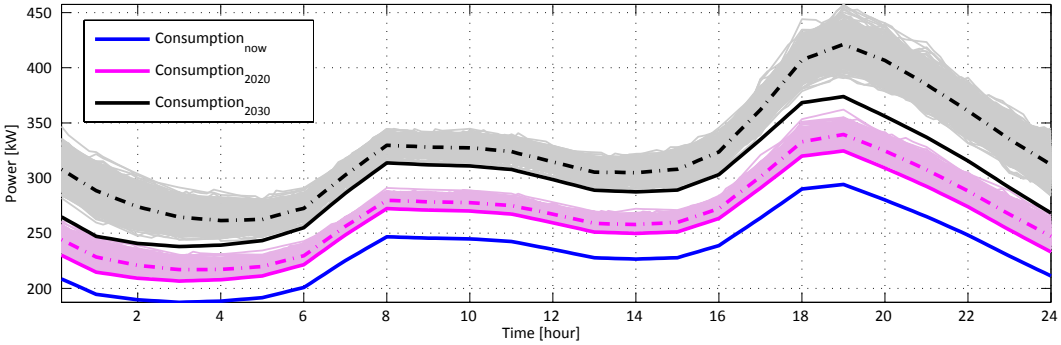

(b) winter cases No. 10, 12, & 14

Figure 40: The load profiles with (dash-dot lines)/ without (solid lines) electric vehicles and heat pumps in different penetration level.

4.2.1 Reference cases (without control No. 9 – 14)

Given the base load in Figure 13 for Node target.1, the load profiles with the integration of electric vehicles and heat pumps are illustrated in Figure 40 (a. summer cases No. 9, 11, & 13; b. winter cases No. 10, 12, & 14).

Peaks occurs in the evening. The power consumption exceed assumed 120% capacity of the transformer during the period 17:30 – 21:20 in winter 2030 (Case 14). With the integration of electric vehicles and heat pumps, the peak value in winter cases increases by 12.7% and 4.5% in 2030 and 2020 respectively.

Winter peak value: 373.8 (2030), 421.3 (2030 with DER), 324.6 (2020), 339.5 (2020 with DER), 294.3 (2013).

Summer peak value: 166.8 (2030), 202.2 (2030 with DER), 145.1 (2020), 153.1 (2020 with DER), 131.7 (2013).

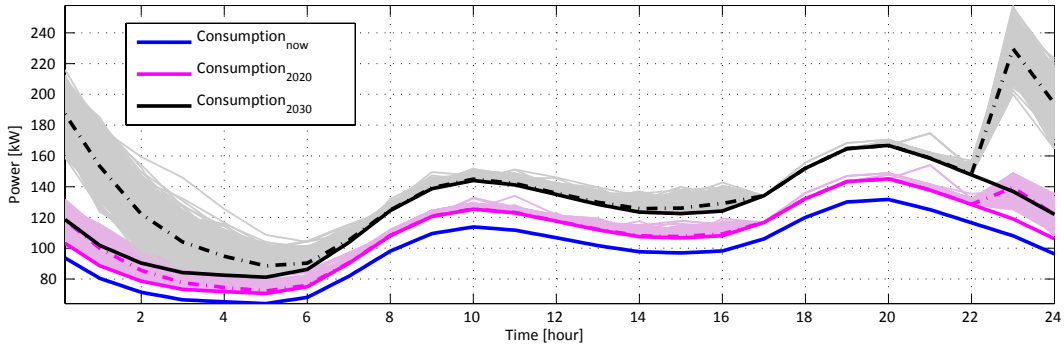

(a) summer cases No. 15 & 17

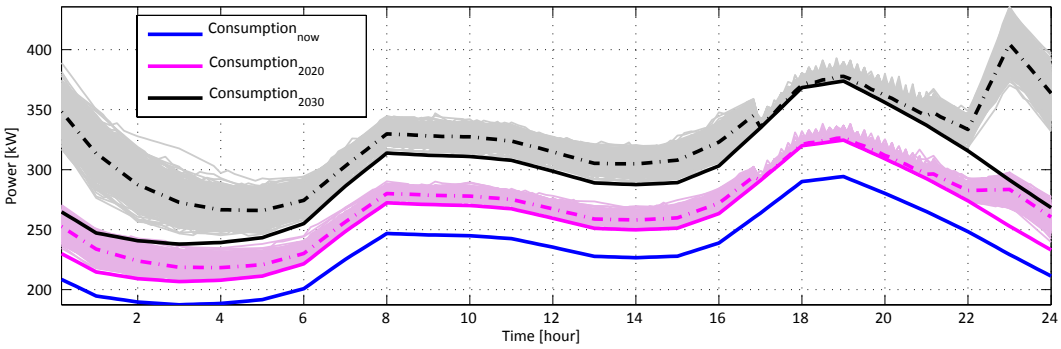

(b) winter cases No. 16 & 18

Figure 41: The load profiles with (dash-dot lines)/ without (solid lines) electric vehicles and heat pumps in different penetration level.

4.2.2 STOP CONTROL CASES (NO. 15 – 18)

In this group, stop control is implemented. The control command asks for curtailment from 17:00 to 22:00. Figure 41 shows the results at different penetration levels. From the figure we can see that a large peak is generated in 23:00 mainly due to the delayed charging activities of electric vehicles, especially in Case 17 and 18 (50 electric vehicles exist under this node in 2030). The load profiles exhibit increases reference (i.e., Case 11 – 14) at approximately 4:00, though the magnitude are comparably low after midnight. The kick-back load of heat pumps comes later due to the thermal inertia of buildings. During the stop period, the power consumption increases gradually to avoid the violation of local constraints (major part is heat pump consumption). The loads that have to be served is due to the reason that the the heating demand is utilized to maintain the indoor temperature above the lower boundary, and the batteries of electric vehicles have to be charged before the deadline expires.

Comparing the peak values with the reference cases (Case 11 – 14), we can observe a slightly drop of the magnitude in Case 16, and the peak is postponed to 23:00. In Case 16, due to that the kick-back peak is smaller than the original peak in 2020 (load curve without DER), the largest load still occurs at 19:00 and is thus reduced comparing to Case 12. Case 17 indicates that this control strategy is not so rational because the peak created by kick-back effect is even higher than the reference case (Case 13). However, it is still effective when the penetration of electric vehicles are rather lower (Case 15).

Winter peak value: 373.8 (2030), 404.6 (2030 with DER), 324.6 (2020), 326.6 (2020 with DER), 294.3 (2013).

Summer peak value: 166.8 (2030), 229.7 (2030 with DER), 145.1 (2020), 145.1 (2020 with DER), 131.7 (2013).

4.2.3 INCENTIVE SIGNAL CONTROL CASES (NO. 19 – 22)

In this group of cases, the incentive signal (i.e., spot price) is used to control the behaviours of flexible demand. In the control strategy, the parameter threshold value $p_{threshold,i}$ [DKK] of individual unit i follows Gaussian distribution as explained in Equation 8.

The service activation period is not exactly follows the peak load hours. We can see from Figure 42 that part of the load is curtailed during the period 8:00 – 11:00, and the period 17:00 – 19:00. More customers start to consume power after the controlling period, due to which a peak load is generated. Comparing to the ordinary cases, it is seen that more power is consumed from 12:00 to 16:00 and less is consumed from 8:00 to 10:00. But around the evening peak, the kick-back power comes too fast so that the peak is generated on the base load in 21:00 (mainly because of the EV charging). In addition, the peak is more severe in 2030 case due to larger penetration of EVs. Not much difference appears on the peak values but only on the time when they occur.

However, comparing to the results in Section 4.2.2, it can be observed that the kick-back does not occur sharply as in stop control cases. It is mainly because that a random term is introduced here in this group, and this diversifies the customer behaviours. A preliminary impression of this phenomenon inspires that the stochastic or diversified terms may flatten the kick-back peak, due to the reason that they are correcting the temporary synchronized behaviours during the kick-back period.

Winter peak value: 373.8 (2030), 417.1 (2030 with DER), 324.6 (2020), 330 (2020 with DER), 294.3 (2013).

Summer peak value: 166.8 (2030), 218 (2030 with DER), 145.1 (2020), 154.2 (2020 with DER), 131.7 (2013).

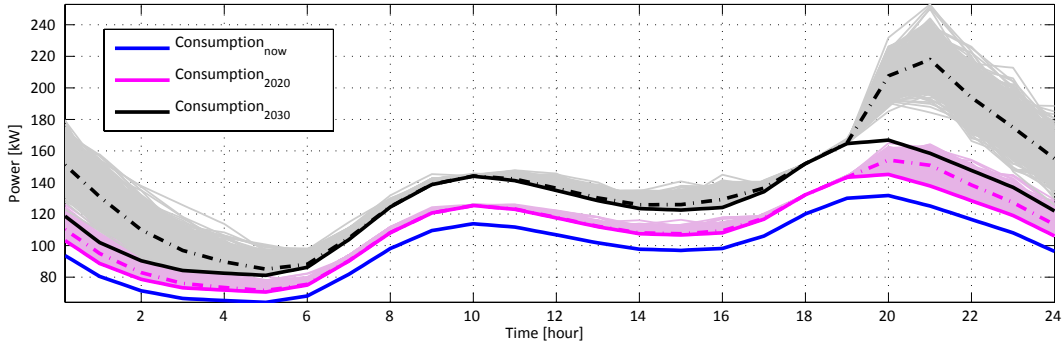

(a) summer cases No. 19 & 21

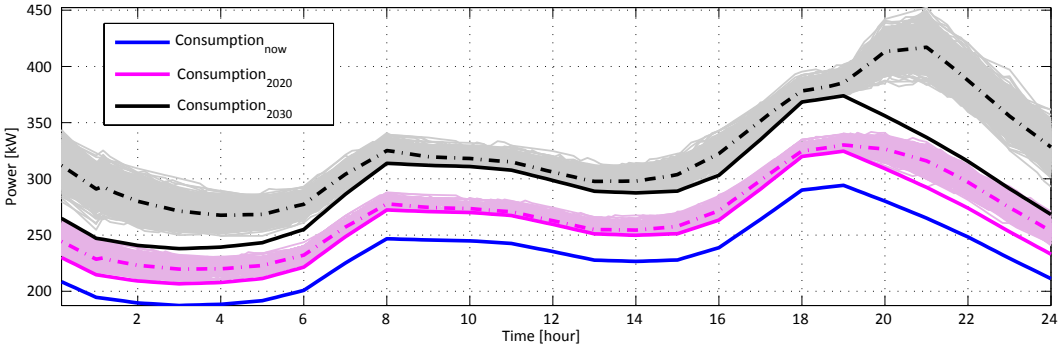

(b) winter cases No. 20 & 22

Figure 42: The load profiles with (dash-dot lines)/ without (solid lines) electric vehicles and heat pumps in different penetration level.

4.3 MV FEEDER ORIENTED SIMULATIONS

In this subsection, the selected feeder B02 is used to simulate and analyse the kickback effect by considering more grid constraints (i.e., peak load, transformer loading, line loading, and voltage deviations). Similar to the Section 4.2, different cases are considered including penetration levels and control strategies. According to the above analysis, it is obvious that the summer cases are not of much interest in terms of the size of peak. So, only winter cases are considered within feeder oriented simulations. To investigate the load kick-back effect to a MV feeder, we rebuilt the feeder for a better illustration. Appendix C includes the color range of the cables and nodes, and the corresponding load flow results in 2013, 2020, and 2030 in a normal weekday in December with the integration of electric vehicles and heat pumps (Case 10, 12, and 14). Appendix D shows in details the load flow results of different cases.

4.3.1 Reference cases (without control No. 10, 12, and 14)

It is observed that both voltage magnitude variations of a single node, and its absolute voltage drop increase along the feeder. The largest voltage drop in MV level is 0.13 kV, occurring at 18:30. The lines' loading varies between 30% and 55%. The peak of the line loading is 54.2% at L_B02_01_1. The peak of the transformer loading is 62.1% at 18:30. Due to the fixed tap of MV/LV transformers (sub-optimal tap positions), the voltage drops are even severe on the secondary side of transformers.

The base loads increase by 12% in Case 12 comparing to Case 10, defined by DONG's long term scaling factors. Some electric vehicles and heat pumps are installed and connected to the feeder. The aggregated loads increase by 0% – 30% respectively. Due to the increase of load, the voltage deviations from nominal value become larger. Some transformers are heavily loaded during peak hours.

In Case 14, the penetration levels of electric vehicles and heat pumps are even higher. The peak of the aggregated load is above 450 kW. The loading of the most critical transformer T_B02.13_1 is above 70% for most of the time. The largest loading is 91% occurs at T_B02.08_1 at 19:00. Some lines are heavily loaded during peak hours. The largest voltage deviation is 8% of all MV nodes, and is 11.2% of all nodes in the feeder. Table 5 summarized the calculation results.

Case	Peak load [kW]	U dev. [kV]	U dev. [%]	Line loading [%]	Tr. loading [%]	No. of lines[7]	No. of Tr.s[8]	No. of nodes[9]
10	275.6	9.87	8.28	54.31	61.84	0	0	0
12	329.4	9.77	9.33	65.24	74.14	0	1	0
14	455.4	9.60	11.24	84.72	90.65	6	7	7

Table 5: The summation of the most critical conditions in the operation.

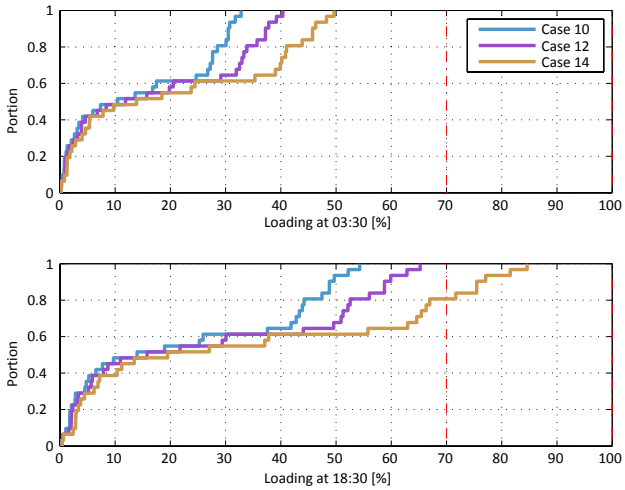

Figure 43: CDF curves of line loadings at different time instants during a working day.

[7]The lines that are heavily loaded (>70% loading).
[8]The transformers that are heavily loaded (>70% loading).
[9]The nodes of which the voltage is below 95%.

Figure 43 shows the cumulative distribution curves of the lines' loading at different time instants. It can be seen from the figure that 20% of lines in the feeder B02 exceed 70% of their loading capacity during peak hours in Case 14. In all cases the loadings are below 70% during non-peak hours. Figure 44 shows the cumulative distribution curve of the transformer loading for different transformers and at different time instants. Two groups of transformers can be identified from Figure 67, 68, and 69: there are very few DERs integrated under the nodes in the first group while there are a lot under the latter ones. Thus, we take T_B02.07_1 and T_B02.08_1 as examples in Figure 44 (a). We can see that the loading value of T_B02.07_1 increases very fast. In Case 14, the loading is over 70% of the transformer capacity for approximately 15% of a day. In Figure 44 (b), the loading at different time instants are illustrated. During peak time, there exist transformers of which the loading is larger than 70% of their capacity in Case 12 and Case 14. Figure 45 illustrates the voltage profile (MV) along the feeder in different cases at peak time. The loading of lines are also marked with different color. In the figure, the X and Y axes indicate the distance between the nodes, Z axis illustrates the voltage magnitudes at different nodes. The color bar on the left is the indicator of the line loading, and the one on the right is the indicator of the voltage deviation. We can easily find out that the loading and voltage deviation from the nominal value is most critical in Case 14.

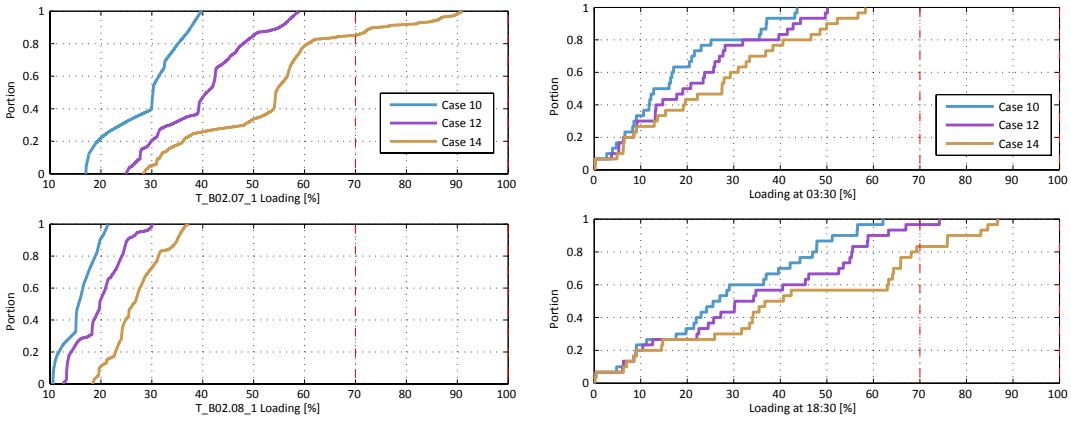

(a) Different transformers

(b) Different time instant

Figure 44: CDF curves of transformer loading.

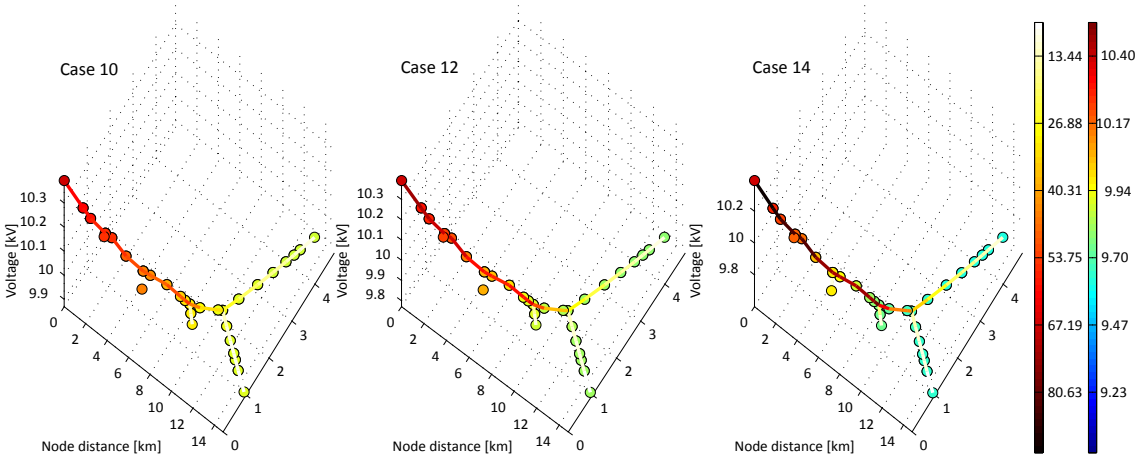

Figure 45: Voltage profile and line loading at 18:30 of the feeder in cases No. 10, 12 and 14.

4.3.2 STOP CONTROL CASES (NO. 16 AND 18)

Applying the stop control during the peak hours (i.e., 08:00 to 09:30 and 17:00 to 21:10), the charging of electric vehicles and the consumption of heat pumps are forbidden. We can find during these two periods, the aggregated loads are reduced. Consequently, the voltage drop is relieved, the loading of transformers and lines are reduced during the corresponding hours. Looking at the most severe transformer, we can see that the kickback load is not dominant in the daily profile. Instead, the peak of the reshaped profile occurs before the control period. It is similar for the lines. The peak loading still appears during the control period but not the kickback load. The heavy loading of the feeder is relieved to some extent.

In Case 18, more flexible demands participate in the control. Thus, the kickback introduced by the control strategies is dominant in the daily profiles. Although under some nodes, the load peaks increase due to the co-occurrence of electric vehicle charging and heat pump consuming activities, the overall peaks (transformers, lines) are reduced slightly, e.g., transformer T_B02.08_1. According to the strategy, the peak hour moves from the original time (around 18:30 in our case) to the end of the control period (21:20 in our case).

4.3.3 INCENTIVE SIGNAL CONTROL CASES (NO. 20 AND 22)

Similar to the MV/LV transformer oriented study, the incentive signals may not reflect exactly the operation conditions in all distribution grid areas. Given the raw market price signals, the curtailment of consumption is released too early. As a consequence, the peak loads are even higher than the original peaks in both Case 16 and Case 18. However, in general, the line loading and voltage deviation conditions are improved a little bit in Case 20.

The condition in Case No. 22 is even worse. Higher or equal line and transformer loading appears. The kickback loads starts at the original peak time and are added on top of the original ones. Due to the dynamics of the thermostats, the kickback peak occurs 20 minutes later.

4.3.4 ANALYSIS AND DISCUSSION

Table 6 sums the results of scenario 2020 and 2030. The most severe moment and the value are listed as below.

	Peak load [kW]		Voltage drop [kV]		Line loading [%]		Tr. loading [%]		No. of	No. of	No. of
Case	size	time	size	time	size	time	size	time	lines[10]	Tr.s[11]	nodes[12]
12	329.4	18:30	9.77	18:30	65.24	18:30	74.14	18:30	0	1	0
16	310.9	18:40	9.81	18:40	61.57	18:50	70.42	16:40	0	1	0
20	335.0	19:40	9.79	19:10	63.56	19:40	73.75	19:40	0	1	0
14	455.4	19:00	9.60	19:00	85.2	19:00	91.33	19:00	6	7	7
18	471.7	21:10	9.64	21:10	81.17	21:10	83.7	21:10	6	8	5
22	460.6	19:40	9.60	19:40	81.42	19:40	91.95	20:00	6	7	5

Table 6: Summation of the most critical moments and the corresponding state values.

[10]The lines that are heavily loaded (>70% loading).

Figure 46 shows daily loading profiles of several most critical lines in the feeder. Similar to results in Section 4.2, the original peaks are cut in cases No. 16 – 22. The kick-back peaks are more severe and visible in 2030 cases. Hence, we looked into the cumulative distribution of loading at peak time for all lines and the distribution of loading of the most critical line but along the entire day (see Figure 47). From the plots we can see that there is very little difference of the CDF curves for all lines at peak time. However, it is noticeable that the control methods force the loading below 70% of the capacity for longer time. Take the line L_B02_01_1 as an example. There is 80% of the time in a day when the loading is below 70% capacity in Case 18 and 22, whereas there is only 63% of the time in Case 14 without applying any control applications. Similar results can be drawn for transformer loading (see Figure 48 and Figure 49).

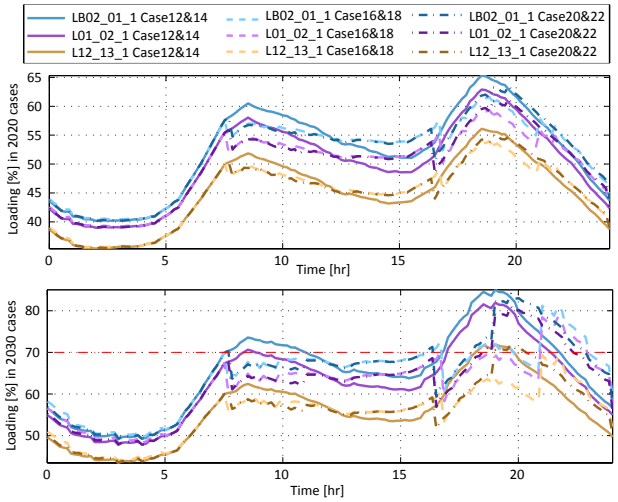

Figure 46: Daily loading profiles of lines.

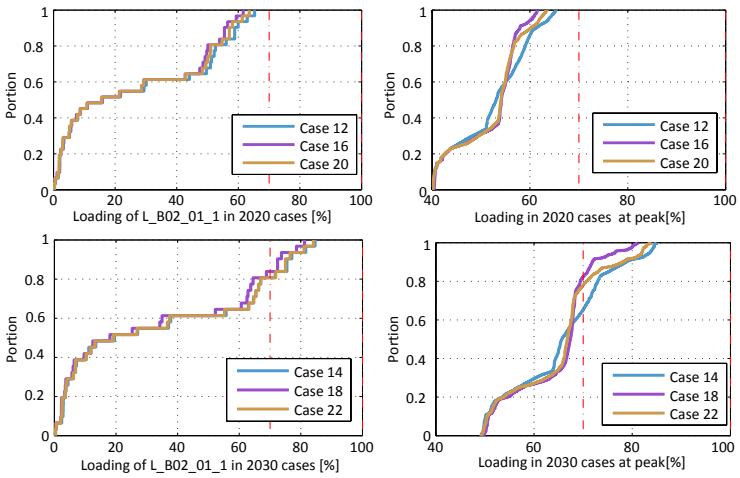

Figure 47: CDF curves of line loading at original peak and new peaks due to control.

[11] The transformers that are heavily loaded (>70% loading).
[12] The nodes of which the voltage is below 95%.

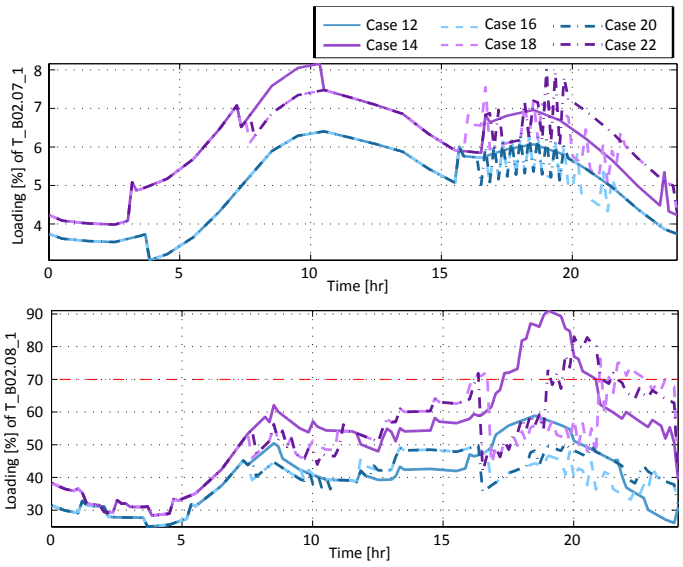

Figure 48: Daily loading profiles of transformers T_B02.07_1 and T_B02.08_1.

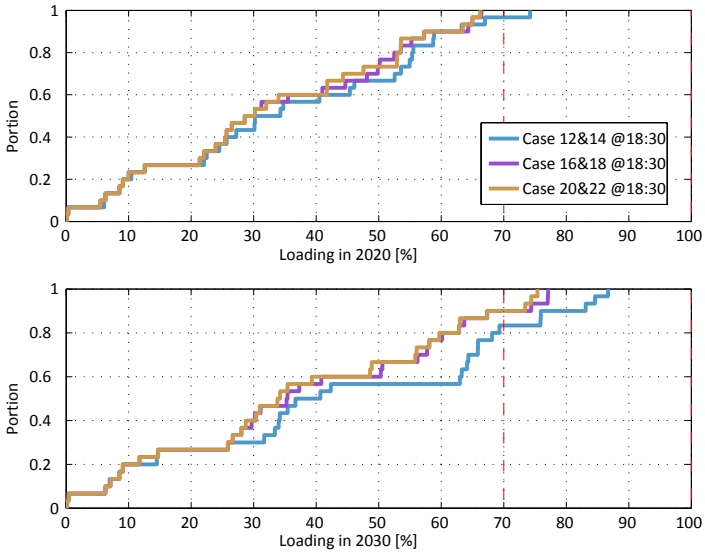

Figure 49: CDF curves of transformer loading during peak time.

Daily voltage profiles of the last node B02.31 in the feeder is plotted in Figure 50. The drop during peak hours are brought back due to the activation of flexibility. Since there is mismatch between high price and local peak, the controlling period does not cover the entire peak period. The lowest voltage magnitude is not improved so much in incentive signal control cases. The comparisons of results between different control strategies in peak time are illustrated in Figure 51 and 52.

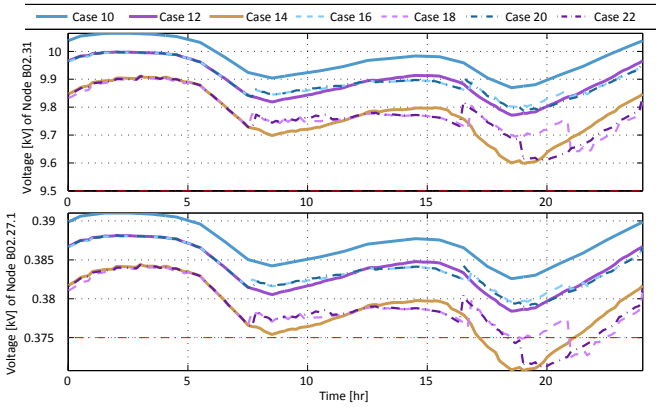

Figure 50: Daily voltage profiles in different cases at the last node in the feeder (MV).

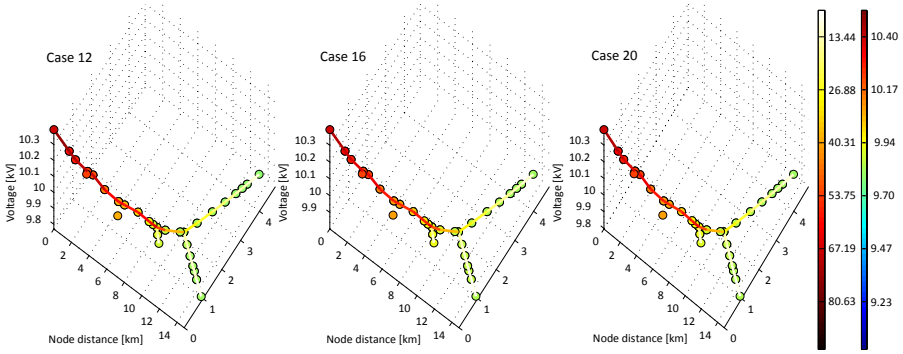

Figure 51: Voltage profile and line loading at 18:30 of the feeder in 2020 cases No. 12, 16 and 20.

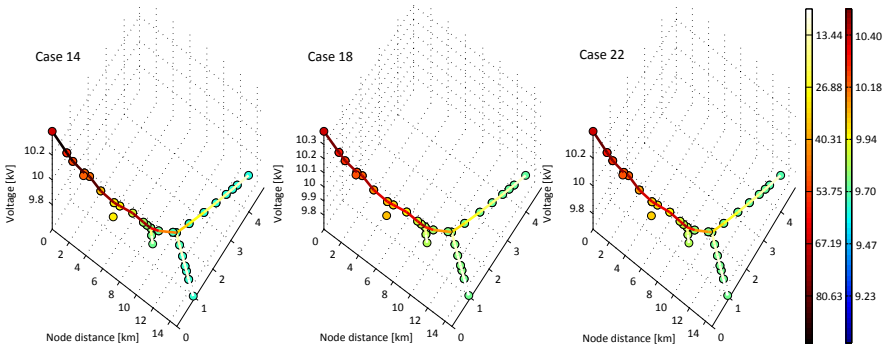

Figure 52: Voltage profile and line loading at 18:30 of the feeder in 2030 cases No. 14, 18 and 22.

5 RECOMMENDATIONS

In this report, we focus on describing the kick-back effects when activating some rather simple control signals to curtail and shift the consumption of heat pumps and electric vehicles during certain periods. The applications and flexibility products are briefly described. The control signal may vary according to the targeting services, which affects when and how to curtail or to shift the flexible consumption. Other activities of customers are not considered in the DER models which may reduce the synchronous behaviours. From the simulation results and the analysis, it is concluded that an open-loop approach could not handle the kick-back effects of a population of homogeneous DERs, due to synchronous behaviours advised by an identical control signal. To limit the size of kick-back peak, the management system should differentiate trivial signals beforehand to reserve some flexibility and diversity, or to alter the signal afterwards accordingly for prevention of critical kick-backs (if the behaviours of the system and DER fleet can be well estimated).

Introduced to prevent critical load during the restoration of blackout, [30], [31], [16], and [32] have proposed some solutions to solve kick-back effects by separating the DERs into several sub-portfolios. Different algorithms were presented to decide the sequence and timing on switching the consumption of different group of loads. The voltage dependent loads (such as pure resistive load) can be controlled by changing the voltage at certain feeders to limit the overall consumption during kick-back [33]. Quick response of distributed generations were proposed in [34] to conserve the diversity of loads. Protection devices also play very important roles in the emergency situations, e.g. load shedding. However, during the emergency conditions, the fulfilment of user's requirement is compromised to the safety of the grid. Instead, flexible topology in normal conditions, e.g., switching some loads to adjacent less-loaded feeders. might support solving kick-back effects. Direct aggregation management were proposed to optimize the profile effectively [33]. [16] presented an indirect way of aggregating and controlling thermostatically-controlled-loads to limit the kick-back peak.

The cause of critical kick-back effects can be classified into the following categories:

- Local constraints, including grid constraints and customer constraints, are invisible during the control process. For instance, when providing ancillary services to TSO, the local constraints may not be described or not be described accurately in the control problem.
- The modelling and forecasting of the system fails. The control signals are generated based on the considerations of response of the models and the forecasting of the system behaviours. In the future grid infrastructure, the randomness of customer behaviour and weather conditions are hard to describe, and may fail due to unexpected disturbance or imperfect model.

A closed-loop predictive control method considering local constraints and using perfect models for prediction, may optimize the control actions by updating the DER states, and send out the differentiated signals to individuals. As long as the flexibility is available for further regulation, the size of kick-back peaks can be properly handled. A closed-loop procedure is used in Case 2, where the DER states are considered while generating the control signals. If the control continue to be performed after the curtailment period by limiting the maximal power consumption, the kick-back effect can be managed within an acceptable size (see Figure 53). The blue curve shows the aggregated consumption curve without setting the maximal value, while the purple one shows the consumption by limiting the overall size using differentiated signals. One step estimation of the state variations (i.e., transactions between "on" and "off" states) are used to modulate the consumption in next instant. An indirect control implementation with similar approach is described in [35], where the composed load consumption is limited by modifying the incentive signal values.

However, in some applications that are constrained by such as IT configurations, the complexity of the system, and activation time, the above mentioned limitations may not be able to improved. A universal method applied locally is able to diversify the DER behaviours, and hence to decrease the impact of the kick-backs. The following statement will present how the kick-back peak can be limited.

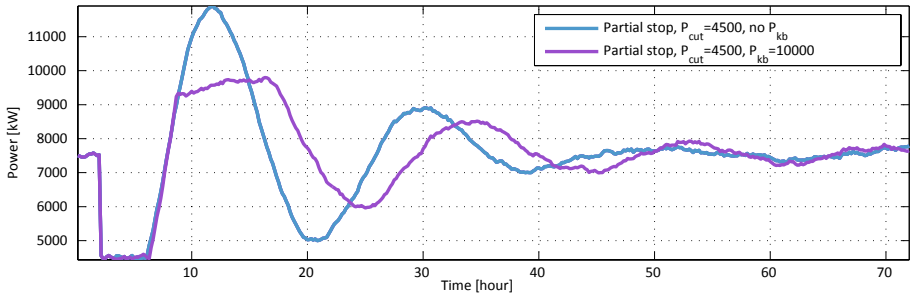

Figure 53: The aggregated consumption by using differentiated signals to limit kick-back peaks.

Here we extend Case 6 for analysis, in which an identical control signal is set for all the units, the remote controller may not consider local constraints. To explicitly shows the impacts, three control signals are used (see Figure 54): a step, a ramp, and a pulse. The original local responsive function is defined in Equation 11. Figure 55 shows the indoor temperature of two houses equipped with heat pump heated space heating system. The temperature set-points vary according to the incentive control signal. How much the set-points deviate from the original ones are depending on the size of the house.

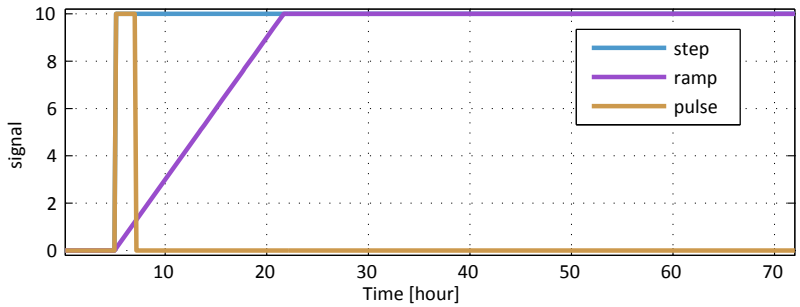

Figure 54: The incentive signals used in the analysis of limiting kick-back peaks.

To differentiate the DER response, small random components, $\epsilon_{p,j}$, and $\epsilon_{k,j}$, are added into the local responsive function, as described in Equation 12.

$$T_{ref,j,t} = 22 - k_j * (p(t) - p_{ref}) + \epsilon_p \quad \text{if} \, T_{ref,min} \leq T_{ref,j,t} \leq T_{ref,max} \tag{12}$$

where,

$$k_j = 0.133 + \epsilon_{k,j}, \quad \epsilon_{k,j} \sim \mathcal{N}(0, 0.01) \tag{13}$$

$$\epsilon_{p,j} \sim \mathcal{N}(0, 0.25) \tag{14}$$

These random components are integrated into the control process, and speed up the diversification of behaviours of DERs. Figure 56 shows the altered temperature set-points and the indoor temperatures accordingly. The mean value of the set-points follows the curves in Figure 55.

In Figure 57, Figure 58, and Figure 59, the aggregated response of step, ramp, and pulse signals are presented respectively. Comparing the purple curves (local control with random components), and the blue one (original control), we can observe that for all three signals, the oscillations in the kick-back effects are damped faster than the original ones. Especially in Figure 57, the oscillations are almost gone in one cycle. The kick-back peaks in Figure 57 and Figure 58 are

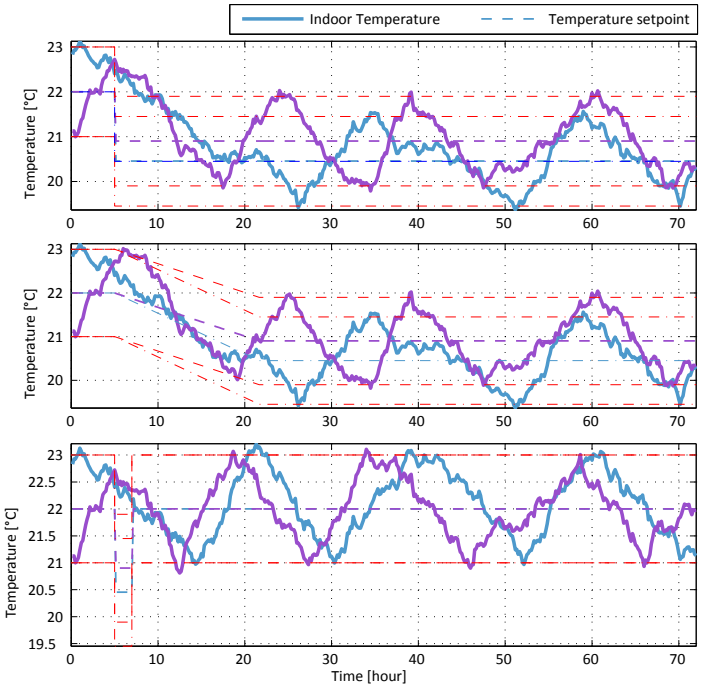

Figure 55: Indoor temperatures and their corresponding temperature set-points responding to step, ramp, and pulse control signals.

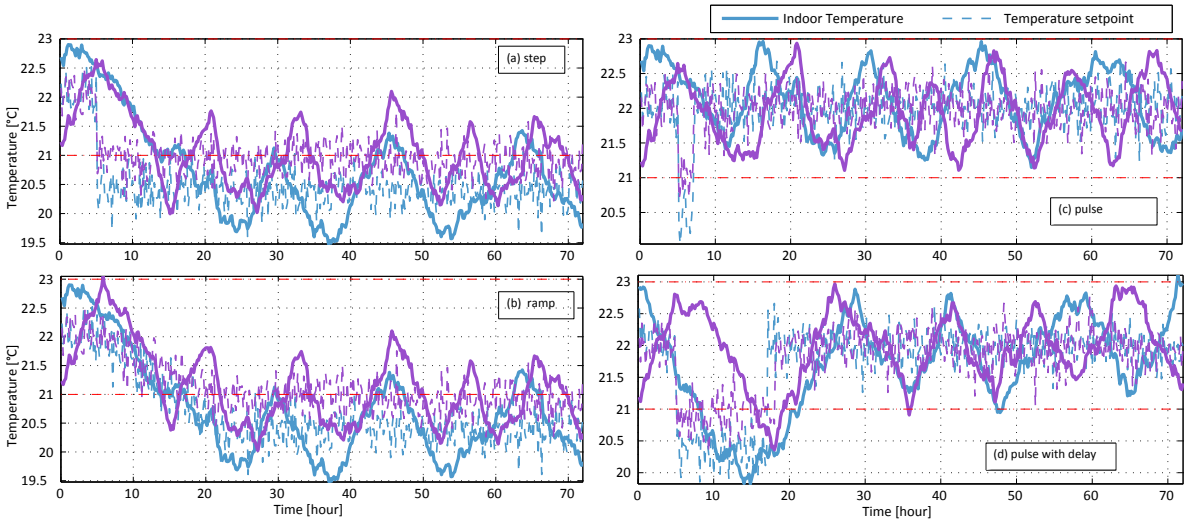

Figure 56: Indoor temperatures and their corresponding temperature set-points responding to step, ramp, and pulse control signals.

reduced by approximately 1000 kW and 500 kW accordingly. The service quality (the size and shape of curtailment) of all cases are close to or even better than the original one. However in Figure 59, the peak is slightly higher than the original one (mainly due to a larger curtailment of consumption during Hour 5 – Hour 7). Therefore, we can conclude that the additional small random components could improve the performance during the kick-back period without losing service quality during the curtailment.

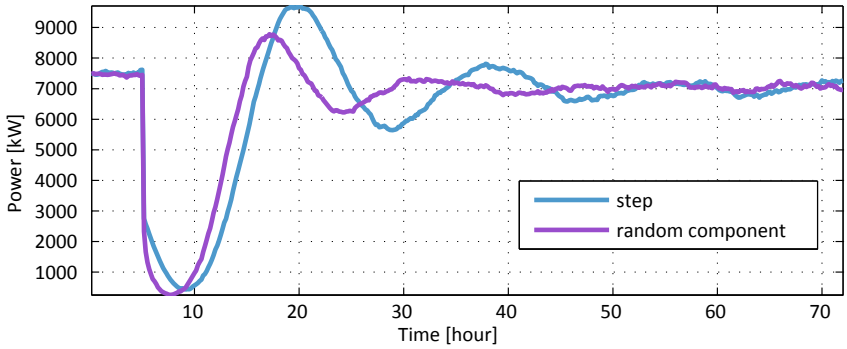

Figure 57: The overall consumption curves of 5000 space heating systems using 'step' control signals.

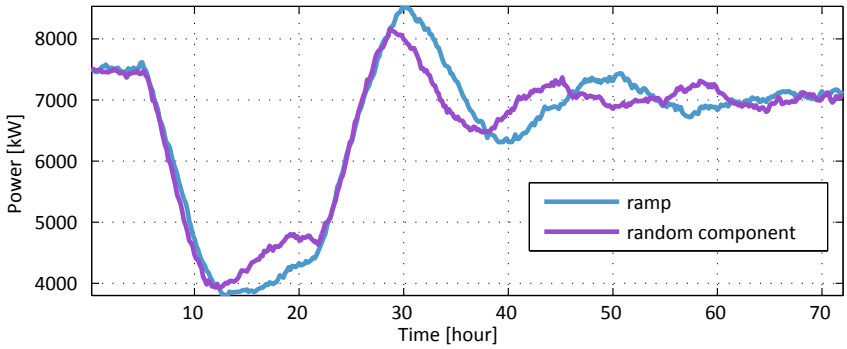

Figure 58: The overall consumption curves of 5000 space heating systems using 'ramp' control signals.

To further limit the kick-back peaks, similar to the approaches after black-out, random delays are added onto the control signals before they are coming back to the original set-points with pulse case. Aggregated load profiles (green and yellow curves) are plotted in Figure 59. In our simulations, two-hour curtailment is required. Comparing to the energy inertia of the thermostats, it is quite short, which means that some flexibility is still available even after the curtailment of consumption. Thus, uniformly distributed numbers between 0 and 2 hours (yellow) / 0 and 4 hours (green) are added to the local responsive functions to delay the recovery of original set-points. The peak size is reduced by approximately 500 kW, if the delays are set up to 2 hours. The peak is reduced by approximately 2500 kW, if the delays can be extended to 5 hours. From the figure, we can also identify that the width of the peak may increase while the magnitude is being reduced.

From the above analysis and discussions, we summarize the following recommendations that would help on avoiding critical kick-back effects when controlling an amount of homogeneous DERs:

- Different DER units exhibit various characterized profiles and dynamic features. The portfolio of thermostatic sys-

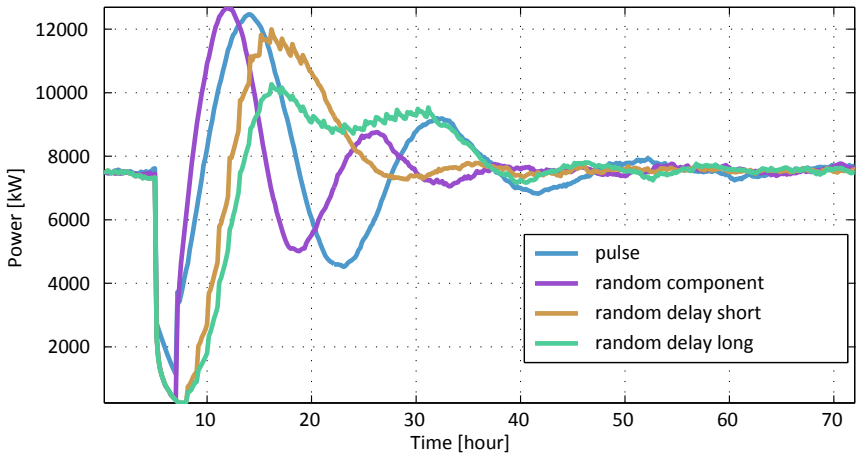

Figure 59: The overall consumption curves of 5000 space heating systems using pulse control signals.

tems can be regarded as a second order system within a certain period [13], given a curtailing signal with limited value. In this case, it simplifies the design of the control strategy and the kick-back is easier to be predicted by estimating the response of a small test signal.

- Trivial feedback signals are essential to improve the controllability of the system. Even though, as mentioned in the last point, the aggregated behaviour can be estimated and modelled, in a more general condition, indirect control without stimulating large kick-backs is hard to be implemented. Feedback signals of individual devices that provide sufficient knowledge of individual states helps the controller to manage the control actions in the next step. In this way, the kick-back effects can be reduced and even eliminated by the following control actions. Another notable issue is that, in order to manage the critical kick-backs, post/pre curtailing control design should be included in the control frame.
- Despite the above listed points, in the condition that there is no way to improve the remote/central control strategy, local random components in the local controller is able to diversify the synchronous behaviours after the curtailment. The damping of oscillations is larger than the original system, and the oscillation magnitude can be reduced accordingly.

[13] Given the simulation results in Case 3, Figure 34 shows that the response behaviour can be represented by a second order system within 10 hours for this homogeneous population of heating systems.

6 CONCLUSION

Demand side DERs and their flexibility provide an alternative way to assist system operations, e.g., power balancing, and congestion management. The services commanded by the remote entity instruct the DER units to perform same or similar actions to their flexibility. The harmonized actions of a large quantity of homogeneous DERs would generate kick-back effects. The kick-back load might increase the network load and power imbalance.

Hence, this report has been focused on investigating such phenomenon when applying different control strategies under normal operation conditions. Furthermore, we have provided some recommendations on how to avoid critical kick-backs in practice. In this report, we have introduced some general concepts: DER, flexibility, and kick-back effect. A Danish MV distribution grid has been presented to analyse the power system operation and to assess the risks by activating the flexibility services.

Electric heating system and EVs, as two typical types of DERs have been modelled. Subsequently, the states of the populations are presented in different stages (i.e., before, during, and after the curtailing period) to describe how the kick-back effects are created. Both remote and local control strategies are considered and described explicitly.

A scenario tree is built to study the kick-back effect with relation to the population of DERs (i.e., penetration level), seasons (i.e., winter and summer), and various control strategies. The simulations and analysis are made on unit level, MV node level, and MV feeder level.

Based on the simulation results, more study is made to test the method to limit the size of kick-back load, and how to mitigate the critical kick-back effects. In the end, some general recommendations on avoiding critical kick-backs are proposed.

As a final remark, the demand side DERs are attractive to provide system services, while the kick-back effects should be taken into account when describing the services and products, and should be managed when designing a control strategy.

A APPENDIX – PENETRATION OF DERS IN THE GRID AREA

	2013		2020		2030			2013		2020		2030			2013		2020		2030	
Node	EV	HP	EV	HP	EV	HP	Node	EV	HP	EV	HP	EV	HP	Node	EV	HP	EV	HP	EV	HP
1016	0	0	0	1	2	1	2979	0	0	2	1	9	2	462	0	0	0	1	4	1
1019	0	0	2	2	12	5	2991	0	0	5	6	22	12	4655	0	0	2	2	6	4
1022	0	0	2	4	8	9	3007	0	0	3	5	13	11	4670	0	0	0	2	2	5
1023	0	0	1	2	4	3	3025	0	0	1	3	3	7	4717	0	0	3	10	13	21
B02.30	0	0	0	0	1	0	3036	0	0	6	3	26	6	4723	0	0	2	4	8	8
1026	0	0	7	10	31	20	3046	0	0	2	2	8	5	4724	0	0	7	3	31	7
1027	0	0	2	1	5	2	3066	0	0	13	6	60	12	4789	0	0	3	2	14	5
1042	0	0	1	1	5	1	3068	0	0	2	1	8	2	4792	0	0	3	3	10	6
1053	0	0	9	3	40	7	3097	0	0	0	0	0	0	4848	0	0	4	14	18	28
1058	0	0	0	0	3	0	B02.12	0	0	3	6	15	12	4864	0	0	2	3	9	7
B02.26	0	0	1	0	5	0	3212	0	0	0	1	2	1	487	0	0	3	2	14	4
1071	0	0	4	3	15	6	3213	0	0	3	4	15	8	4895	0	0	2	2	5	3
1072	0	0	7	4	29	9	3215	0	0	4	6	20	13	4901	0	0	3	2	10	3
1109	0	0	4	13	18	27	322	0	0	7	1	30	2	4945	0	0	16	3	69	7
1119	0	0	0	0	0	0	3258	0	0	0	1	3	2	4958	0	0	11	2	51	3
1140	0	0	0	1	3	1	3262	0	0	5	4	21	8	505	0	0	2	2	6	3
1152	0	0	0	1	1	2	3269	0	0	1	2	7	3	5069	0	0	4	0	21	0
1165	0	0	1	4	4	9	3311	0	0	4	5	16	10	5071	0	0	7	12	33	24
1169	0	0	11	5	49	11	3314	0	0	14	9	63	19	5085	0	0	0	1	2	1
1178	0	0	7	9	31	18	3322	0	0	0	2	4	3	5095	0	0	3	3	11	6
118	0	0	2	5	10	11	3334	0	0	7	3	28	7	5166	0	0	0	1	0	1
1252	0	0	5	2	24	5	3343	0	0	1	3	6	7	5177	0	0	14	13	62	27
1411	0	0	0	2	3	3	3353	0	0	5	8	26	17	5178	0	0	8	7	35	15
1422	0	0	1	3	8	7	3371	0	0	7	5	29	10	5283	0	0	9	2	42	3
1441	0	0	5	14	23	28	3378	0	0	1	0	3	0	5291	0	0	1	2	8	4
1444	0	0	9	19	40	39	3380	0	0	5	6	21	13	5293	0	0	4	3	17	6
B02.14	0	0	9	7	41	14	3387	0	0	1	4	6	9	5313	0	0	1	3	4	7
1451	0	0	6	8	29	17	3391	0	0	1	1	3	1	B02.03	0	0	1	4	5	8
1496	0	0	21	21	93	43	B02.15	0	0	4	4	17	8	5331	0	0	6	0	28	0
1501	0	0	2	5	10	11	3398	0	0	0	0	2	0	5337	0	0	2	3	9	6
1564	0	0	1	2	5	3	3399	0	0	2	0	8	0	5355	0	0	10	1	43	1
1565	0	0	0	0	0	0	3401	0	0	2	1	8	2	5374	0	0	1	1	3	2
1649	0	0	4	12	17	24	3404	0	0	2	1	6	1	5380	0	0	3	2	13	3
166	0	0	2	1	8	2	3410	0	0	2	2	6	3	5409	0	0	0	1	1	1
1686	0	0	2	4	10	8	3422	0	0	11	10	50	20	5410	0	0	5	2	22	4
1688	1	0	24	24	104	48	3493	0	0	0	2	3	3	5435	0	0	2	3	7	7
1716	0	0	0	0	1	0	3509	0	0	3	7	14	14	5455	0	0	5	17	20	34
1717	0	0	2	1	7	2	3565	0	0	12	17	51	34	5470	0	0	1	2	3	4
1737	0	0	1	3	8	6	B02.10	0	0	2	4	9	8	548	0	0	3	9	12	18
B02.21	0	0	0	0	0	0	3637	0	0	17	6	73	12	5488	0	0	0	2	1	3
176	0	0	1	4	4	8	3644	0	0	1	1	2	1	5510	0	0	2	5	11	11
1765	0	0	1	5	6	10	3677	0	0	5	5	25	10	5512	0	0	2	10	9	20
1772	0	0	1	2	5	5	3713	0	0	4	5	15	11	5520	0	0	1	3	2	6
1796	0	0	12	8	51	16	3714	0	0	1	1	3	2	5537	0	0	2	2	11	4
180	0	0	10	8	42	17	3717	0	0	2	1	7	2	B02.08	0	0	1	5	8	10
1813	0	0	5	14	22	28	3724	0	0	2	4	7	8	5597	0	0	0	2	2	3
182	0	0	3	7	13	14	3763	0	0	10	6	44	13	B02.20	0	0	1	2	4	3
1825	0	0	2	3	6	6	3772	0	0	3	3	11	7	B02.23	0	0	1	3	7	7
184	0	0	1	2	4	5	B02.18	0	0	3	7	14	14	5635	0	0	2	2	7	4
1847	0	0	2	3	9	6	3881	0	0	2	4	8	9	5648	0	0	1	0	5	0
1863	0	0	4	4	20	8	3919	0	0	3	5	13	10	5650	0	0	6	10	24	20
1929	0	0	2	7	8	14	3931	0	0	1	1	6	1	5652	0	0	0	1	1	2
194	0	0	8	0	34	0	3946	0	0	0	1	1	2	5697	0	0	1	1	5	1
195	0	0	2	11	9	22	3961	0	0	0	0	2	0	5703	0	0	7	5	28	10
200	0	0	10	35	44	71	3964	0	0	4	3	17	7	573	0	0	0	4	4	8
2023	0	0	2	4	11	8	3986	0	0	6	7	25	14	5762	0	0	0	1	1	1
2057	0	0	6	7	29	15	3991	0	0	1	1	5	1	5766	0	0	5	0	22	0
2079	0	0	0	0	0	0	3999	0	0	4	3	18	6	5773	0	0	4	18	18	37
2081	0	0	1	1	5	1	4006	0	0	0	1	1	1	5774	0	0	0	0	3	0

2085	0	0	5	12	23	24	4017	0	0	0	1	2	2	5823	0	0	0	0	0	0
2143	0	0	6	12	26	24	4051	0	0	1	2	6	3	5825	0	0	1	1	4	1
2149	0	0	1	3	5	6	B02.01	0	0	2	1	9	1	5B02.31	0	0	0	2	3	5
target	0	0	8	5	36	10	4071	0	0	1	0	4	0	5828	0	0	0	2	1	3
2160	0	0	3	2	12	4	4134	0	0	15	38	65	77	5829	0	0	2	5	10	11
2196	0	0	2	0	10	0	4145	0	0	0	2	0	3	5876	0	0	0	2	3	3
2204	0	0	8	15	35	30	4148	0	0	2	1	7	1	5877	0	0	4	4	18	9
2212	0	0	6	4	28	8	4152	0	0	0	0	0	0	5881	0	0	0	0	2	0
222	0	0	0	2	1	4	4158	0	0	5	9	20	19	5883	0	0	1	2	4	3
2248	0	0	4	7	19	14	416	0	0	4	5	16	11	5884	0	0	1	2	4	5
2252	1	0	27	32	117	65	B02.13	0	0	3	7	12	14	5908	0	0	1	2	5	4
2288	0	0	1	1	3	1	425	0	0	0	1	3	2	5913	0	0	1	1	5	2
B02.09	0	0	2	3	9	6	4250	0	0	5	6	22	13	5915	0	0	0	1	1	2
2371	0	0	2	1	11	1	4254	0	0	4	1	21	1	6011	0	0	1	0	4	0
2379	0	0	4	3	14	6	426	0	0	1	1	6	2	6012	0	0	1	2	6	4
2380	0	0	3	2	14	5	4272	0	0	3	8	12	16	602	0	0	7	14	34	28
B02.27	0	0	2	1	5	2	B02.28	0	0	0	1	3	1	6226	0	0	5	4	20	8
2423	0	0	0	1	4	1	4321	0	0	13	25	59	51	6278	0	0	5	2	19	3
2443	0	0	1	1	3	1	4322	0	0	1	1	4	2	6371	0	0	0	2	2	4
B02.16	0	0	8	12	34	25	4323	0	0	0	2	1	3	641	0	0	3	2	11	4
247	0	0	1	1	6	2	4324	0	0	1	3	7	7	643	0	0	2	1	6	2
2508	0	0	0	0	0	0	4337	0	0	7	8	29	17	6481	0	0	0	0	0	0
2534	0	0	19	71	85	144	B02.19	0	0	1	1	5	1	6521	0	0	0	2	3	4
2561	0	0	1	2	5	3	4385	0	0	0	0	1	0	6532	0	0	7	33	33	66
2566	0	0	3	2	11	3	4410	0	0	2	3	7	7	6584	0	0	0	1	1	2
2567	0	0	2	2	9	5	4415	0	0	5	2	25	5	661	0	0	3	7	14	15
2573	0	0	3	4	11	9	B02.07	0	0	0	1	2	2	6626	0	0	7	26	31	53
2613	0	0	0	1	1	2	4442	0	0	1	2	5	5	664	0	0	7	13	31	27
2696	0	0	4	2	17	5	446	0	0	1	1	3	1	665	0	0	1	3	5	7
2697	0	0	7	9	32	19	4461	0	0	0	0	0	0	666	0	0	2	6	8	12
2747	0	0	1	6	6	13	4464	0	0	4	12	19	25	6763	0	0	2	0	10	0
2749	0	0	2	5	7	11	4489	0	0	12	14	53	28	6868	0	0	3	3	16	7
B02.25	0	0	6	5	29	11	4491	0	0	2	1	7	1	6901	0	0	1	3	5	7
2770	0	0	7	0	32	0	B02.24	0	0	0	1	2	1	691	0	0	6	8	27	16
2773	0	0	2	1	7	1	4518	0	0	2	2	10	3	6949	0	0	3	0	12	0
2776	0	0	8	32	37	64	4523	0	0	0	0	1	0	7059	0	0	1	0	4	0
2838	0	0	1	0	2	0	4530	0	0	1	1	2	1	720	0	0	4	6	18	13
2841	0	0	2	0	8	0	B02.04	0	0	0	0	0	0	767	0	0	9	26	39	52
2862	0	0	2	2	8	5	4547	0	0	8	6	38	12	770	0	0	0	2	1	3
2890	0	0	12	18	54	37	4583	0	0	1	2	5	5	B02.31	0	0	0	1	2	2
2892	0	0	2	2	8	3	4596	0	0	6	0	25	0	874	0	0	0	0	1	0
2985	0	0	2	1	4	2	4608	0	0	1	1	6	2	B02.02	0	0	14	19	59	38
2967	0	0	8	30	37	60	4609	0	0	2	3	12	6	960	0	0	2	6	7	13
B02.06	0	0	3	10	11	21														

Table 7: Penetration information corresponding to individual nodes.

B APPENDIX – PROCEDUE TO DERIVE THE LOAD PROFILES (AN EXAMPLE)

Figure 60 shows a load template (i.e., normalized scales along time) of a load category 'DETAILHANDEL'. The maximal power consumption P_{max} [kWh/h] is calculated by

$$P_{max,i,k} = \alpha_k \times E_{i,k} + \beta_k \times \sqrt{E_{i,k}} \tag{15}$$

where, $E_{i,k}$ is the annual consumption [MWh] of this particular load category k, under a certain node i. α_k and β_k are the parameters for the category. . For the category 'DETAILHANDEL', α_k = 0.21 and β_k = 0.85.

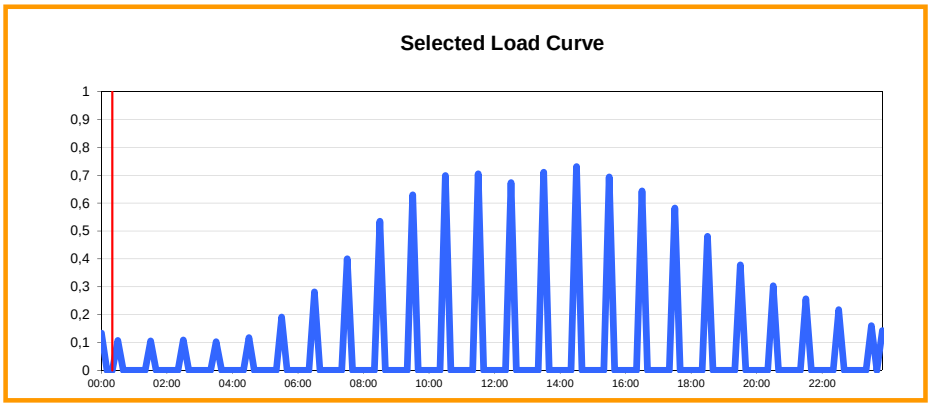

Figure 60: Load template of category 'DETAILHANDEL'.

The power factor is also specified in the load template, which is 0.981 for the load category âĂŸDETAILHANDELâĂŹ. For most categories, the power factor is larger than 0.9, which indicate that little reactive power is consumed.

$E_{i,k}$ can be derived by knowing the annual consumption of the node i, and the portion of the category under this node. For Node target.1, the portions can be found in the grid model as in Figure 61.

The annual consumption of the future is estimated as in Figure 62 by DONG Energy A/S [18]. By taking the annual consumption in 2013, and multiplying by the increasing rate, we can therefor estimate the annual consumption in 2020 and 2030 respectively. Having the information above, the load profile can be derived accordingly.

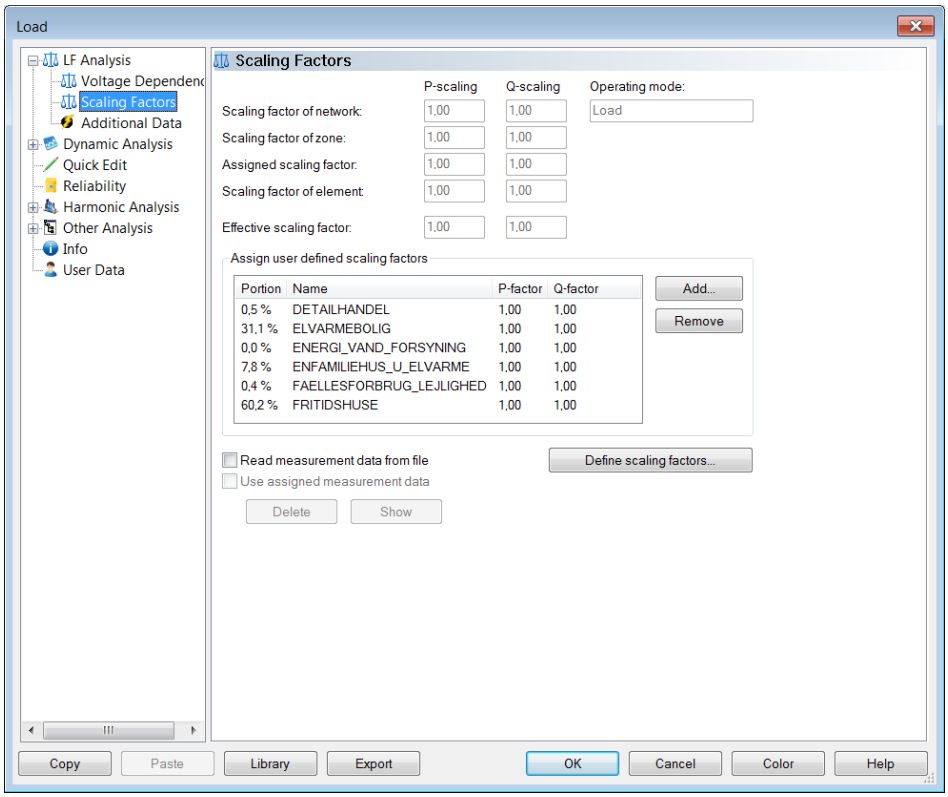

Figure 61: Portions of load under Node target.1.

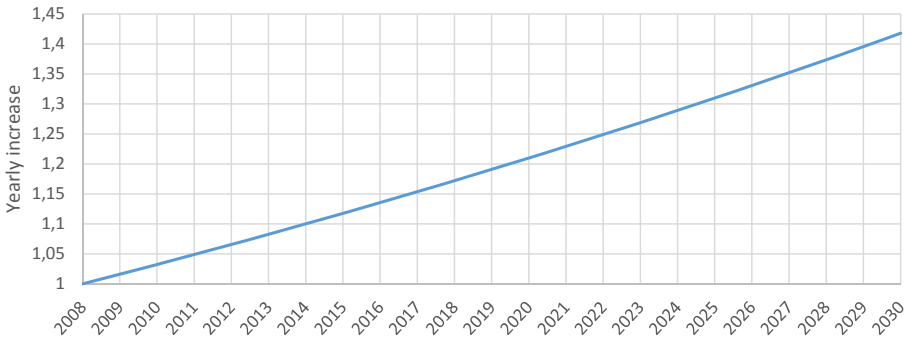

Figure 62: Yearly increase of load estimated by DONG Energy.

C APPENDIX – LOAD FLOW RESULTS OF FEEDER B02 UNDER REFERENCE CASES IN NEPLAN

Figure 63 shows the color ranges used for the elements and the nodes.

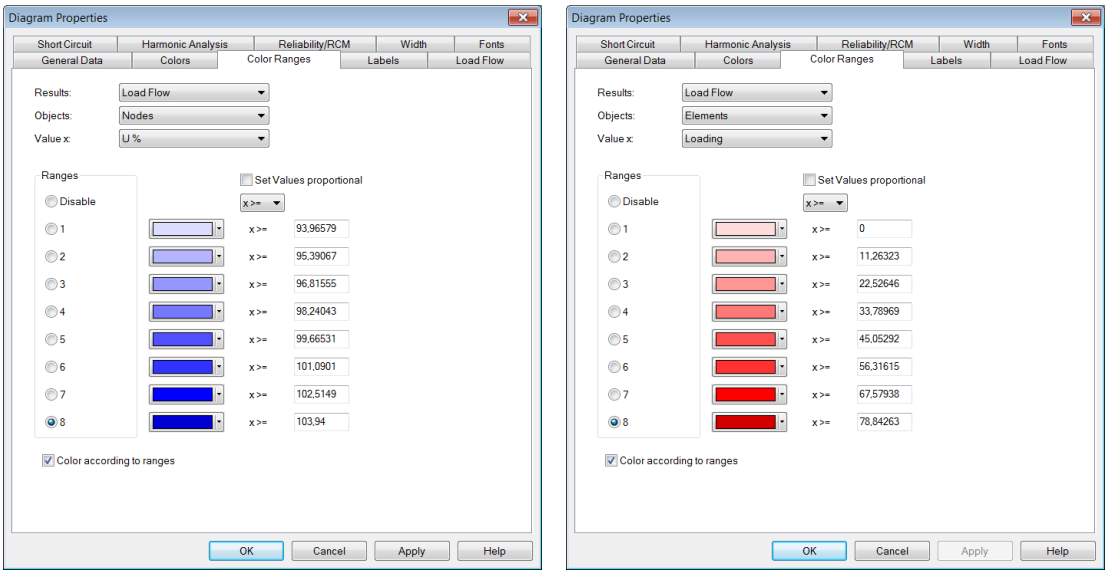

(a) Element loading (b) voltage deviation

Figure 63: Color range definition in NEPLAN.

The following figures are the load flow results of the reference cases at 18:30 in a normal weekday in December 2013. From the changes of colors, we can see the trends of variation along feeder (geographical location), and along time.

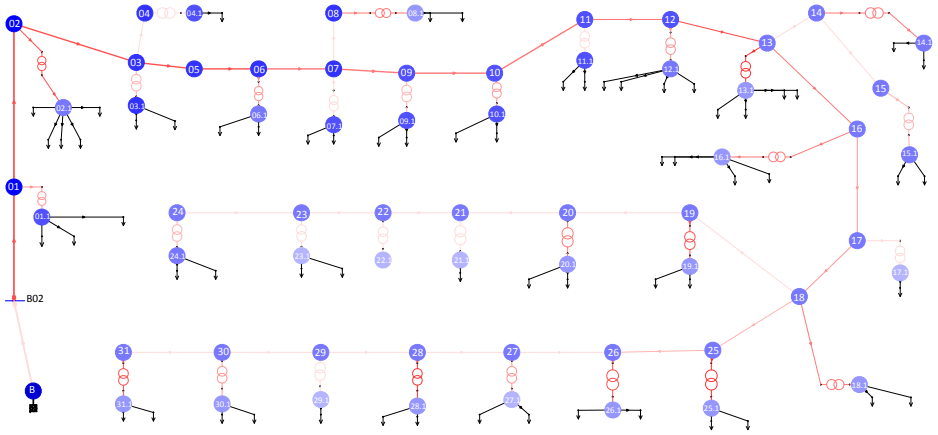

Figure 64: Load flow screenshot of the feeder under 2013 reference case.

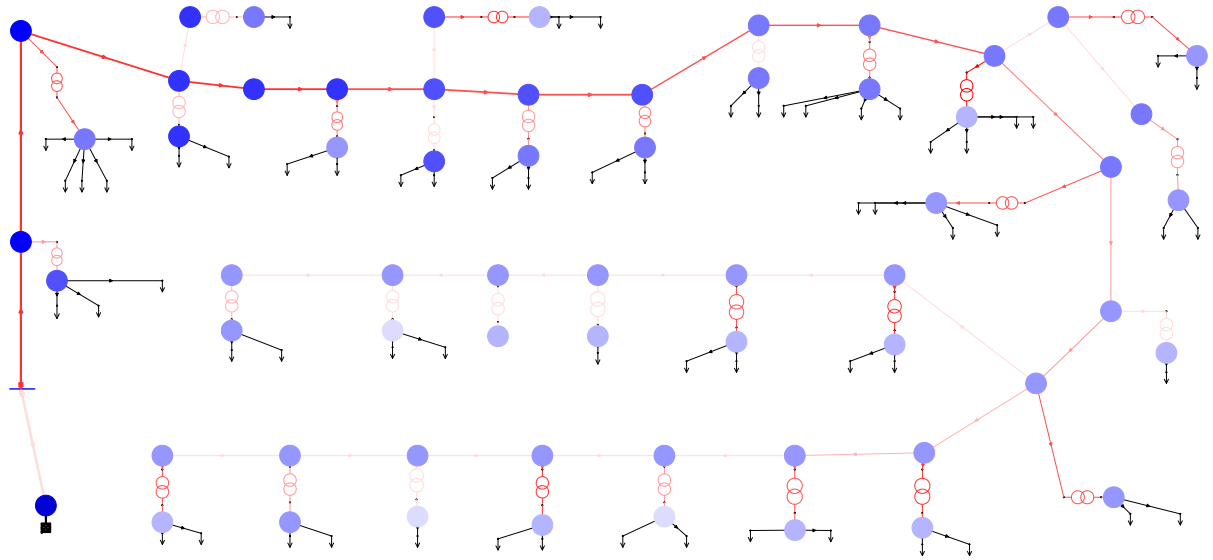

Figure 65: Load flow screenshot of the feeder under 2020 reference case.

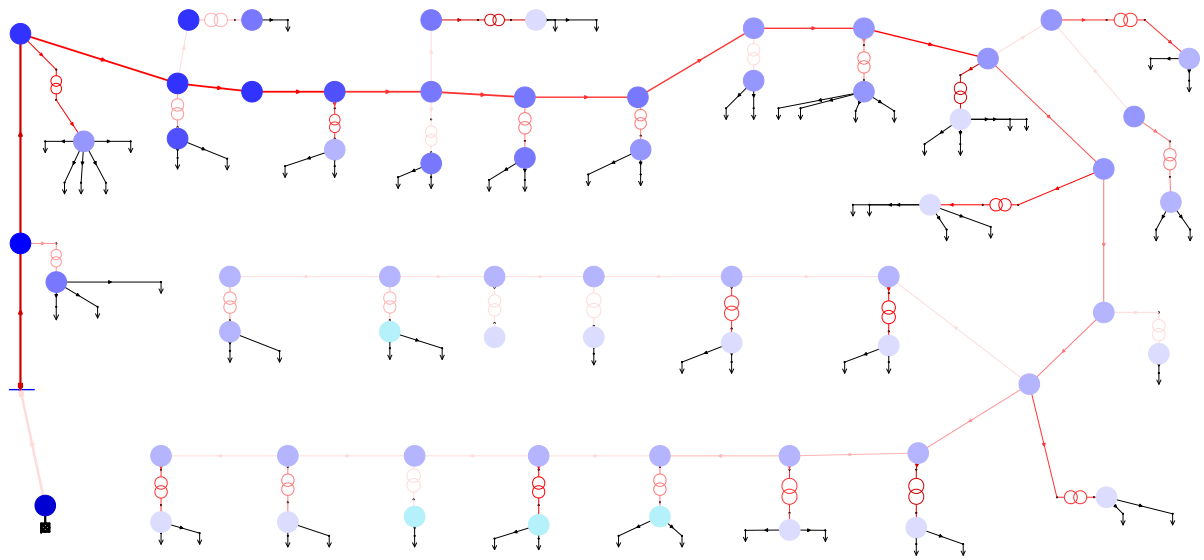

Figure 66: Load flow screenshot of the feeder under 2030 reference case.

D APPENDIX – PLOTS OF LOAD FLOW RESULTS OF FEEDER B02

Figure 67 (a) shows the composition of load profiles under arbitrary nodes in the MV feeder: the upper-left plot shows the ordinary load profiles using load templates (EC load); the upper-right plot shows the additional load due to the integration of electric vehicles and heat pumps; the lower-left plot shows the load of large customers (PQ load); the lower-right plot shows the composed load profile under each node from different portions. Figure 67 (b) shows the profiles of grid states along time. The upper-left plot shows the voltage variation of selected nodes. Both variation and drop of voltage magnitudes increase along the feeder. The largest voltage drop is 9.87 kV, occurring at 18:30. The upper-right plot illustrate the current and loading of the most critical lines in the feeder. We can see that the loading varies between 30% and 55%. The peak of the line loading is 54.2% at L_B02_01_1. The lower-left plot shows the curves of active power, reactive power, and loading of certain transformers that are most loaded. The peak is 62.1% at 18:30. Due to the fixed tap of MV/LV transformers, the voltage drops are even severe in LV side of transformers. The lower-right plot shows the voltage curves of the most critical nodes on LV side. The loading of all elements and the normalized voltage of all nodes are plotted in Figure 67 (c) and (d) respectively.

The counterparts of Case 12 and Case 14 are illustrated in Figure 68 and Figure 69 respectively. If applied the control, modified load profiles can be observed in Figure 70 and Figure 71 (stop control, Case 16 and 18), and in Figure 72 and Figure 73 (stop control, Case 20 and 22).

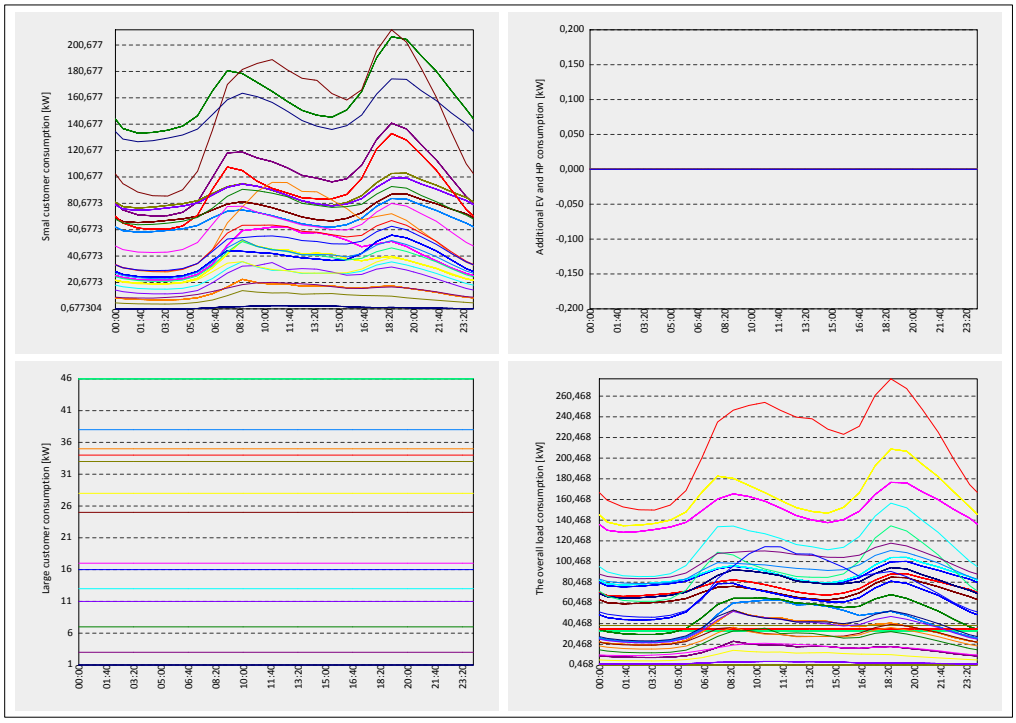

(a) load compositions

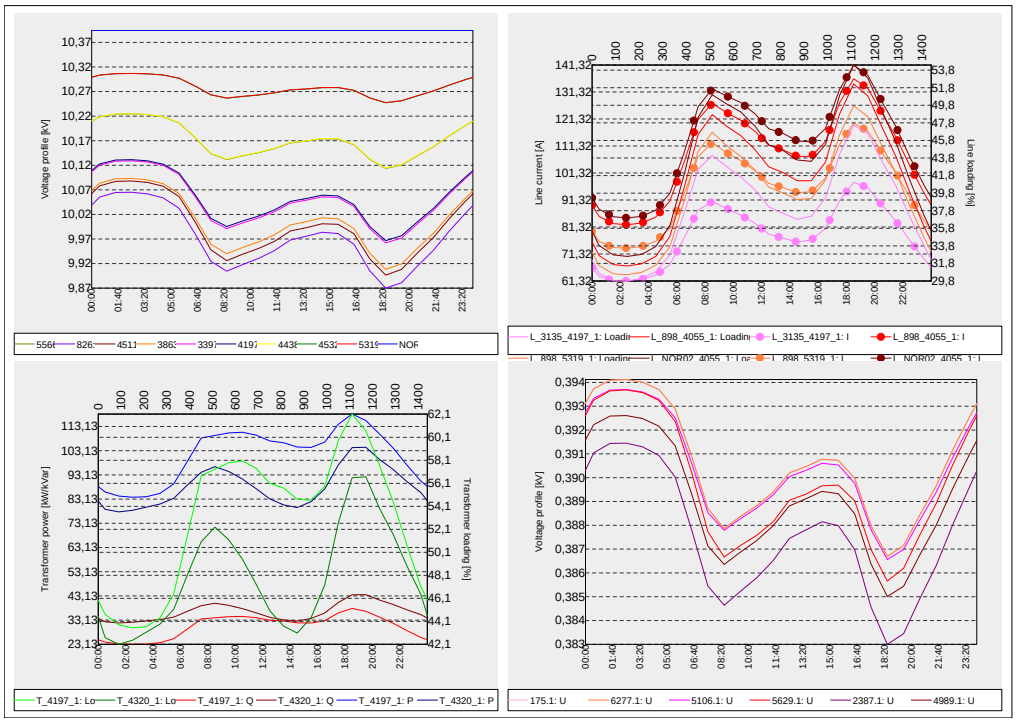

(b) voltage, current, power, and loading profiles along time

Figure 67: Load flow results of the feeder for 2013 reference case No. 10.

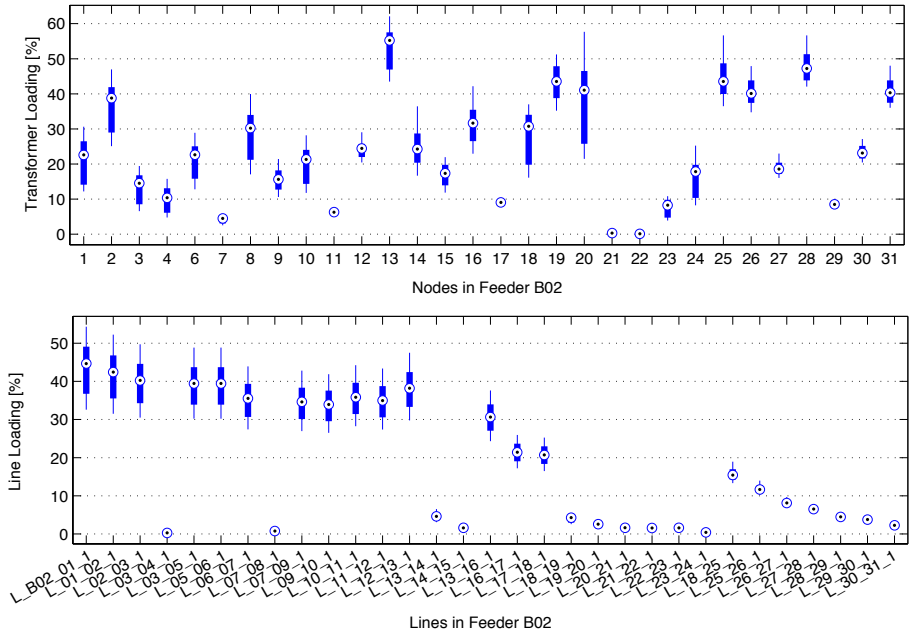

(c) loading of all lines and transformers

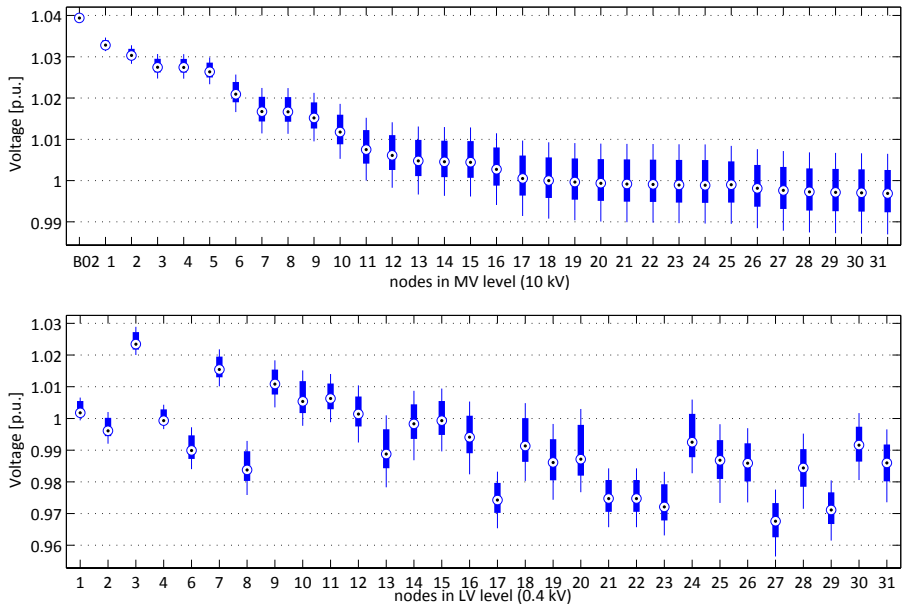

(d) voltage deviations of all the nodes

Figure 67: Load flow results of the feeder for 2013 reference case No. 10. (cont.)

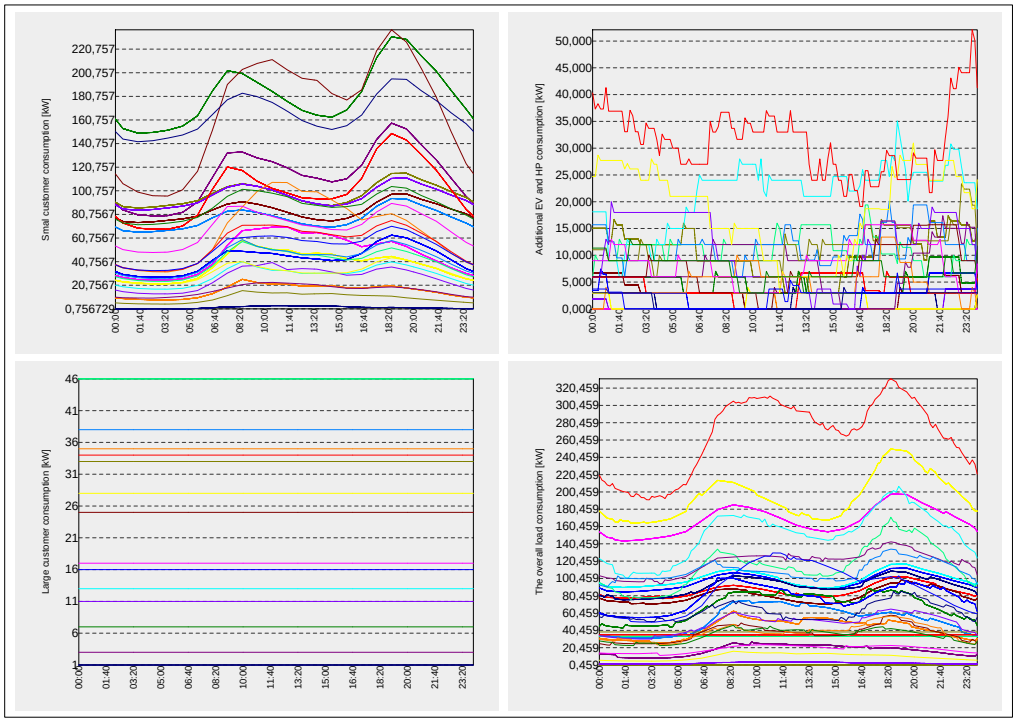

(a) load compositions

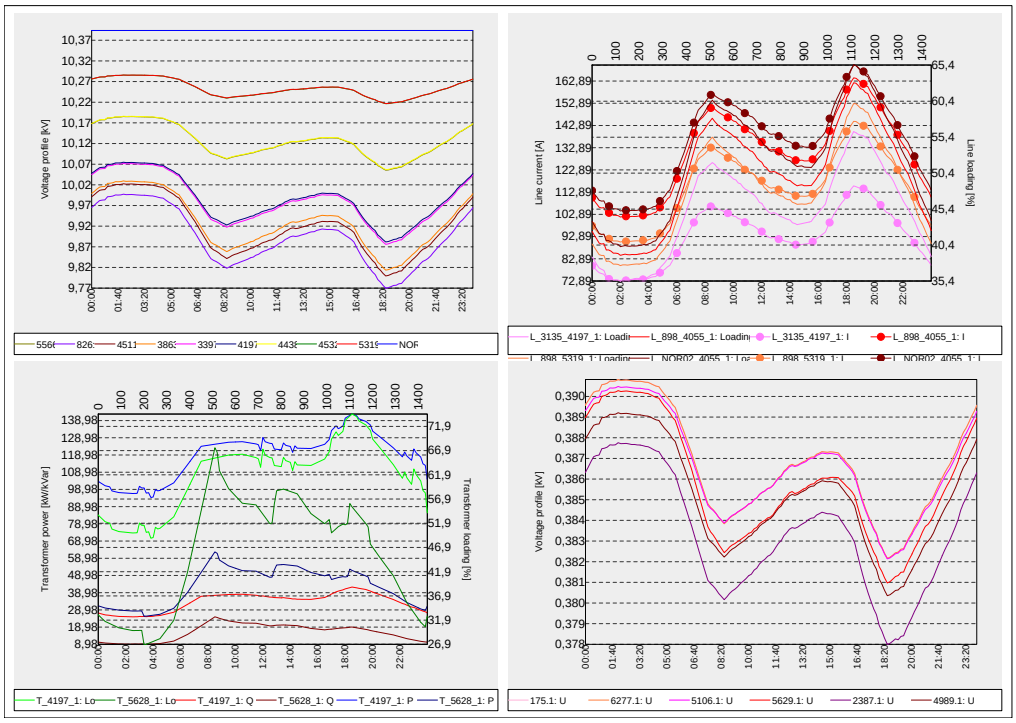

(b) voltage, current, power, and loading profiles along time

Figure 68: Load flow results of the feeder for 2020 reference case No. 12.

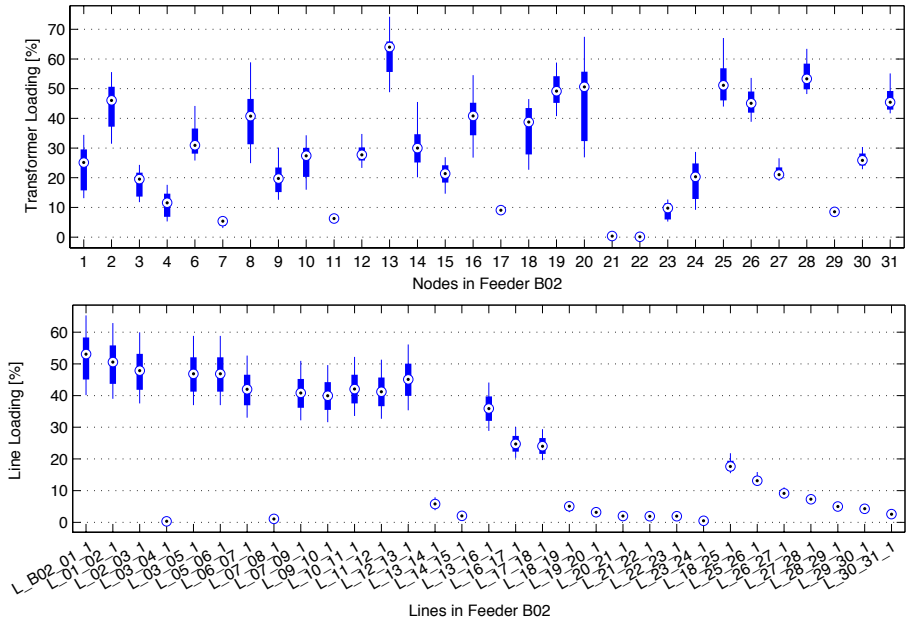

(c) loading of all lines and transformers

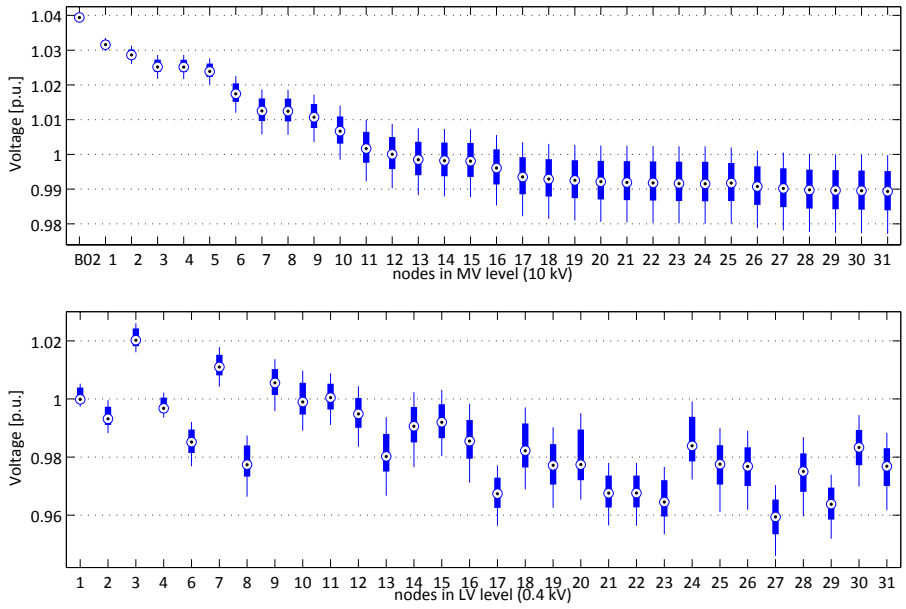

(d) voltage deviations of all the nodes

Figure 68: Load flow results of the feeder for 2020 reference case No. 12. (cont.)

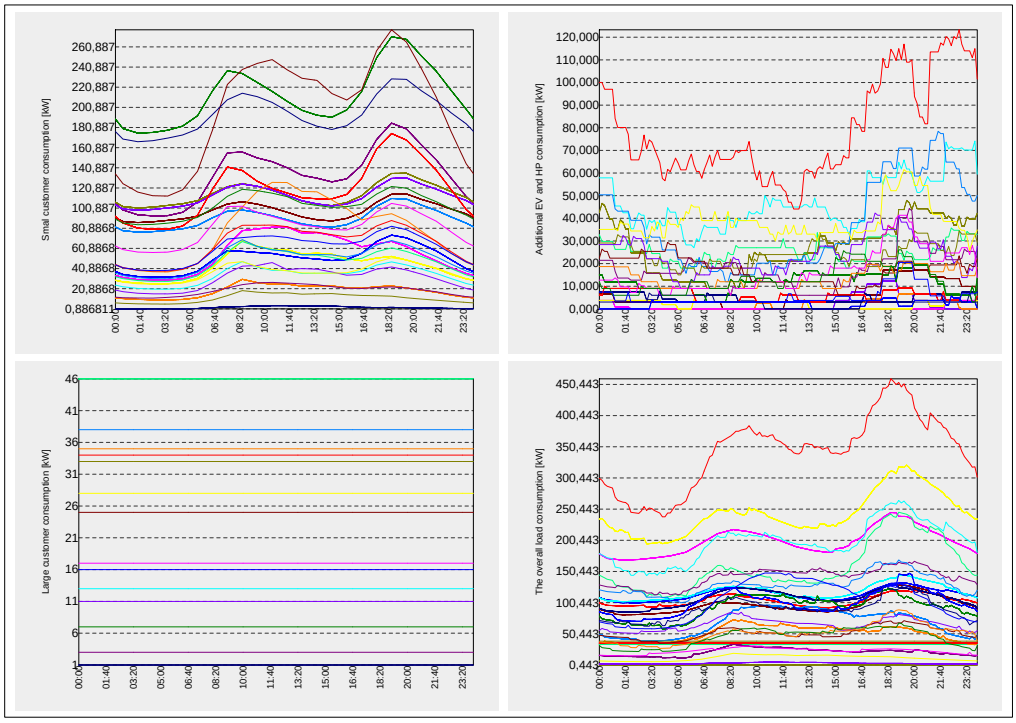

(a) load compositions

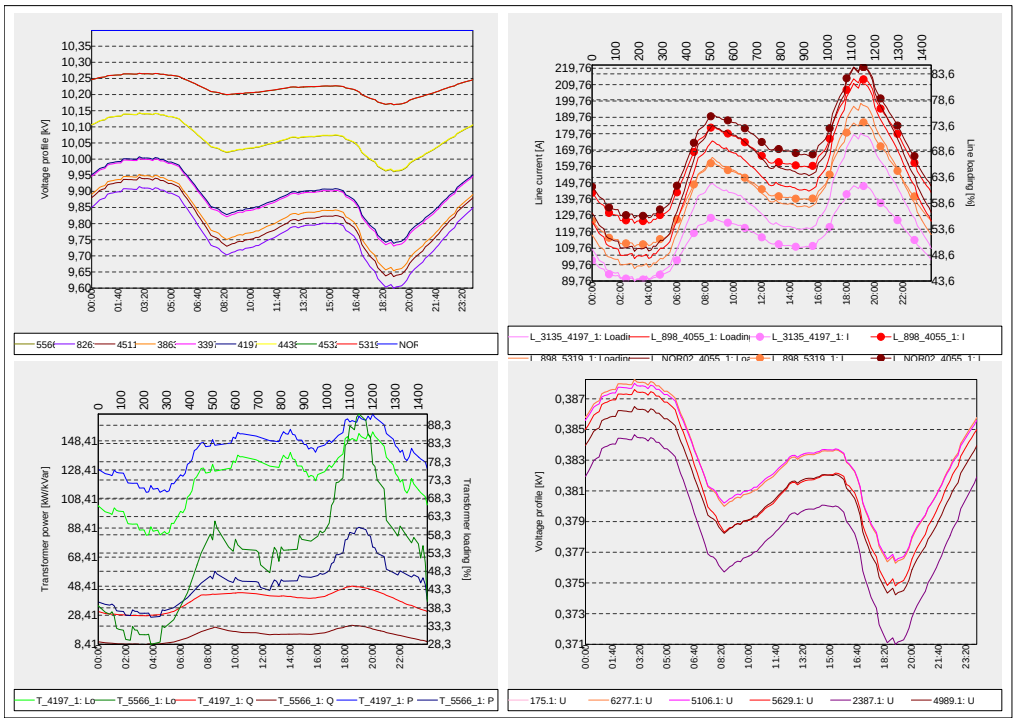

(b) voltage, current, power, and loading profiles along time

Figure 69: Load flow results of the feeder for 2030 reference case No. 14.

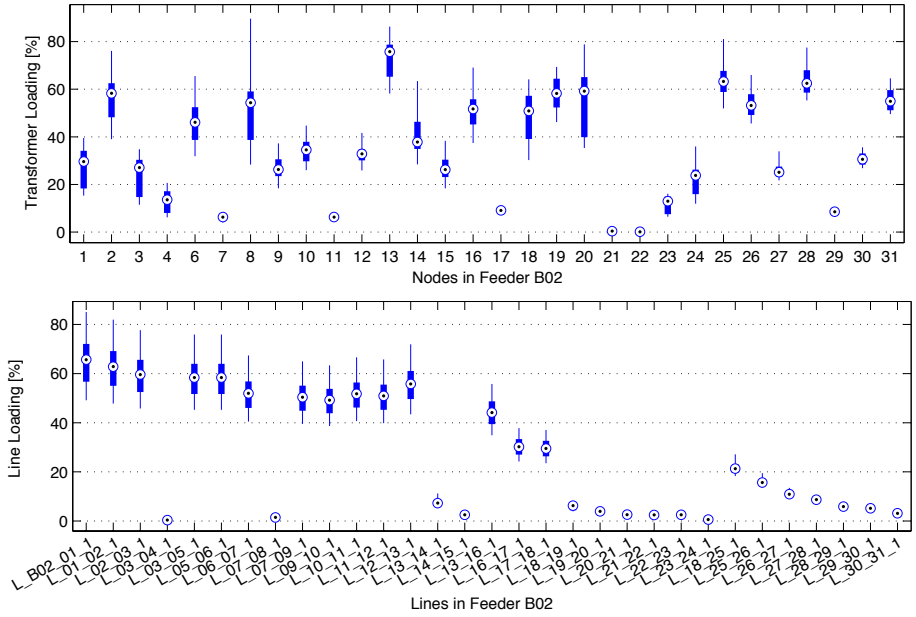

(c) loading of all lines and transformers

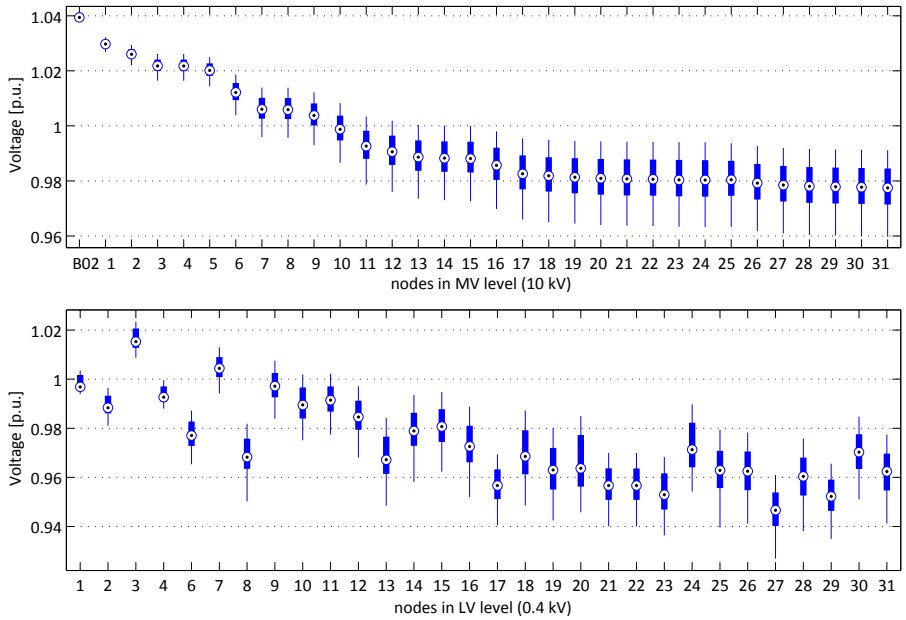

(d) voltage deviations of all the nodes

Figure 69: Load flow results of the feeder for 2030 reference case No. 14. (cont.)

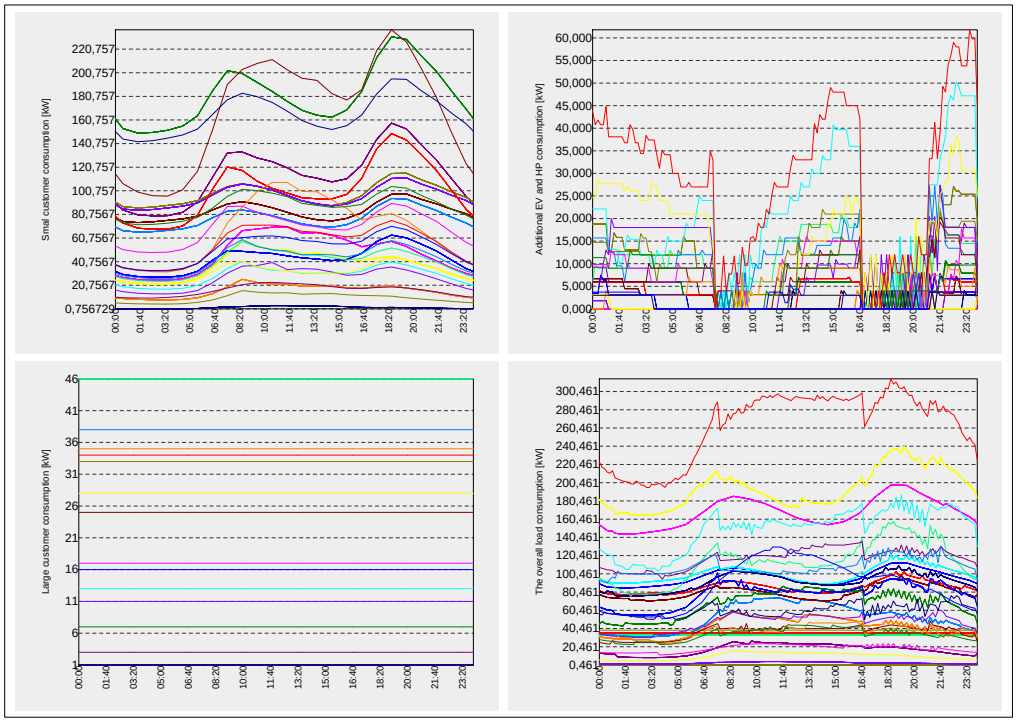

(a) load compositions

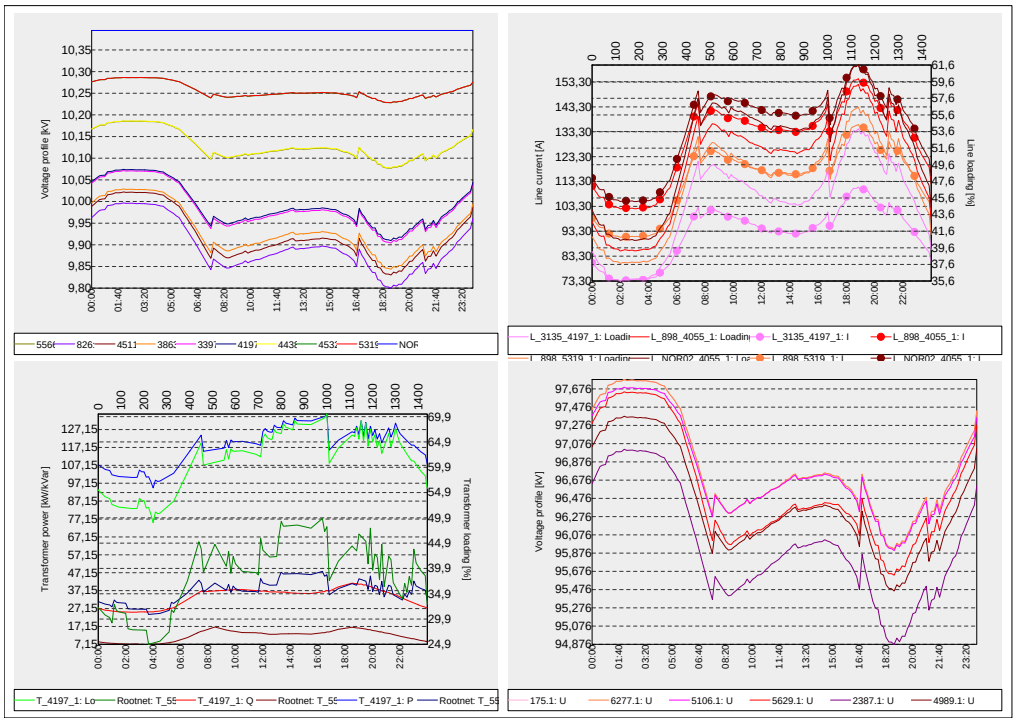

(b) voltage, current, power, and loading profiles along time

Figure 70: Load flow results of the feeder for 2020 stop control case No. 16.

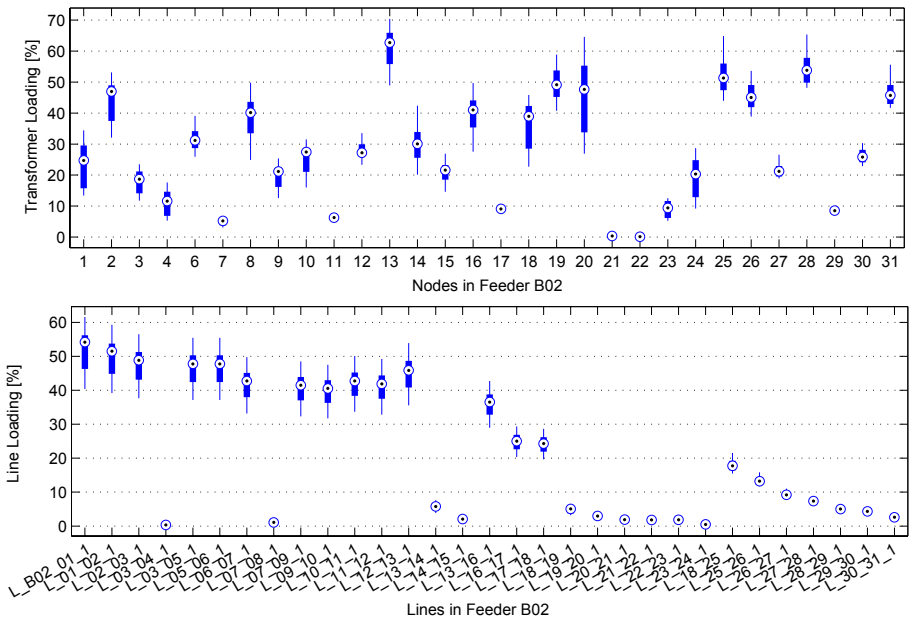

(c) loading of all lines and transformers

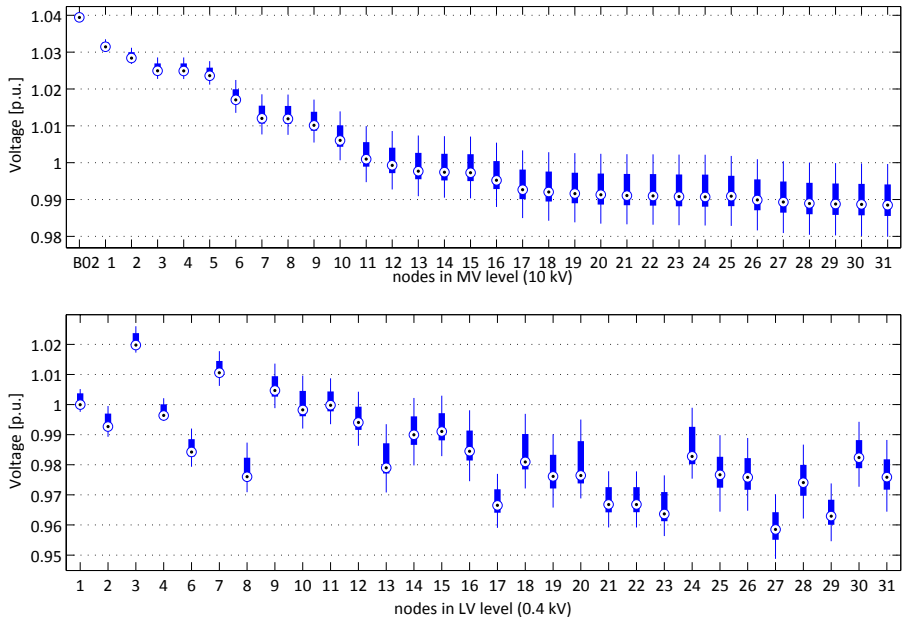

(d) voltage deviations of all the nodes

Figure 70: Load flow results of the feeder for 2020 stop control case No. 16. (cont.)

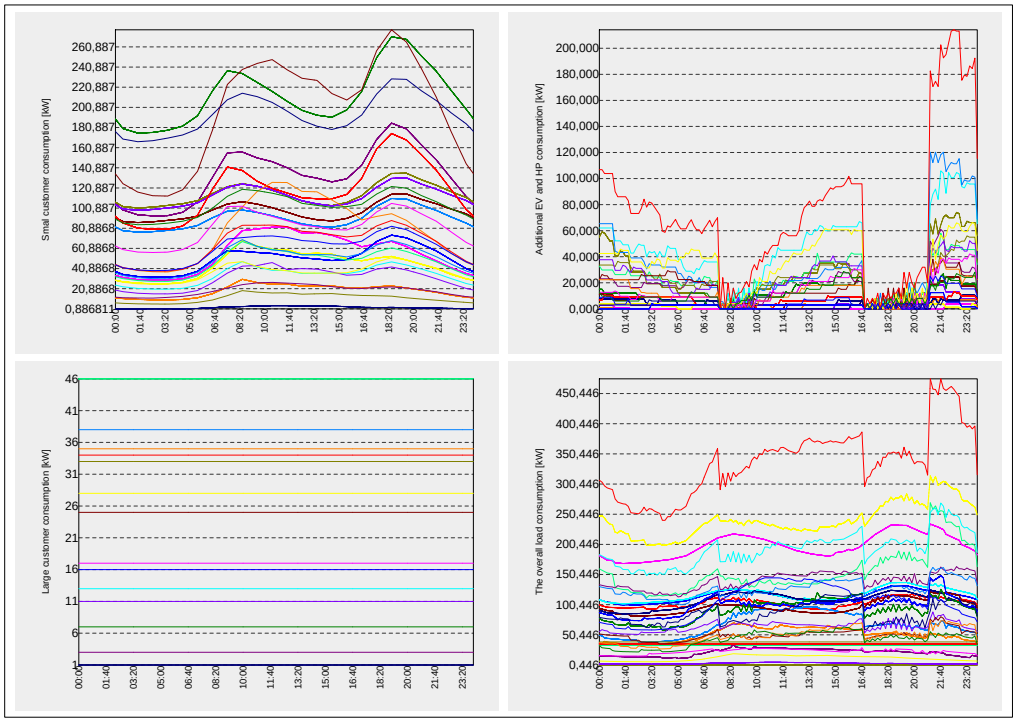

(a) load compositions

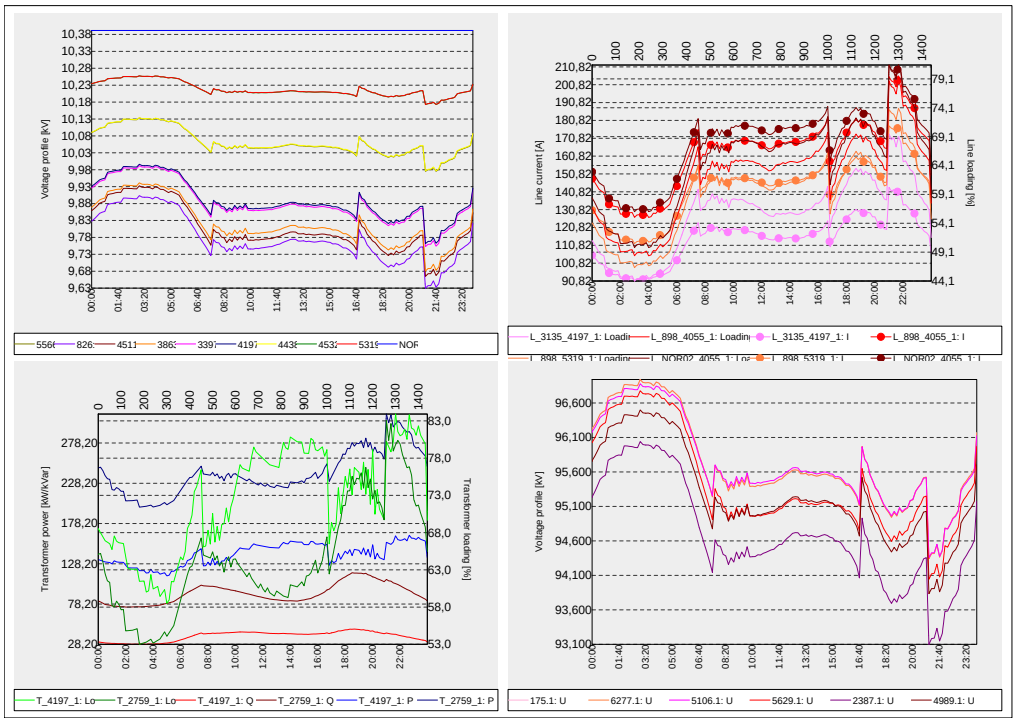

(b) voltage, current, power, and loading profiles along time

Figure 71: Load flow results of the feeder for 2030 stop control case No. 18.

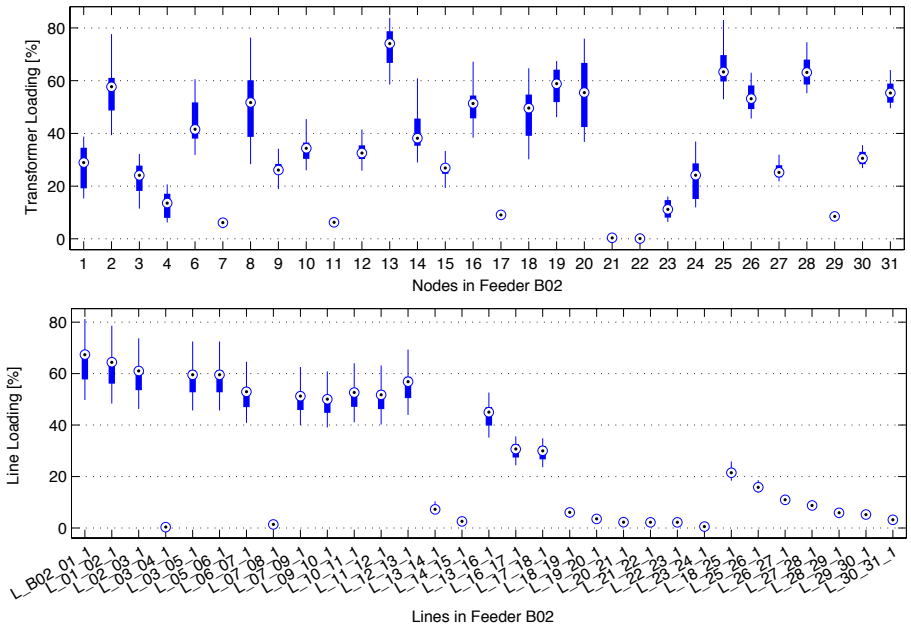

(c) loading of all lines and transformers

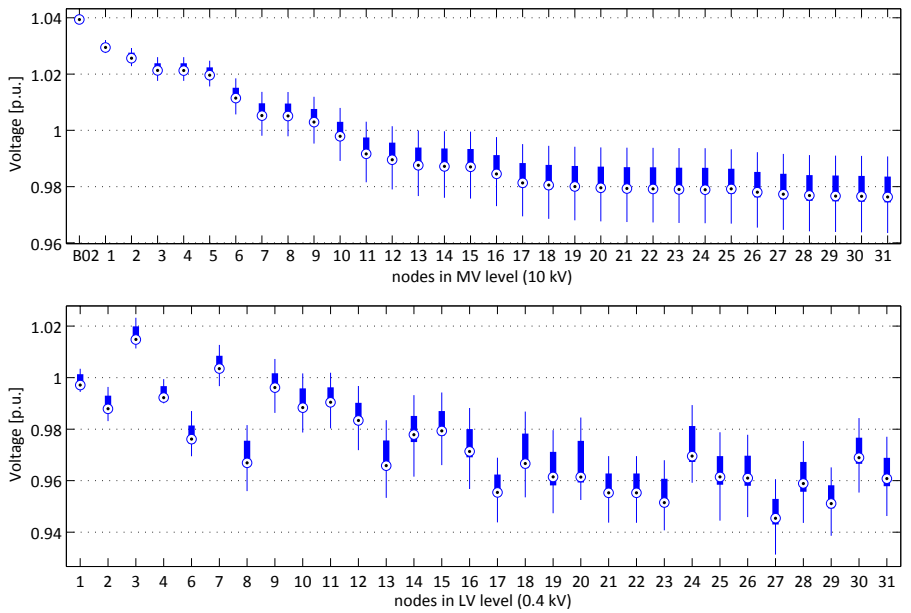

(d) voltage deviations of all the nodes

Figure 71: Load flow results of the feeder for 2030 stop control case No. 18. (cont.)

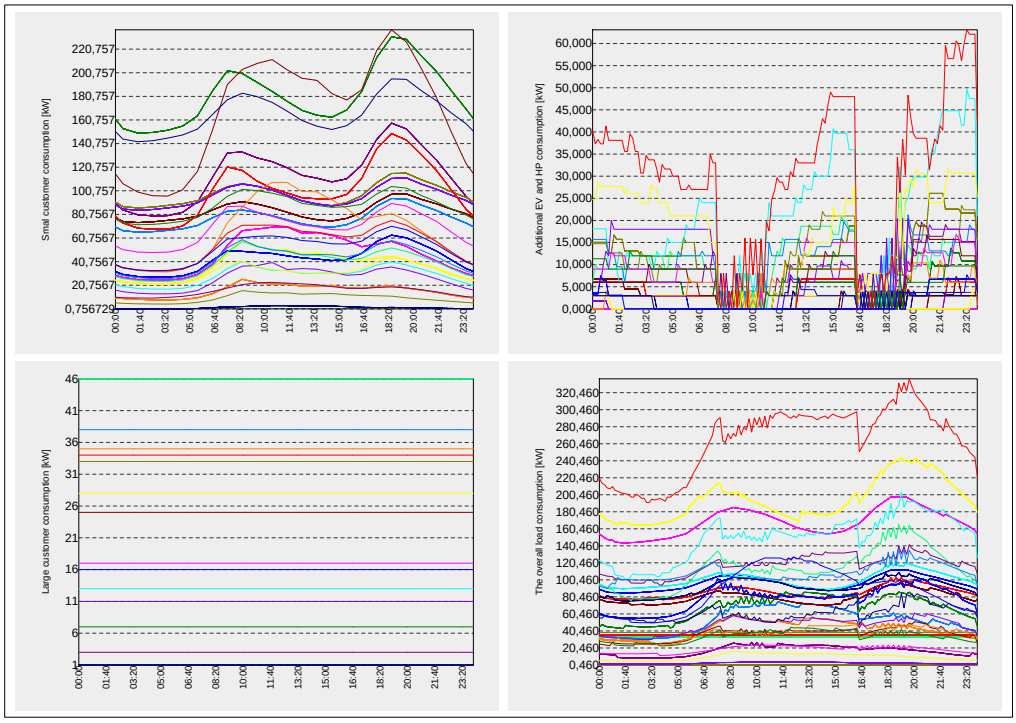

(a) load compositions

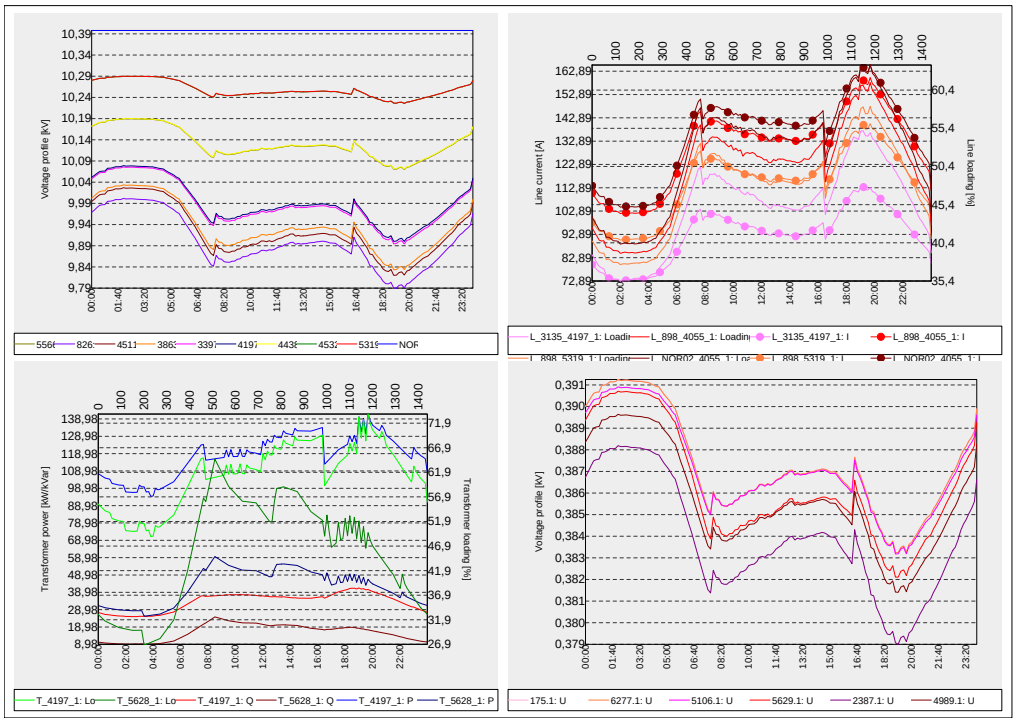

(b) voltage, current, power, and loading profiles along time

Figure 72: Load flow results of the feeder for 2020 incentive-based control case No. 20.

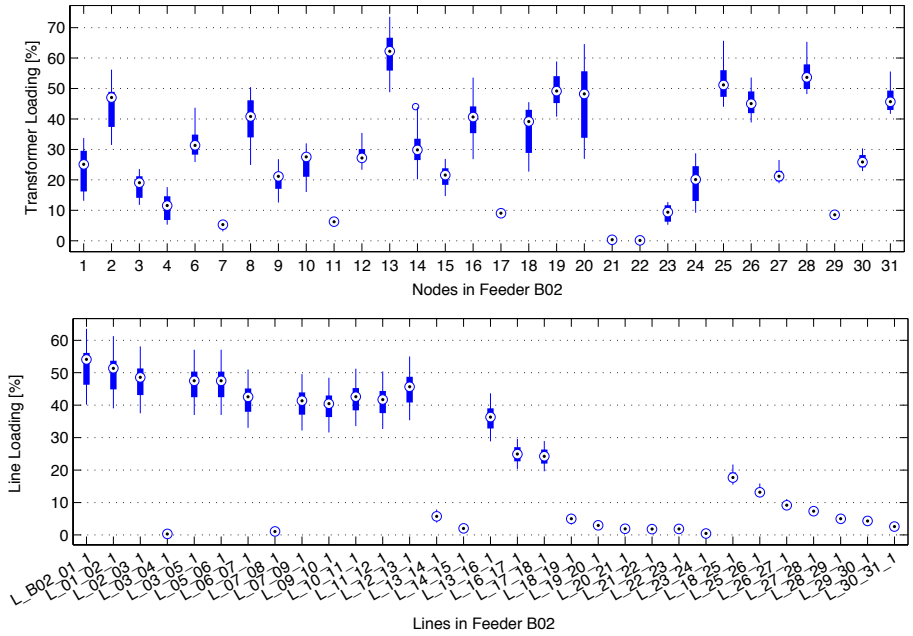

(c) loading of all lines and transformers

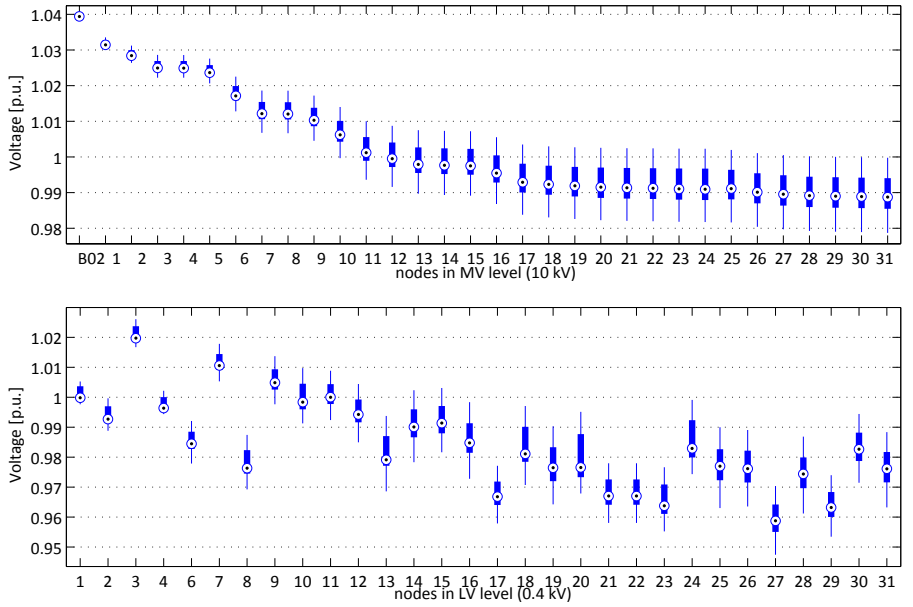

(d) voltage deviations of all the nodes

Figure 72: Load flow results of the feeder for 2020 incentive-based control case No. 20. (cont.)

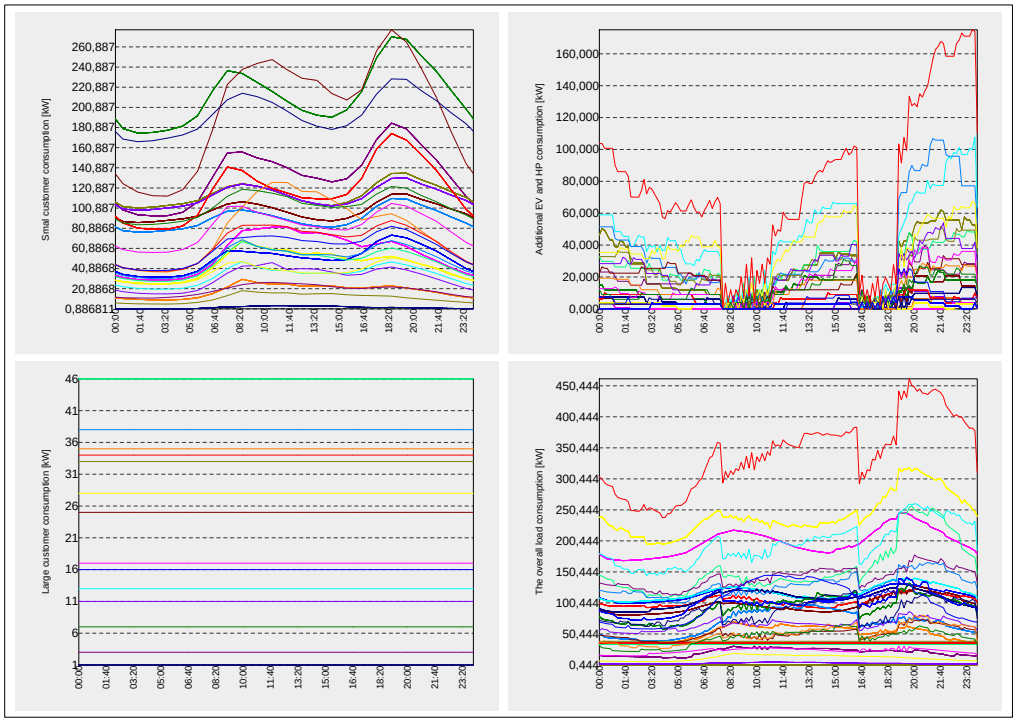

(a) load compositions

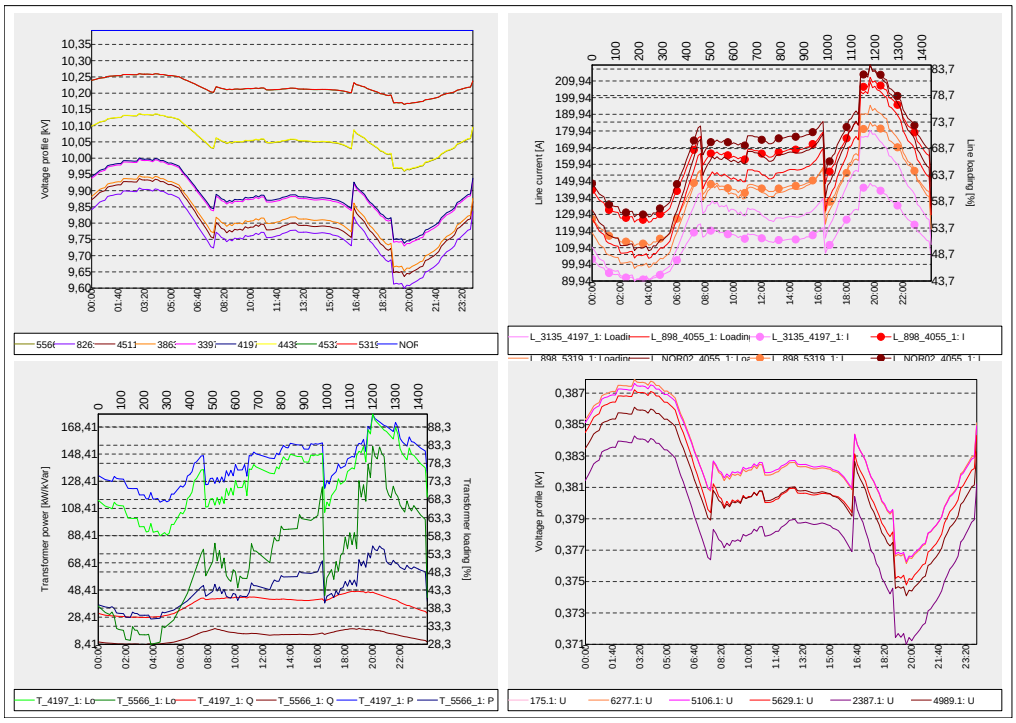

(b) voltage, current, power, and loading profiles along time

Figure 73: Load flow results of the feeder for 2030 incentive-based control case No. 22.

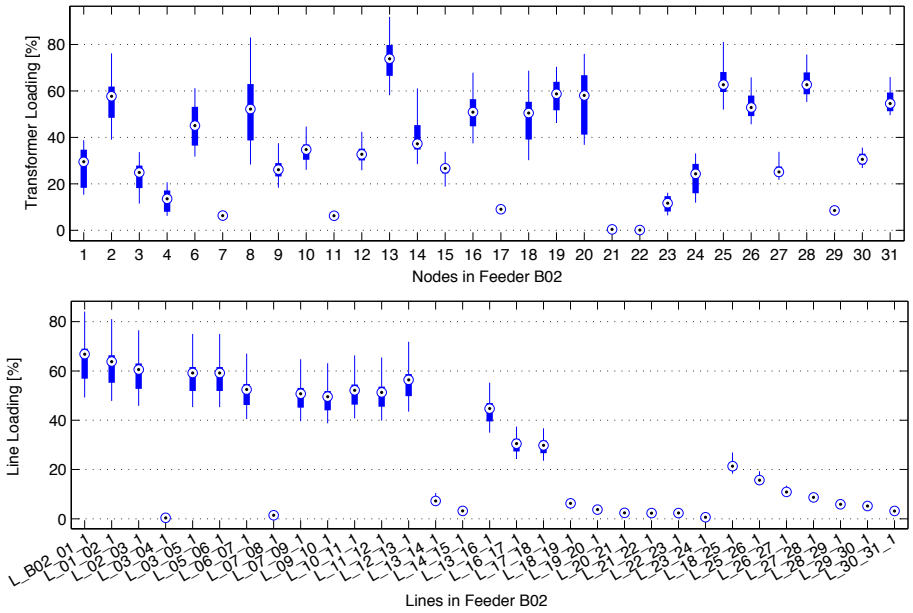

(c) loading of all lines and transformers

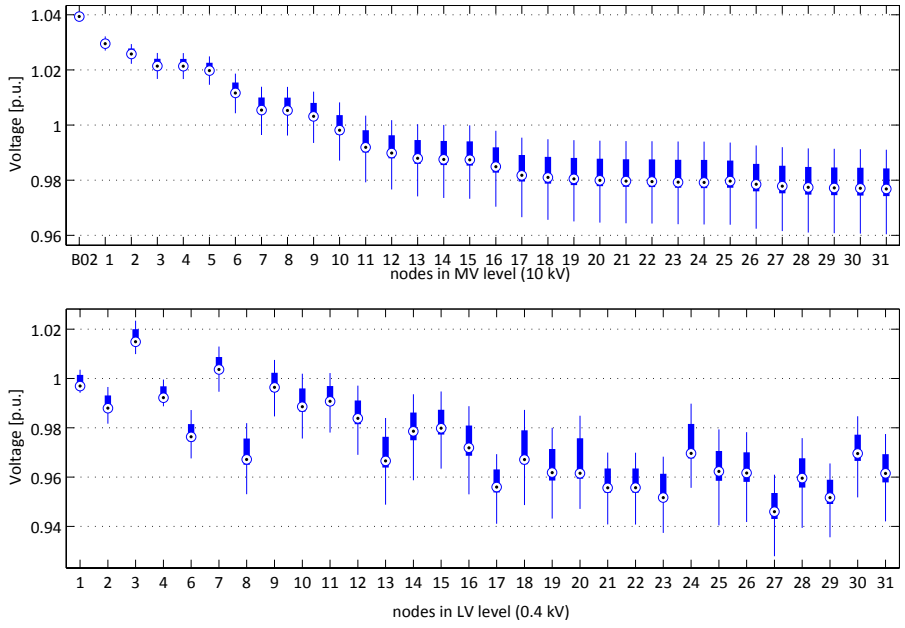

(d) voltage deviations of all the nodes

Figure 73: Load flow results of the feeder for 2030 incentive-based control case No. 22. (cont.)

REFERENCES

[1] Danish Energy Agency, "Energy statistics 2009," 2009.

[2] Commission of the European Communities, "A european strategy for sustainable, competitive and secure energy," 2006, COM(2006) 105 final.

[3] Danish Government, "energy strategy 2050 – from coal, oil and gas to green energy," 2011.

[4] H. Hansen, L. H. Hansen, H. Jóhannsson, H.-H. Holm-Hansen, H. W. Bindner, P. Cajar, D. Energy-Denmark, and O. Samuelsson, "Coordination of system needs and provision of services," in *22nd International Conference on Electricity Distribution*, Jun. 2013, p. Paper No 0261.

[5] T. Kapetanovic, K. Takac, and M. S. Jimenez, "Task force for smart grids expert group 3: Roles and responsibilities of actors involved in the smart grids deployment," EU Commission, Tech. Rep., Apr. 2011.

[6] K. Moslehi and R. Kumar, "A reliability perspective of the smart grid," *IEEE Transactions on Smart Grid*, vol. 1, no. 1, pp. 57–64, 2010.

[7] B. Biegel, "Flexibility interface – information modeling for direct control," iPower Project Work Package 4, Tech. Rep., May 2011.

[8] P. Pinson, T. Jónsson, and H. Madsen, "Indirect control by prices – basic concepts, applications and requirements," iPower Project Work Package 4, Tech. Rep., Jul. 2012.

[9] D. Miller and T. Sleva, "Cold load pickup issues," Power System Relay Committee of The IEEE Power Engineering Society, Tech. Rep., May 2008.

[10] S. Lee and C. Wilkins, "A practical approach to appliance load control analysis: a water heater case study," *power apparatus and systems, ieee transactions on*, no. 4, pp. 1007–1013, 1983.

[11] C. Kurucz, D. Brandt, and S. Sim, "A linear programming model for reducing system peak through customer load control programs," *Power Systems, IEEE Transactions on*, vol. 11, no. 4, pp. 1817–1824, 1996.

[12] N. Ruiz, I. Cobelo, and J. Oyarzabal, "A direct load control model for virtual power plant management," *Power Systems, IEEE Transactions on*, vol. 24, no. 2, pp. 959–966, 2009.

[13] S. Paoletti, M. Casini, A. Giannitrapani, A. Facchini, A. Garulli, and A. Vicino, "Load forecasting for active distribution networks," in *Innovative Smart Grid Technologies (ISGT Europe), 2011 2nd IEEE PES International Conference and Exhibition on*. IEEE, 2011, pp. 1–6.

[14] C. Perfumo, E. Kofman, J. H. Braslavsky, and J. K. Ward, "Load management: Model-based control of aggregate power for populations of thermostatically controlled loads," *Energy Conversion and Management*, vol. 55, pp. 36–48, 2012.

[15] S. Kundu, N. Sinitsyn, S. Backhaus, and I. Hiskens, "Modeling and control of thermostatically controlled loads," *arXiv preprint arXiv:1101.2157*, 2011.

[16] N. A. Sinitsyn, S. Kundu, and S. Backhaus, "Safe protocols for generating power pulses with heterogeneous populations of thermostatically controlled loads," *Energy Conversion and Management*, vol. 67, pp. 297–308, 2013.

[17] R. Belhomme and F. Bouffard, "ADDRESS technical and commercial conceptual architectures," Active Distribution network with full integration of Demand and distributed energy RESourceS Project, Tech. Rep., Oct. 2009.

[18] Dong Energy. (2013). [Online]. Available: www.dongenergy-distribution.dk

[19] NEPLAN. (2013). [Online]. Available: www.neplan.ch

[20] "Standard EN 50160 -Voltage Characteristics in Public Distribution Systems," http://www.copperinfo.co.uk/power-quality/downloads/pqug/542-standard-en-50160-voltage-characteristics-in.pdf.

[21] A. H. F. s, "EDISON wp1.1 electric vehicle technology," EDISON Consortium, Tech. Rep., Nov. 2010, http://www.edison-net.dk/Dissemination/Reports.

[22] Tesla Moter. (2009). [Online]. Available: http://www.teslamotors.com/goelectric/efficiency

[23] S. You, J. Hu, A. B. Pedersen, P. B. Andersen, C. N. Rasmussen, and S. Cha, "Numerical comparison of optimal charging schemes for electric vehicles," in *Power and Energy Society General Meeting, 2012 IEEE*. IEEE, 2012, pp. 1–6.

[24] M. Miara, "Performance/optimization of state-of-the art residential heat pump," IEA-Annex 32, Expert meeting, Kyoto, Dec. 2007.

[25] M. Miara, D. Günser, T. Kramer, T. Oltersdorf, and J. Wapler, "Analysis and evaluation of heat pump efficiency in real-life conditions," Fraunhofer Institute for. Solar Energy Systems ISE, Tech. Rep., May 2011.

[26] "Demand response – the eFlex project report," DONG Energy Eldistribution A/S Department of Grid Strategy, Tech. Rep., Nov. 2012.

[27] F. Sossan, X. Han, and H. Bindner, "Dynamic behaviour of a population of controlled-by-price demand side resources," in *Proceedings of the IEEE Power Energy System General Meeting, 2014*. IEEE, submitted for publication.

[28] "Bygnings-og boligregistret," www.bbr.dk.

[29] DTU. (2013) Powerflexhouse. [Online]. Available: http://www.powerlab.dk/English/facilities/PowerFlexHouse.aspx

[30] C. Ucak and A. Pahwa, "An analytical approach for step-by-step restoration of distribution systems following extended outages," *Power Delivery, IEEE Transactions on*, vol. 9, no. 3, pp. 1717–1723, 1994.

[31] E. Agneholm and J. Daalder, "Cold load pick-up of residential load," in *Generation, Transmission and Distribution, IEE Proceedings-*, vol. 147, no. 1. IET, 2000, pp. 44–50.

[32] N. Saker, M. Petit, and J. Coullon, "Demand side management of electrical water heaters and evaluation of the cold load pick-up characteristics (clpu)," in *PowerTech, 2011 IEEE Trondheim*. IEEE, 2011, pp. 1–8.

[33] S. Lefebvre and C. Desbiens, "Residential load modeling for predicting distribution transformer load behavior, feeder load and cold load pickup," *International journal of electrical power & energy systems*, vol. 24, no. 4, pp. 285–293, 2002.

[34] V. Kumar, H. R. Kumar, I. Gupta, and H. O. Gupta, "Dg integrated approach for service restoration under cold load pickup," *Power Delivery, IEEE Transactions on*, vol. 25, no. 1, pp. 398–406, 2010.

[35] F. Sossan and M. Marinelli, "An auto tuning substation peak shaving controller for congestion management using flexible demand," in *Universities Power Engineering Conference, 2013. UPEC 2013. 48th International*, 2013, pp. 1–5.

